LOAN DOCUMENT

PHOTOGRAPH THIS SHEET

AD-A253 722

DTIC ACCESSION NUMBER

LEVEL

1

INVENTORY

NSTL-TR-294

DOCUMENT IDENTIFICATION

Apr 85

DISTRIBUTION STATEMENT A
Approved for public release;
Distribution Unlimited

DISTRIBUTION STATEMENT

HANDLE WITH CARE

ACCESSION FOR
NTIS GRA&I ☑
DTIC TRAC ☐
UNANNOUNCED ☐
JUSTIFICATION

BY

DISTRIBUTION/

AVAILABILITY CODES

DISTRIBUTION	AVAILABILITY AND/OR SPECIAL
A-1	

DISTRIBUTION STAMP

DTIC
ELECTE
AUG 4 1992
S C D

DATE ACCESSIONED

DTIC QUALITY INSPECTED 5

DATE RETURNED

92 7 30 004

DATE RECEIVED IN DTIC

92-20659

REGISTERED OR CERTIFIED NUMBER

PHOTOGRAPH THIS SHEET AND RETURN TO DTIC-FDAC

DTIC FORM 70A JUN 90

DOCUMENT PROCESSING SHEET

PREVIOUS EDITIONS MAY BE USED UNTIL STOCK IS EXHAUSTED.

LOAN DOCUMENT

Naval Oceanographic Office
Bay St. Louis,
NSTL,
Mississippi 39522-5001

Technical Report
TR-294
April 1985

CTD ALIASING INVESTIGATION

ERNEST L. BURDETTE

Prepared by
Triton Systems, Incorporated
Contract Number N62306-82-M-2222

Prepared under the authority of
Commander,
Naval Oceanography Command

FOREWORD

This report gives the results of an investigation of aliasing in the data from conductivity/temperature/depth (CTD) instruments used by the Naval Oceanographic Office (NAVOCEANO). The U.S. Navy Fleet requirements for environmental data presently are supported through measurements made with the CTD. Investigation was undertaken to determine what errors could be expected in survey data products due to aliasing in the CTD data.

This effort was performed under a contract awarded to Triton Systems, Inc., of Pass Christian, MS. Dr. Ernest L. Burdette was the principal investigator for Triton Systems. The empirical data used in the analysis were obtained using the unique facilities and specialized techniques developed in the Engineering Department of NAVOCEANO.

J. M. Sears
Captain, USN
Commanding Officer

Triton Systems, Incorporated
Contract No. N62306-82-M-2222
Pass Christian, MS. 39571

REPORT DOCUMENTATION PAGE

READ INSTRUCTIONS BEFORE COMPLETING FORM

1. REPORT NUMBER: TR-294	2. GOVT ACCESSION NO.: N/A
3. RECIPIENT'S CATALOG NUMBER: N/A	
4. TITLE (and Subtitle): CTD DATA ALIASING INVESTIGATION	5. TYPE OF REPORT & PERIOD COVERED: Technical Report - Final SEP 82 - DEC 83
6. PERFORMING ORG. REPORT NUMBER: N/A	
7. AUTHOR(s): ERNEST L. BURDETTE	8. CONTRACT OR GRANT NUMBER(s): N62306-82-M-2222
9. PERFORMING ORGANIZATION NAME AND ADDRESS: Triton Systems, Incorporated, 109 East Scenic Drive, Pass Christian, MS 39571	10. PROGRAM ELEMENT, PROJECT, TASK AREA & WORK UNIT NUMBERS: N/A
11. CONTROLLING OFFICE NAME AND ADDRESS: Naval Oceanographic Office, Bay St. Louis, NSTL, MS 39522-5001	12. REPORT DATE: April 1985
	13. NUMBER OF PAGES: 158
14. MONITORING AGENCY NAME & ADDRESS (if different from Controlling Office): Instrumentation and Metrology Branch, Naval Oceanographic Office, Bay St. Louis, NSTL, MS 39522-5000	15. SECURITY CLASS. (of this report): UNCLASSIFIED
	15a. DECLASSIFICATION/DOWNGRADING SCHEDULE

16. DISTRIBUTION STATEMENT (of this Report)

Approved for public release; distribution unlimited

17. DISTRIBUTION STATEMENT (of the abstract entered in Block 20, if different from Report)

N/A

18. SUPPLEMENTARY NOTES

"The inclusion of names of any specific commercial product, commodity, or service in this publication is for information purposes only and does not imply endorsement by the Navy or NAVOCEANO."

19. KEY WORDS (Continue on reverse side if necessary and identify by block number)

Aliasing; spectral analysis; power spectral analysis; variance; digital filtering; time-series analysis

20. ABSTRACT (Continue on reverse side if necessary and identify by block number)

The Neil Brown Instrument Systems Mark IIIb Conductivity, Temperature, and Depth (CTD) instrument is used by the Naval Oceanographic Office to satisfy requirements for environmental data. Computed parameters such as salinity are calculated from those directly measured. An investigation is described which evaluates the effect of aliasing on CTD data acquired at the standard sampling rate of 15.63 Hz.

A method is developed for determining the transfer functions for conductivity

and temperature from a modified CTD at three times the normal data sampling frequency. Because the modified sampling arrangement introduces jitter in the sample timing, it is necessary to use a modified spectral estimation technique. Results of a literature survey of such techniques are presented. One of the techniques, developed by Shaw, was adopted to estimate the conductivity- and temperature-transfer functions. Conductivity-transfer functions obtained in this way are compared with published results. Agreement is to within the margin of error introduced by sample timing jitter for most frequencies.

The temperature- and conductivity-transfer functions are used to predict an upper limit to the spectral error due to aliasing. These results are extended to include a corresponding estimate for salinity.

It is concluded that aliasing is not a significant source of error in present data products at 1.0-m resolution, and that error due to aliasing would be less than 10% in products with resolutions as fine as 0.1 m. Thus, limits on high resolution data products are not due to aliasing, but instead are due to other phenomena associated with the instrument.

TABLE OF CONTENTS

LIST OF FIGURES

LIST OF TABLES

APPENDIXES

1.0 INTRODUCTION

1.1 BACKGROUND

U.S. Navy requirements for environmental data presently are supported through measurements made with a conductivity/temperature/depth (CTD) instrument. Data products are developed from the CTD data. A typical example is salinity, a function of all three measured parameters.

The instrument used by the Naval Oceanographic Office (NAVOCEANO) is the Mark IIIb CTD manufactured by Neil Brown Instrument Systems, Inc. (NBIS). Data are acquired by operating the CTD in an over-the-side downcast mode. The standard profiling deployment rate for the instrument is 1 m/s. Time series data are digitized at a rate of approximately 32 ms per sample of pressure, temperature and conductivity. This corresponds to a spatial sampling rate of approximately 31.2 samples per meter (0.032 m between samples) in the vertical direction. Standard data products are obtained by applying a low-pass filter to the vertical data sequence, followed by sub-sampling at 1 sample per meter. This approach is followed for directly measured parameters, such as temperature and conductivity, as well as computed parameters such as salinity.

The Nyquist criterion for the spatial data sequence states that a vertical sampling frequency of 31.2 m^{-1} is adequate to resolve spatial frequencies as high as 15.6 m^{-1}. This is equivalent to resolving wavelengths greater than 0.064 m. The vertical dimension of the NBIS conductivity cell is 0.03 m which should approximate the spatial resolution of the sensor. Thus, it is clear that the spatial resolution of the sensor is approximately two times that specified by the Nyquist criterion for the given sampling rate.

As this simplistic analysis demonstrates, the present 1-m^{-1} data products are an order of magnitude poorer in resolution than is dictated by the fundamental limitations of the sampling rate and the NBIS CTD conductivity cell resolution. However, due to other characteristics of this instrument, at least two barriers to higher resolution data products exist.

One well-known problem is created by mismatching of the time response characteristics for the conductivity and temperature transducers. Changes in temperature and conductivity are measured with different responses, the temperature circuitry responding more slowly than conductivity. If these changes are of the same order of magnitude in duration as the response times of the sensors, the computed salinity will temporarily overshoot the correct value, producing a transient but relatively large error in salinity, termed a salinity spike. Several methods exist for correcting salinity spikes, including:

1) Electronic correction by attempting to match physically the time responses of the temperature and conductivity transducers;
2) low-pass filtering of the temperature and conductivity data to remove the high frequency spikes in computed salinity as is done in the operational data; and
3) numerically filtering the individual temperature and conductivity data sets to correct for the time response of the respective transducer.

The third method theoretically has the potential for producing the most accurate results and for retaining a relatively larger amount of high frequency information as required for improvement of resolution. It has the disadvantage of requiring accurate knowledge of the transducer transfer function, including both amplitude and phase.

A second potential problem is presented by sampling of CTD transducers at a frequency of approximately 31.2 Hz without prior filtering to eliminate high frequency information. Aliasing occurs when frequencies greater than one-half the sampling frequency are present in the digitized analog signal. Thus, if either transducer is capable of responding to frequencies higher than approximately 15.6 Hz, the potential exists for data at lower frequencies to be contaminated by the aliased high-frequency data. The nature and extent of the potential aliasing problem can be addressed only if the transfer functions of the transducers are known.

The transfer function of any device may be determined by observing the response of the device to known inputs, provided that the input contains information covering the entire range of frequencies of interest. One common method is to apply a step function as input, since a time domain step is composed of an infinity of frequencies. This method is described in some detail in Section 2.4.

The NAVOCEANO Maintenance Engineering Division has developed a laboratory test to determine time responses of the individual NBIS CTD transducers. The test, described in Section 2.1, subjects the transducers to step changes in temperature and/or conductivity by dropping the sensor through a stratified layer, while acquiring digitized data from the CTD via normal means. Data digitized at the normal 31.2 Hz sampling frequency are Nyquist limited to approximately 15.6 Hz.

NAVOCEANO has modified selected units to acquire data from a single channel, either temperature or conductivity, at approximately 93 Hz. Frequency-domain analysis of step-response data acquired at this higher rate provides a determination of transducer response up to the Nyquist limit of 46.5 Hz. This should be adequate to evaluate performance over the frequency range of the normal CTD data, 0 to 15.6 Hz.

A consequence of the modification to enable high-speed sampling of a single channel is that data are sampled at unerual time intervals, while conventional spectral analysis techniques require that data be sampled at equally spaced times. Equally spaced time series could be acquired for the purposes of this investigation by developing specialized instrumentation at a significant cost. However, it was decided that the objectives of this investigation could be satisfied by analysis of readily available unequally spaced step response data.

1.2 OBJECTIVE

The CTD Data Aliasing Investigation was undertaken in order to determine if aliasing from the NBIS Mark IIIb CTD may, in fact, represent a problem to present or future operational data requirements. Existing laboratory testing techniques and data acquisition equipment employed made the investigation possible at minimal cost.

The specific objectives of the investigation may be summarized as follows:

1) Adapt or develop means of determining the transfer function of a sensor from unequally spaced time series data,
2) Using data acquired by NAVOCEANO in laboratory tests, determine the transfer function of the NBIS Mark IIIb temperature and conductivity sensors,
3) Based upon these experimentally determined transfer functions, determine the nature and extent of aliasing in CTD data acquired at 15.6 Hz,
4) Quantify the effect of aliasing on the accuracy of measured data, and
5) Attempt to extend the accuracy conclusions to a typical data product, such as salinity.

2.0 APPROACH

The initial activity of the investigation was a survey of available literature to identify techniques for analysis of unequally spaced time series data, with emphasis placed on techniques for estimation of the spectrum. As a result of the literature survey, a spectral estimation technique was identified, and this technique was adapted for use in the study.

Individual conductivity and temperature time series data sampled at a nominal rate of 93 Hz were obtained from laboratory response tests performed at the NAVOCEANO environmental test facilities. These step response time series were processed into individual spectra which were then averaged to obtain mean conductivity and temperature spectra. The amplitude portion of the sensor transfer function was then obtained from the respective mean spectrum.

By assuming a spectral form for the data input sampled by the sensor, it was possible to predict the frequency domain response of the sensor to that spectral form over the bandwidth 0 to 46.5 Hz. From this response, the spectral effect of aliasing within the more limited operational data bandwidth, 0 to 15.6 Hz, could be quantified. The aliasing effect on both sensors was examined for two spectral form models. The effect of error due to aliasing was also extended to the estimation of variance in the conductivity and temperature data.

The error in computed salinity was approximated by a linear first-order form involving the errors in temperature and conductivity. Based on results obtained for the individual sensed parameters, a numerical approximation for the error in salinity was used to quantify the effect of aliasing upon the accuracy of the salinity data product when spatial resolution is extended beyond the present 1-m level.

A detailed explanation of the approach taken for each stage of the investigation is provided in the remaining portions of this section.

2.1 SPECTRAL ANALYSIS OF UNEQUALLY-SPACED TIME SERIES

A literature survey, undertaken to identify the present state of knowledge concerning techniques of spectral estimation from unequally spaced time series, produced several valuable references. Three different spectral estimation approaches were identified:

1) Prediction and/or interpolation to synthesize missing data samples, making an unequally spaced sequence into a uniformly sampled one which may then be processed by conventional methods,

2) Analysis of unequally spaced sequences when sampling instants are known, and

3) Spectral analysis when sampling instants are unknown, but statistics of sampling times are known.

A brief description of the significant references for each approach is provided below.

Results of Literature Survey

Bowling and Lai[1] have applied a linear prediction algorithm to fill gaps of missing data in an unequally spaced sequence. The technique produces spectral estimates which are consistent with the data observed. The authors provide listings of programs which perform extrapolation and interpolation, as required.

Ackerman[2] has investigated non-uniform sampling as a means for reducing odd harmonic terms in the correlation function of clipped signals. These arise due to synchronism between the periodicity of uniform samples and the periodicity of odd signal harmonics produced by clipping. Sampling times must be known in order to compute the correlation function from non-uniform samples.

Jones[3] reported a spectral estimation technique using unequally spaced observations taken at known times. It is assumed that the time intervals are not multiples of some real number, since this case may be treated as missing data points in a uniformly sampled time series. If x_ν represents the complex value sampled at time t_ν while x_ν^* is the complex conjugate value, the spectral estimate is

$$\hat{s}(f) = \sum_{\nu=1}^{n} \sum_{\mu=1}^{n} w_{\nu\mu} x_\nu x_\mu^* e^{2\pi i(t_\nu - t_\mu)f}$$

where $w_{\nu\mu}$ are real weights satisfying

$$w_{\nu\mu} = w_{\mu\nu}$$

Weight functions are developed for three special cases:
Poisson sampling, random sampling, and ordered time differences.

A Fourier-series approach has been adapted by Singleton and Larson[4] to obtain a spectral estimate from an unequally spaced time series with known sampling times. The case of random timing is considered.

Masry[5] has developed a method for estimating the spectral density function when the times of individual samples are not known. Consideration is restricted to a stationary Poisson point process wherein samples are acquired at times

$$t_\emptyset = \emptyset, \ldots, t_n = t_{n-1} + T_n, \ldots, n = 1,2,\ldots$$

with the T_n independently distributed random variables possessing an exponential distribution

$$F(x) = 1 - e^{-\beta x}$$

where β is known. The spectral estimate is obtained by weighted series expansion of the discrete covariance function associated with the sampled data sequence. The expansion is constructed from a basis set of modified cosine functions. A class of exponential-type weight functions is shown to be acceptable from the point of view of series convergence.

A procedure for estimating sinusoids in a background of noise with known spectral content but unknown total power has been reported by McClellan[6]. This maximum entropy method is extended also to multi-dimensional signals.

Shaw[7] considers the effect of processing data acquired in a non-uniform fashion as though they were sampled uniformly. He shows that such treatment introduces a non-negative error component into the power spectrum. The spectral error is expressed as a function of the true power spectral density (PSD) of the process and the variance of the timing errors. The result is a powerful one since it enables a bound to be placed upon the error of spectra obtained by processing non-uniformly sampled data via standard FFT-based time-series analysis methods.

Since Shaw's approach minimized the amount of additional software required for analysis, this method was adopted for computation of error bounds on all power spectra utilized in the CTD Data Aliasing Investigation. The method is summarized below for the sake of completeness.

Conventional Spectral Analysis Using Non-Uniform Samples

For the purposes of conventional time-series analysis, a stationary, random process, $x(t)$, is sampled at points spaced uniformly along the time line to produce a discrete sequence of samples, $x(i \Delta t) \quad x_i$.* If, due to error in the sampling procedure, samples actually are acquired at other times, producing a sequence $x(i \Delta t + e_i)$ which is treated subsequently as uniformly sampled, the error is introduced into the spectral estimate for the process. The derivation of an expression for the spectral error is presented in some detail by Shaw[7]. A summary of the major steps follows.

---

*Jenkins and Watts[8] provide the following description: "Qualitatively, a stationary series is one which is in statistical equilibrium, in the sense that it contains no trends, whereas a non-stationary series is such that its properties change with time."

It is assumed that the individual position or timing errors, e_i, also referred to as "jitter", are small compared to Δt. Under this condition we may obtain an expression for the non-uniformly sampled sequence as a perturbation of the process x(t):

$$h(t) = x(t) + e(t) \cdot \frac{\partial x}{\partial t} \tag{1}$$

Equation (1) assumes that x(t) is differentiable, a condition which should readily be satisfied for a real-world physical process such as temperature or conductivity.

The autocorrelation functions of the process h(t) is

$$R_{hh}(\tau) = R_{xx}(\tau) - R_{ee}(\tau) \cdot \frac{\partial^2}{\partial \tau^2} R_{xx}(\tau), \tag{2}$$

where R_{xx} and R_{ee} are autocorrelation functions of the processes, x(t) and e(t), respectively. The power spectrum of h(t) is obtained by Fourier transformation of Eq. (2),

$$S_h(f) = S_x(f) + S_e(f) * \{(2 \pi f)^2 S_x(f)\}, \tag{3}$$

where S_x and S_e are the PSDs for x(t) and e(t), respectively, and * means convolution.

The second term in the RHS of Eq. (3), a frequency domain convolution, represents the error component in the computed PSD when non-uniformly sampled data are treated as uniform samples. An expression for the error term is derived for the case of stationary jitter.

Recall that the process x(t) is sampled at times

$$t_i = i \Delta t + e_i, \tag{4}$$

where e_i represents the jitter in the i^{th} sample. The e_i may be thought of as discrete samples of e(t), a stationary, zero-mean process. Further, assume that the variance of e(t) is well approximated by

$$\sigma_e^2 = \sum_{i=1}^{N} e_i^2 \tag{5}$$

Then, the autocorrelation function of the continuous error function, e(t), is

$$R_{ee}(\tau) = \frac{N\sigma_e^2}{12} \left\{ 1 - \frac{6|\tau|}{T} \left(1 - \frac{|\tau|}{T}\right) \right\}, \tag{6}$$

for $|\tau| \leq T$,

where

N = number of samples in the sequence and

T = N Δ T = length of sample sequence.

The PSD for the error function is then

$$S_e(f) = N\sigma_e^2 \sum_{\substack{n=-\infty \\ n\neq 0}}^{\infty} \frac{1}{n^2} \delta(f - n\Delta f) \tag{7}$$

The error term in Eq. (3) becomes $\Delta S(f) = S_e(f) * \{(2\pi f)^2 S_x(f)\}$

$$= N\sigma_e^2 \sum_{n\neq 0} \frac{1}{n^2} (f - n\Delta f)^2 \, S_x(f - n\Delta f) \tag{8}$$

However, since a power spectral density function computed by means of an FFT is discrete with frequencies k Δ f, Eq. (3) will only be evaluated for f = k Δ f. Hence, Eq. (8) will, likewise, only be evaluated

for the same discrete frequencies. Substitution for f in eq. (8) together with the change of variables j = k-n yields an error term

$$\Delta S(k\Delta f) = \frac{\sigma_e^2}{N\Delta t^2} \sum_{j \neq k} \left(\frac{j}{j-k}\right)^2 S_x(j\Delta f) \qquad (9)$$

where

$$f = \frac{1}{T} = \frac{1}{N\Delta t} \quad .$$

Note that the error term is a weighted summation over all frequencies of the true power spectral density of the process x(t).

Equation (9) demonstrates that the exact PSD obtained by processing non-uniformly sampled data as uniform may be predicted if the true PSD of the process and the variance of the jitter are known. This investigation, however, posed an inverse problem: Given a spectrum obtained by conventional processing of unequally spaced data, $S_h(k\Delta f)$, what is the true spectrum of the process? The true PSD may not be calculated directly but may be bounded in the following fashion.

From Eq. (3), we know that

$$S_h(k\Delta f) \geq S_x(k\Delta f) \qquad (10)$$

Assume that,

$$S_h(k\Delta f) = S_x(k\Delta f) \qquad (11)$$

Then, substituting into Eq. (9), we have

$$\Delta S'(k\Delta f) = \frac{\sigma_e^2}{N\Delta t^2} \sum_{j \neq k} \left(\frac{j}{j-k}\right)^2 S_h(j\Delta f) \qquad (12)$$

Now from (10)

$$\Delta S'(k\Delta f) \geq \Delta S(k\Delta f) \tag{13}$$

Then

$$S_h(k\Delta f) \leq S_x(k\Delta f) + \Delta S'(k\Delta f) \tag{14}$$

or

$$S_x(k\Delta f) \geq S_h(k\Delta f) - \Delta S'(k\Delta f) \tag{15}$$

We define

$$S_x'(k\Delta f) = S_h(k\Delta f) - \Delta S'(k\Delta f) \tag{16}$$

Then, from Eq. (15), Eq. (16) and Eq. (10), we have

$$S_h(k\Delta f) \geq S_x(k\Delta f) \geq S_x'(k\Delta f) \tag{17}$$

Equation (17) allows upper and lower bounds to be established for the spectrum of the true process, x(t). Required for calculation of upper and lower bounds are: (1) a spectral estimate obtained by processing the time series in conventional fashion as though it were equally spaced, and (2) the variance of the timing errors.

2.2 DATA ACQUISITION

The laboratory procedure which produced the data sets analyzed for this report was developed by NAVOCEANO for routine measurement of CTD sensor response functions. A summary description of the test procedure is provided here for the sake of completeness; (Mayoral, 1982) provides a more detailed description.

Essential to the procedure is a stable and well-defined artificial thermocline which is created in a precision environmental test facility operated by NAVOCEANO. The thermocline consists of two homogeneous, horizontal water layers of different temperatures, separated by a gradient layer less than 1 cm in thickness. The stability of the thermocline and the dimension of the gradient layer have been investigated by Paige.[10] The upper layer typically is maintained at a temperature approximately 0.5°C higher than the lower layer. The two layers are of approximately equal salinity so that the conductivity difference between the two layers is approximately 0.7 mS/cm.

The arrangement of the laboratory apparatus is such that the sensors drop through the thermocline at a rate of approximately 0.75 m/s, near the operational deployment rate of 1.0 m/s. In the process, a pseudo-step change in temperature and conductivity is sensed by the CTD sensors. Digitized time series of each transducer output are produced by the instrument and these are recorded under computer control for subsequent analysis to obtain the transducer response function.

Standard Data Sampling

In normal operation, the Mark IIIb CTD produces one scan of each of the three measured parameters -- pressure, temperature, and conductivity -- on a nominal 32-ms timing cycle. The equivalent sampling frequency is 31.25 Hz. Each analog sensor signal is digitized to 16 bit accuracy using a successive approximation scheme. Sampling resolution for each of the parameters is, respectively: pressure, 0.1 dbar, temperature, 0.0005°C, and conductivity, 0.001 mS/cm.

The analog to digital (A/D) conversion scheme is implemented in an adaptive fashion so that conversion requires the minimum time consistent with error free operation. The digitizing time for each bit may be as short as 0.3 ms or as long as 1.6 ms. Start of digitization of the pressure signal is synchronized to the 32-ms timing signal. However, subsequent sensors in the scan, temperature and conductivity, are digitized at varying times after the start of the scan, depending upon the time required to digitize the preceding parameters.

Figure 1 is a time series plot of temperature obtained from a response test of an instrument operating in the normal mode, i.e., sequential sampling of pressure, temperature, and conductivity. Figure 2 is a time series plot of conductivity obtained during the same test. The difference in response times of the two sensors is apparent in a comparison of the two curves. A time series of salinity was constructed by applying the standard salinity algorithm[11] to corresponding pairs of temperature and conductivity data from this response test. The salinity time series is shown in figure 3. The transient decrease in salinity, as the sensors cross the thermocline, is typical of the "salinity spike" which appears as an artifact in uncorrected salinity time series data obtained with the Mark IIIb CTD.

High-Speed Sampling

In order to address the subject of aliasing in data sampled at 31.25 Hz, it is necessary to evaluate data which are digitized at a much higher rate. To this end, NAVOCEANO has modified a Mark IIIb CTD to acquire data from a single sensor at three times the normal sampling rate. This modification replaces the sensor inputs to each of the other two analog channels by the single sensor to be sampled. For example, if the conductivity parameterwere to be sampled at a high rate, analog-input select lines for digitizing pressure and temperature measurements each would be changed to select conductivity. Conductivity then is sampled successively three times in a single instrument scan. Since only the start of each scan is synchronized by the CTD sampling clock, the second and third samples are converted at times which vary slightly from scan to scan, but all are contained within a 32-ms scan interval.

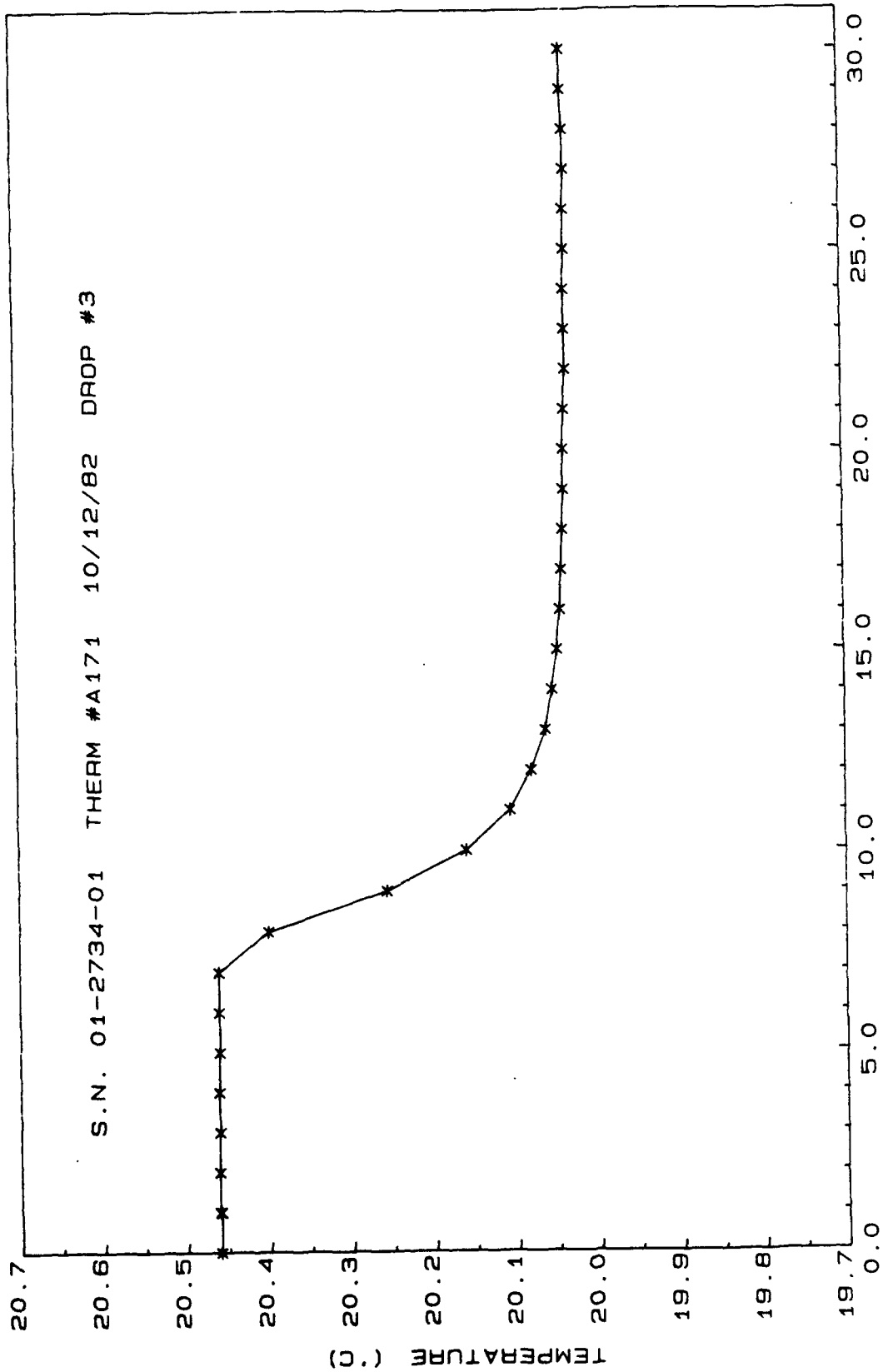

Figure 1. Time series of temperature acquired at the standard data rate.

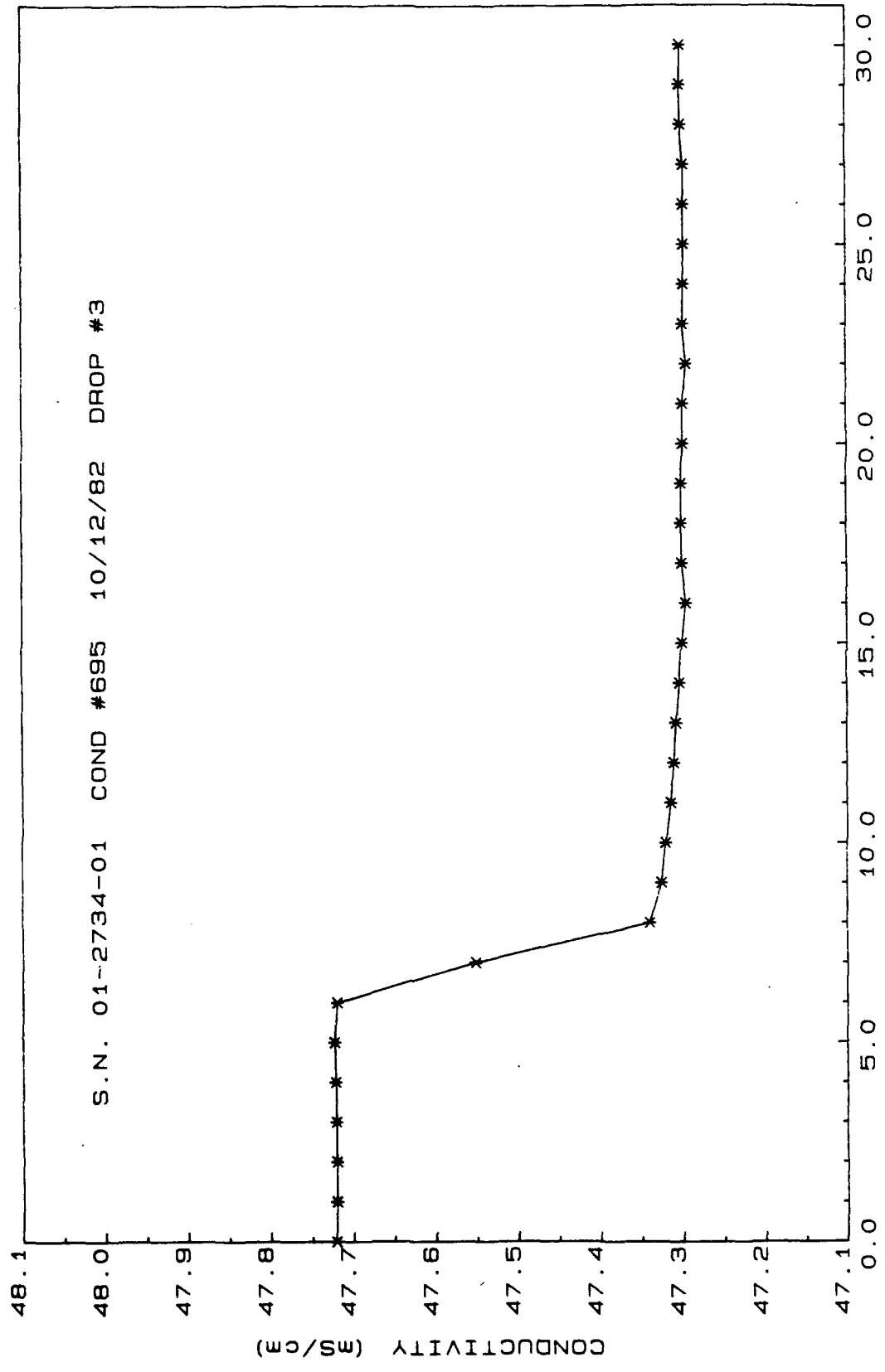

Figure 2. Time series of conductivity acquired at the standard data rate.

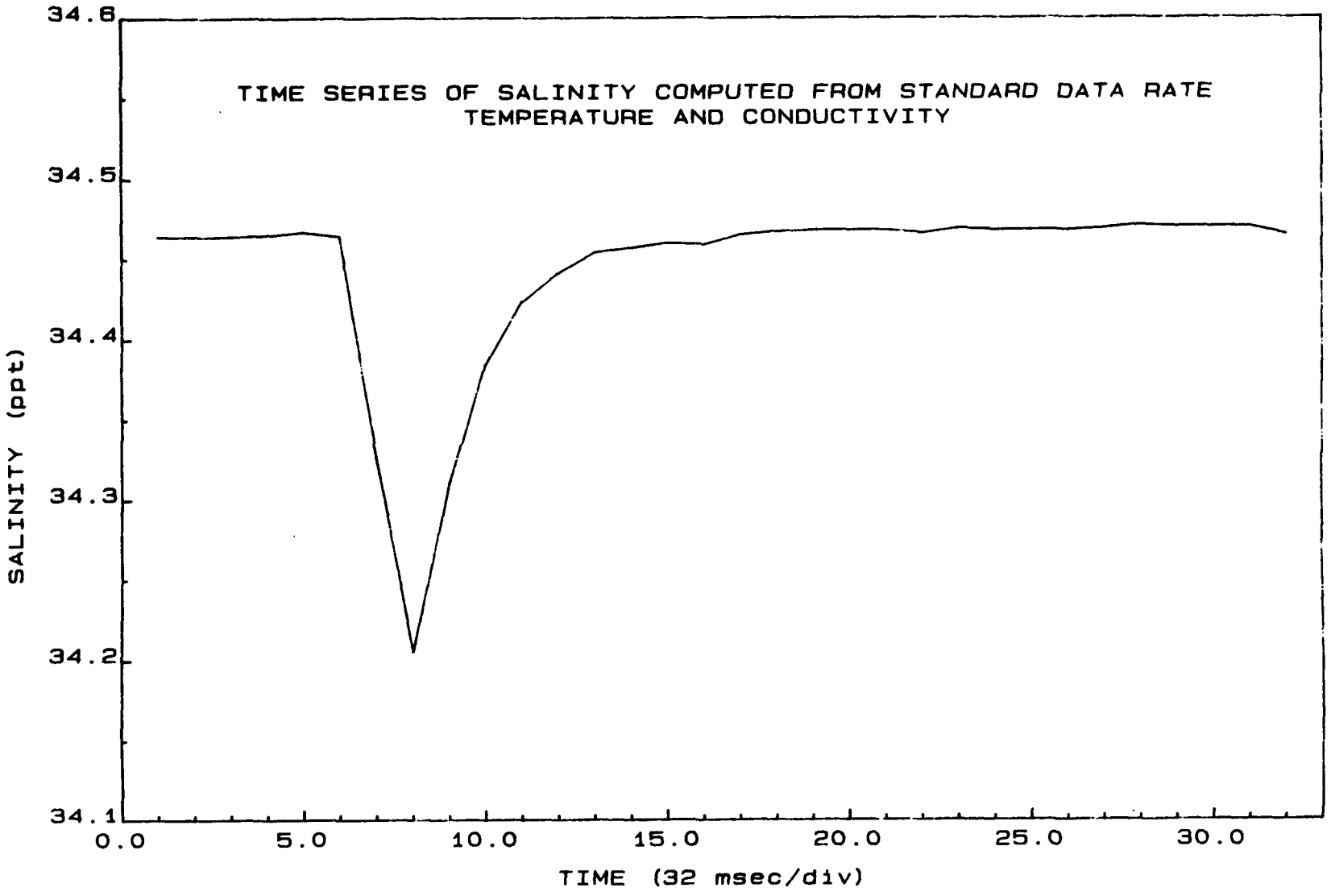

Figure 3. Time series of salinity computed from conductivity and temperature acquired at the standard data rate.

The average sampling frequency, however, is three times the normal rate. For the particular CTD used in these tests, the scan period of the data-sampling clock was measured at 31.9986 ms. The equivalent sampling frequency is 31.25 Hz for standard sampling, while the average frequency for high-speed sampling is 93.75 Hz.

Data Description

Two sets of high-speed data were acquired for use in this investigation. The initial set consisted of five response tests digitizing conductivity only and five tests digitizing temperature only. Preliminary analysis of the first data set revealed essentially no variability between the five temperature response tests. Such was not the case for the conductivity data and so a second set of data was acquired. Twelve additional response tests were made digitizing conductivity only. Both the initial and second data sets were acquired using the same CTD and sensors.

Figure 4 is a time series of temperature acquired at 93.75 Hz, while figure 5 is a time series of conductivity. For the purpose of plotting, it was assumed that the data samples were acquired within a scan at intervals of 10, 10, and 12 ms, respectively, rather than at equal intervals. Some irregularity is evident in the step region of the curves, particularly for temperature (fig. 4), demonstrating the irregular sample timing characteristic of the high data rate. Plots of all high-data-rate response-test time series used in this study are presented in Appendix A.

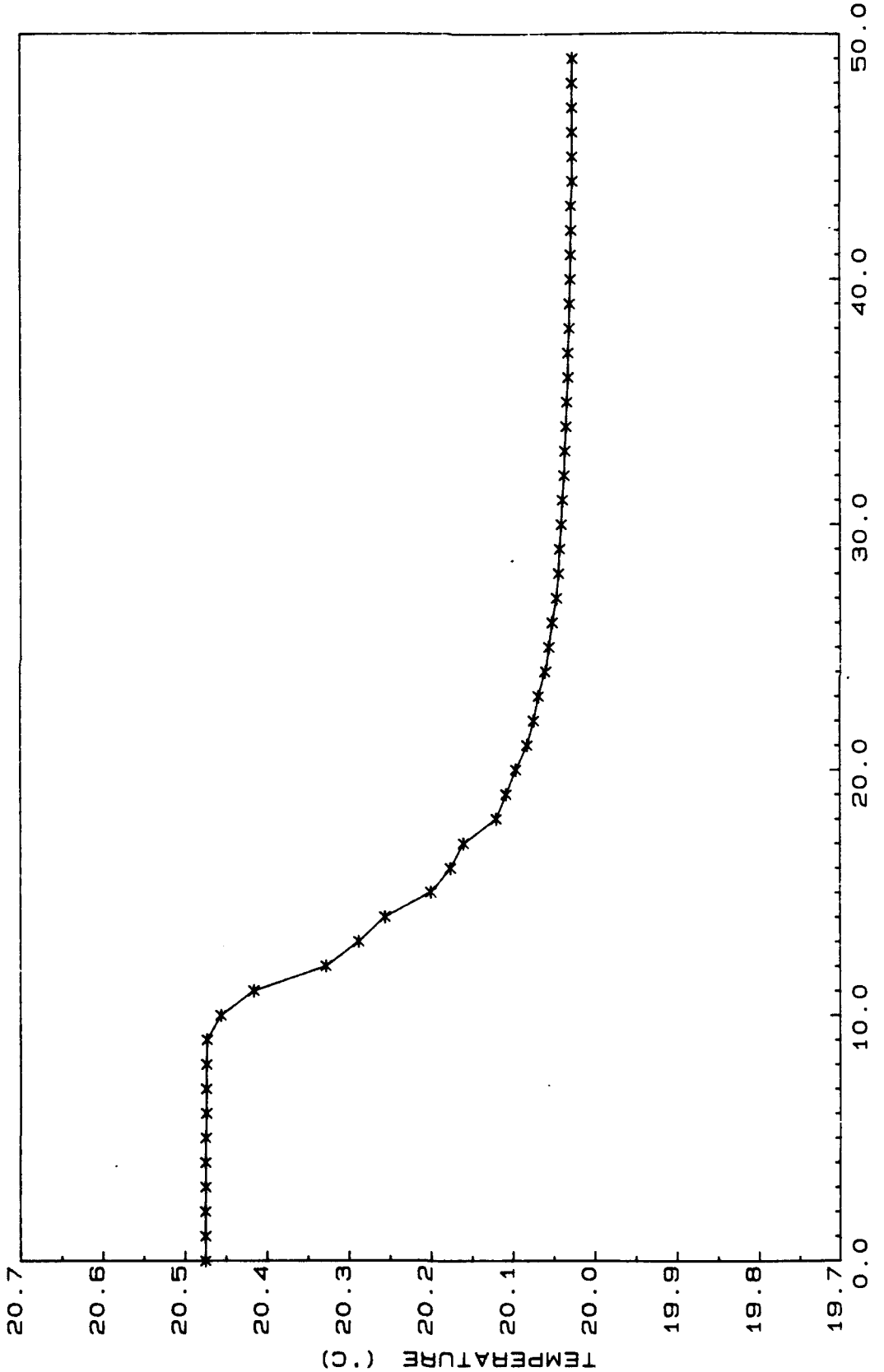

Figure 4. Time series of temperature acquired at the high data rate.

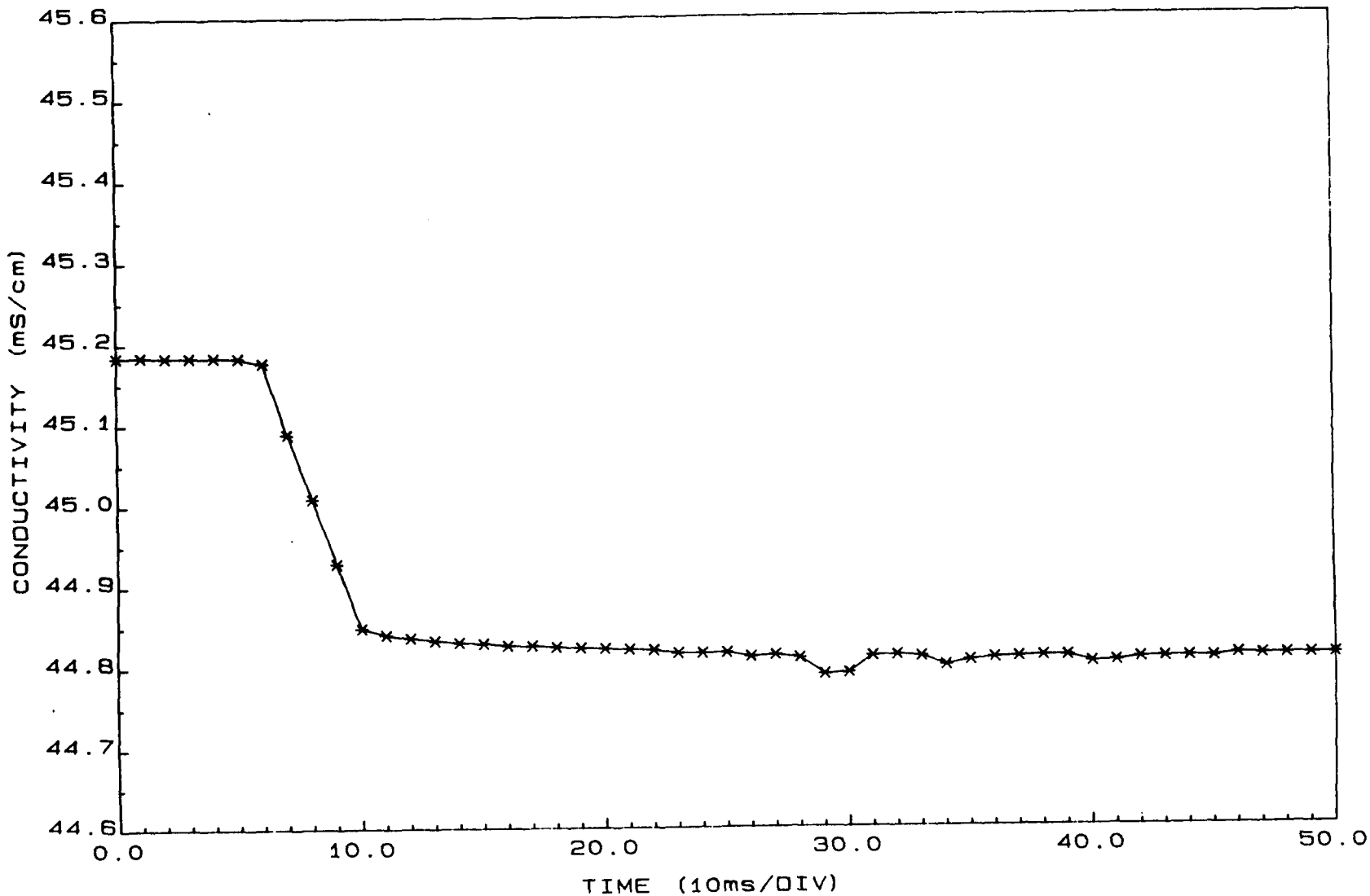

Figure 5. Time series of conductivity acquired at the high data rate.

2.3 ANALYSIS OF TIMING ERRORS

As indicated in Section 2.1, bounds may be established for the spectrum of the CTD step response computed from high-speed data if the variance of the timing errors is known. The time of acquisition of both the second and third samples in a high-speed data scan is dependent in each case upon the time required to convert the previous sample.[12] Therefore, the timing errors and their statistics are data-dependent quantities most accurately measured under conditions which produce the actual response-test time-series themselves. A technique devised for measuring the timing-error variance, based on this concept, is described below.

Evaluation of the first set of response-test data showed that sensor response to the pseudo-step function input of the tests approximated the classical exponential decay curve, as can be seen in figure 4 and figure 5. An exponential response to a unit amplitude step is shown for comparison in figure 6, where the mathematical form of the curve is

$$x(t) = \begin{cases} 1, & t < t_0 \\ e^{-\alpha(t-t_0)}, & t \geq t_0 \end{cases} \qquad (18)$$

where α is the time constant for the exponential decay, and t_0 is the time corresponding to the start of the step input.

Since a plot of the logarithm of x(t) vs. t is a straight line, comparison of measured data values to an exponential decay is simplified by plotting the measured parameter vs. time in logarithmic form. Figure 7 is a plot of a hypothetical time series such as might be encountered in either the conductivity or temperature-response-test data when plotted as though acquired at regular intervals. If the data values are truly those of

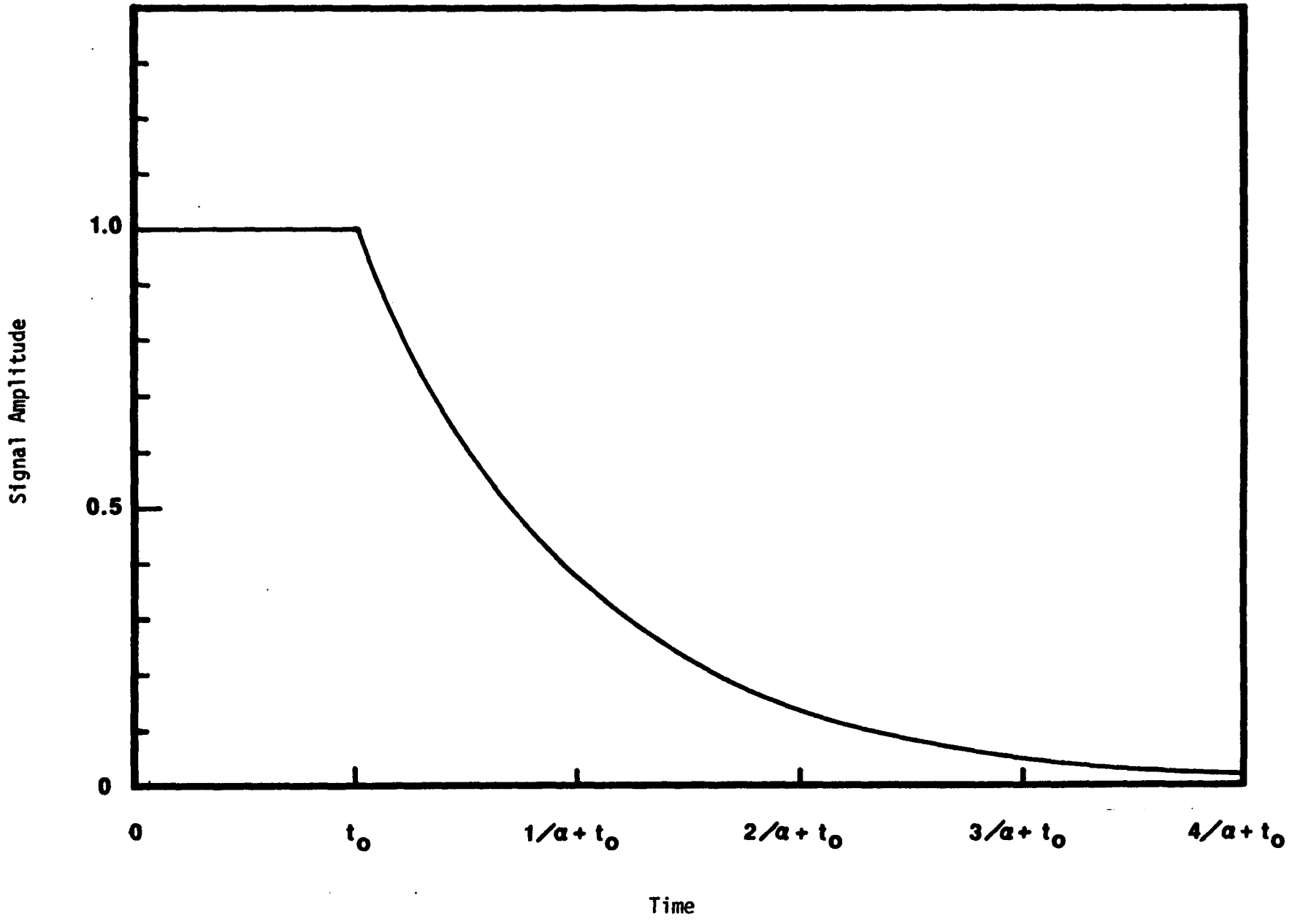

Figure 6. An Exponential Response to a Unit Step Input

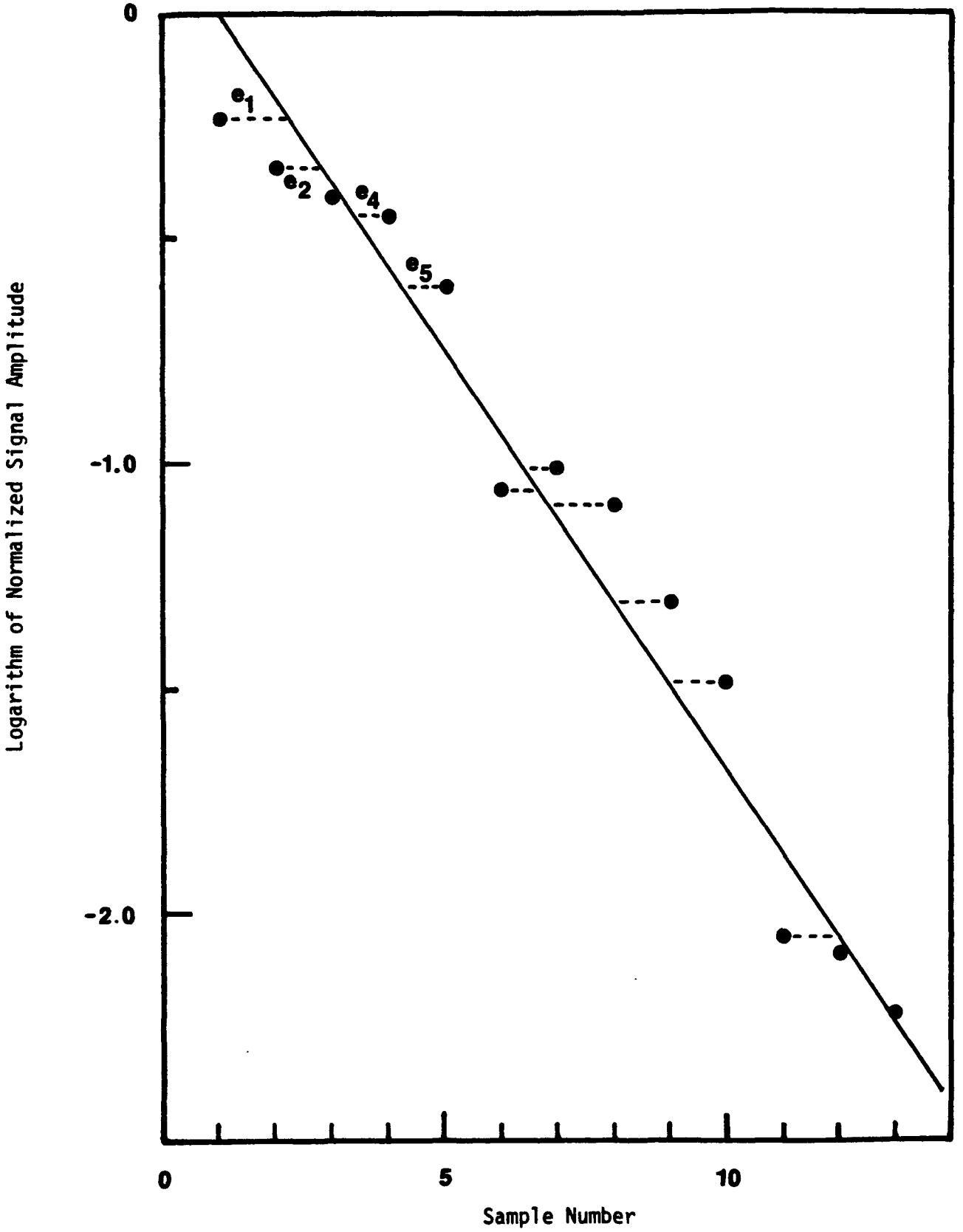

Figure 7. Logarithmic Plot of a Hypothetical Time Series. Solid line is the least squares fit to the points shown. Timing error of an individual point, e_i, is the horizontal distance from the point to the line (length of broken line).

an exponential response process, then it may be assumed that any deviation of a measured value from the straight line is due to an error in timing and not in the measurement of x(t) itself. As will be seen, the actual sensor responses are not simple exponentials. However, the exponential model provides worst case values for the timing errors, since it also includes the residuals to the exponential fit.

The timing error for the i^{th} point, e_i, is given by the difference between the assumed time for equal spaced sampling,

$$t_i = i \Delta t, \tag{19}$$

and the sampling time which corresponds to the ordinate of the i^{th} data value

$$t_i' = t_0 - \frac{1}{\alpha} \ln x_i \tag{20}$$

or

$$e_i = t_i - t_i' \quad . \tag{21}$$

The variance of the timing error is then given by

$$\sigma_e^2 = \frac{1}{N} \sum_{i=1}^{N} (e_i - \bar{e})^2 \tag{22}$$

where $\bar{e}$ is the mean of the timing errors. However, determination of the e_i is possible only if the constants α and t_0 are known for the particular response test.

The response constants were determined for each individual test sequence in a three-step process. First, data were normalized to a unit amplitude step based upon the difference between stabilized "before" and "after" values ascertained from the two equilibrium portions of the response curve. The normalized data were then plotted in logarithmic form, assuming an equal sampling interval. This enabled selection of a subset of the data

sequence which most closely approximated an exponential response. Finally, the subset of the data sequence was fit to an exponential by actually fitting the logarithm of the parameter to a linear form

$$t = t_0 + \beta y, \tag{23}$$

where

$$\beta = -1/\alpha$$

and

$$y = \ln x$$

using traditional least-squares methods and assuming all error to be associated with the parameter t.

Temperature response was found to be closely approximated by the exponential decay, so that the data subset chosen for analysis typically included fourteen to eighteen points beginning immediately after the step (at time = t_0 in figure 6). Conductivity was seen to be more complex in its response to the step change, exhibiting two distinctly different behaviors within the same data set. A rapid exponential decay characterized the early stages of the response curve, so that the first seven to nine points following the break were well represented by the exponential. This was followed by a clear change in the logarithmic curve to a less steeply sloped line which was somewhat less linear and less consistent in slope from test to test. The physical significance of this change is not immediately obvious. It is apparently a consequence of a complex fluid flow pattern caused by the shape of the conductivity cell.[13] From the point of view of potential aliasing, the more rapid response is of greater concern, since rapid response in the time domain suggests greater response to high frequency inputs and therefore greater susceptibility to aliasing. Furthermore, any subset will be valid if the process causing the jitter is truly stationary. This being the case, attention was focused upon the steeper portion of the curve, and the constants α and t_0 for the conductivity response were determined by fitting to this subset. This region typically comprised the first seven to nine data points following the initial break at time t_0.

2.4 TRANSFER FUNCTION DETERMINATION

A continuous, real function, $x(t)$, such as the physical input to a sensor or its analog voltage output, possesses a complex Fourier transform, $X(f)$, given by

$$X(f) = \int_{-\infty}^{\infty} x(t)e^{-i2\pi ft}dt \quad . \tag{24}$$

The function $x(t)$ may be recovered from $X(f)$ by the inverse transform

$$x(t) = \int_{-\infty}^{\infty} X(f)e^{i2\pi ft}df \quad . \tag{25}$$

The frequency-domain transfer function of a sensor or other measurement process relates the input and output of such a device. If $x_1(t)$ and $x_2(t)$ are, respectively, the input and output to the measurement process, the Fourier transforms are related by

$$X_2(f) = T(f)X_1(f), \tag{26}$$

where $T(f)$ is the transfer function for the process, in general a complex quantity. The value of knowing the transfer function for a sensor, and particularly the importance to this project of knowing the CTD sensor transfer functions, has been discussed previously in Section 1.1. A means for obtaining these transfer functions is described below.

Determination of the Transfer Function From a Step-Function Input

From Eq. (26) we have

$$T(f) = \frac{X_2(f)}{X_1(f)} \tag{27}$$

If the input function applied to a sensor is a unit step function

$$x_1(t) = \begin{cases} 1 , & t < 0 \\ \frac{1}{2} , & t = 0 \\ 0 , & t > 0 , \end{cases} \tag{28}$$

or, following the notation of Bracewell[14],

$$x_1(t) = 1 - H(t) \tag{29}$$

where H(t) is the Heaviside step function, a measured response

$$x_2(t) = \int_{-\infty}^{\infty} X_2(f) e^{i2\pi ft} df$$

$$= \int_{-\infty}^{\infty} T(f) X_1(f) e^{i2\pi ft} df \tag{30}$$

will be produced.

If, on the other hand, the measured response, $x_2(t)$, to an input of the form of Eq. (29) is transformed to obtain $X_2(f)$, then the transfer function may be readily determined from Eq. (27) where

$$X_1(f) = \int_{-\infty}^{\infty} (1 - H(t)) e^{-i2\pi ft} dt \quad . \tag{31}$$

Expanding, we have,

$$X_1(f) = \int_{-\infty}^{\infty} e^{-i2\pi ft} dt - \int_{-\infty}^{\infty} H(t) e^{-i2\pi ft} dt \quad . \tag{32}$$

The integrals may be evaluated separately. After Bracewell[14]

$$\int_{-\infty}^{\infty} e^{-i2\pi ft} dt = \delta(f) \tag{33}$$

and

$$\int_{-\infty}^{\infty} H(t)e^{-i2\pi ft} dt = \tfrac{1}{2}\delta(f) - i\left(\frac{1}{2\pi f}\right) . \tag{34}$$

Combining, we obtain

$$X_1(f) = \delta(f) - \left(\tfrac{1}{2}\delta(f) - i\left(\frac{1}{2\pi f}\right)\right)$$

$$= \tfrac{1}{2}\left(\delta(f) + i\left(\frac{1}{\pi f}\right)\right) . \tag{35}$$

By substituting Eq. (35) into Eq. (27), we obtain

$$T(f) = X_2(f) \left\{ \frac{1}{\tfrac{1}{2}\left(\delta(f) + i\left(\frac{1}{\pi f}\right)\right)} \right\}$$

$$= -2\pi i f X_2(f) . \tag{36}$$

In summary, if the response of a sensor to a unit step-function input is measured and its Fourier transform, $X_2(f)$, computed, then the sensor transfer function, $T(f)$, may be readily computed using Eq. (36).

Computation of the Step-Response Spectrum

The power spectrum of a continuous function is related to its Fourier transform by

$$s_x(f) = X^*(f)\ \ X(f), \tag{37}$$

where X^* is the complex conjugate of $X(f)$, the Fourier transform of $x(t)$, as defined by Eq. (24). In this definition, $x(t)$ is defined for all t and, likewise, $X(f)$ is defined for all f in $(-\infty, \infty)$. $s_x(f)$ is often referred to as the two-sided spectrum, since it is defined for both positive and negative f and since

$$s_x(-f) = s_x(f). \tag{38}$$

We are only concerned with the spectrum for non-negative f, and therefore make use of the single-sided spectrum

$$S_x(f) = 2s_x(f), \tag{39}$$

defined on $(0, \infty)$.

A corresponding spectral-density function may be computed for a discrete time series of finite length, consisting of N samples acquired at times Δt apart. The equivalent of the single-sided spectrum for such a time series is termed the periodogram and is given by

$$P_x(k\Delta f) = \frac{2}{N\Delta t}\ \ X^*(k\Delta f)\ X(k\Delta f), \tag{40}$$

where $X(k\Delta f)$ is the discrete Fourier transform of $x(j\Delta t)$ given by

$$X(k\Delta f) = \Delta t \sum_{\text{all } j} x(j\Delta t) e^{-2\pi i \left(\frac{jk}{N}\right)} , \qquad (41)$$

$$j = 0, \ldots, N-1, \quad k = 0, \ldots, N/2,$$

and

$$\Delta f = \frac{1}{N\Delta t} .$$

However, the periodogram is not the best estimate, in the statistical sense, of the spectrum.[8] Welch[15] has described a procedure for obtaining a statistically stable spectrum by dividing a time series into L equal length segments, computing the periodogram of each segment, and averaging the periodograms to yield

$$\hat{S}_x(k\Delta f) = \frac{1}{L} \sum_{\ell=1}^{L} P_{x_\ell}(k\Delta f) . \qquad (42)$$

The periodograms are treated as independent samples of the same process. The averaging indicated by Eq. (42) is referred to as an ensemble average since the L segments taken together form an ensemble of realizations of the process under consideration.

The frequency resolution of the spectral estimate, $\hat{S}_x(k\Delta f)$, given by Eq. (42) is

$$\Delta f = \frac{1}{N_s \Delta t} , \qquad (43)$$

where N_s is the number of samples in a segment. Since the discrete time series acquired from the CTD step response tests were short in length (on the order of 400 ms), division into segments would have

resulted in a coarse frequency resolution for $\hat{S}_x$. In order to achieve the maximum possible resolution, each response-test time-series was treated as an independent realization of the sensor's response to the same step change input. Periodograms for all conductivity response tests were computed and averaged to obtain a conductivity response spectrum via Eq. (42); a temperature response spectrum was obtained in the same way.

Computation of the Periodogram

Computation of the periodogram of the step response function was performed by treating the high-speed time series data as though they were equally spaced in the following manner. A subset of thirty-two consecutive samples was selected from the original forty-plus available samples, taking care to center this subset so that both upper and lower levels of the step were present. The data were then normalized to a unit step in the manner described in Section 2.3. Using the method described by Blackman and Tuckey[16], a linear trend was removed from the time series, the trend having been determined by fitting a linear form to the original data.

For high speed CTD data, the average difference between samples,

$$\overline{\Delta x} = \frac{x((N_s-1) \cdot \Delta t) - x(0)}{N_s-1} \qquad (44)$$

was used to estimate trend,

$$\tau(j) = (j - (\frac{N_s-1}{2})) \cdot \overline{\Delta x} \ . \qquad (45)$$

Each sample in the sequence was then corrected for this trend as well as any offset in the sequence to obtain a corrected time series

$$x_c(j\Delta t) = x(j\Delta t) - \tau(j) - \bar{x} \ , \qquad (46)$$

where the offset is

$$\bar{x} = \frac{1}{N_s} \sum_{j=0}^{N_s-1} x(j\Delta t) \quad . \tag{47}$$

A discrete transform of the corrected time series was computed using a 32 point fast Fourier transform (FFT) routine due to Brenner[17]. The routine computes

$$F(k\Delta f) = \sum_{j=0}^{N_s-1} x_c(j\Delta t) e^{-2\pi i(\frac{jk}{N_s})} \tag{48}$$

for $k = 0, \ldots, N_s-1$. Then from Eqs. (40) and (41) the periodogram is

$$P_x(k\Delta f) = \frac{2\Delta t}{N_s} F^*(k\Delta f)\, F(k\Delta f) \tag{49}$$

and a power spectrum is computed by averaging the periodograms of L different response tests using Eq. (42).

Transfer-Function Estimation from Unequally Spaced Data

Recall that in Section 2.1, Shaw's method was applied to obtain bounds on the power spectrum of a process when unequally spaced time-series data are processed via a discrete Fourier transform into a spectral estimate. To consider the effects of aliasing, it is not necessary to have phase information from the transfer function, $T(f)$, and, hence, it is sufficient to know only the amplitude, $|T(f)|$ or equivalently the power transfer function $|T(f)|^2$.

From Eq. (36), we have

$$T^*(f)T(f) = |T(f)|^2 = (2\pi f)^2 X_2^*(f)X_2(f) \tag{50}$$

In discrete notation, substituting for $X_2^*(f)X_2(f)$ from Eq. (40), we have

$$|T(k\Delta f)|^2 = \frac{(2\pi f)^2 \cdot N_s \Delta t \cdot P_x(k\Delta f)}{2} \tag{51}$$

Since the best estimate of $P_x(k\Delta f)$ is the ensemble average, the estimation of the power transfer function is

$$|\hat{T}(k\Delta f)|^2 = \tfrac{1}{2}(2\pi f)^2 N_s \Delta t \, \hat{S}_x(k\Delta f) \tag{52}$$

But, we may also show that

$$|\hat{T}(k\Delta f)|^2 = \frac{1}{L} \sum_{\ell=1}^{L} |T(k\Delta f)|_\ell^2 \tag{53}$$

where $|T(k\Delta f)|_\ell^2$ is computed from P_{x_ℓ} via Eq. (51).

Aside from the statistical problem of spectral estimation using discrete data, which has been dealt with through ensemble averaging, an additional problem exists in that it is not possible to estimate the output spectrum, $S_2(f)$, directly due to the unequal spacing of data. However, it is possible to place bounds on $S_2(f)$ using Eq. (17). Extending this bounding concept to the transfer function, we have

$$|T_h(k\Delta f)| \geq |T(k\Delta f)| \geq |T'(k\Delta f)|, \tag{54}$$

where $|T_h(k\Delta f)|$ is the transfer function computed from the transfer function estimate of the unequally spaced data,

$$|T_h(k\Delta f)| = \sqrt{\hat{T}(k\Delta f)^2} \tag{55}$$

and

$$|T'(k\Delta f)| = \left(|T(k\Delta f)|^2 - 2N_s\Delta t(\pi k\Delta f)^2\Delta\hat{S}_x(k\Delta f)\right)^{\frac{1}{2}} \tag{56}$$

with

$$\Delta\hat{S}_x(k\Delta f) = \frac{\sigma_e^2}{N_s\Delta t^2} \sum_{l\neq k} \left(\frac{1}{l-k}\right)^2 \hat{S}_x(l\Delta f) \tag{57}$$

To summarize, we determine the conductivity-sensor transfer function in the following way: The periodogram of each conductivity response test is computed, treating the high-speed sensor-output time series as though the data were equally spaced. Then, periodograms of all conductivity tests are averaged to obtain an estimate of the step-response spectrum which is used in Eq. (54) to place upper and lower limits on the true transfer function of the conductivity sensor. Limits for the temperature-sensor transfer function are obtained in a corresponding fashion.

2.5 EFFECT OF ALIASING UPON SPECTRAL DATA

In Section 2.4, the relationship between input and output of a sensor was described in the frequency domain. Extending this concept to the power spectrum, we have

$$S_2(f) = |T(f)|^2 S_1(f) \tag{58}$$

where $S_1(f)$ and $S_2(f)$ are, respectively, the power spectrum of the physical process being measured and the spectrum of the sensor output signal.

In compensating for the transfer effect of a sensor in the frequency domain when discrete calculations are employed, the measured spectral estimate is corrected

$$\hat{S}_1(k\Delta f) = \frac{1}{|T(k\Delta f)|^2} \hat{S}_2(k\Delta f) \tag{59}$$

to obtain an estimate of the spectrum of the physical process. While Eq. (59) is mathematically correct for all frequencies in $S_2(k\Delta f)$, in practice it may not be used for frequencies at which $|T(k\Delta f)|$ becomes small. This is because errors in the measured spectrum which occur as a result of the discrete spectral-estimation process and instrument noise, as well as uncertainty in the transfer function itself, are greatly magnified. Figure 8 shows a hypothetical sensor and the relationship between its input, the transfer function, the measured spectrum, and the corrected result.

Aliasing

When a continuous time signal is digitized into discrete samples taken at times Δt apart, a discrete transform (and a periodogram) of the time series may be computed using Eqs. (40) and (41). However, these frequency-domain functions are defined only for discrete frequencies up to the Nyquist frequency

$$f_N = \frac{1}{2} f_s = \frac{1}{2\Delta t} . \tag{60}$$

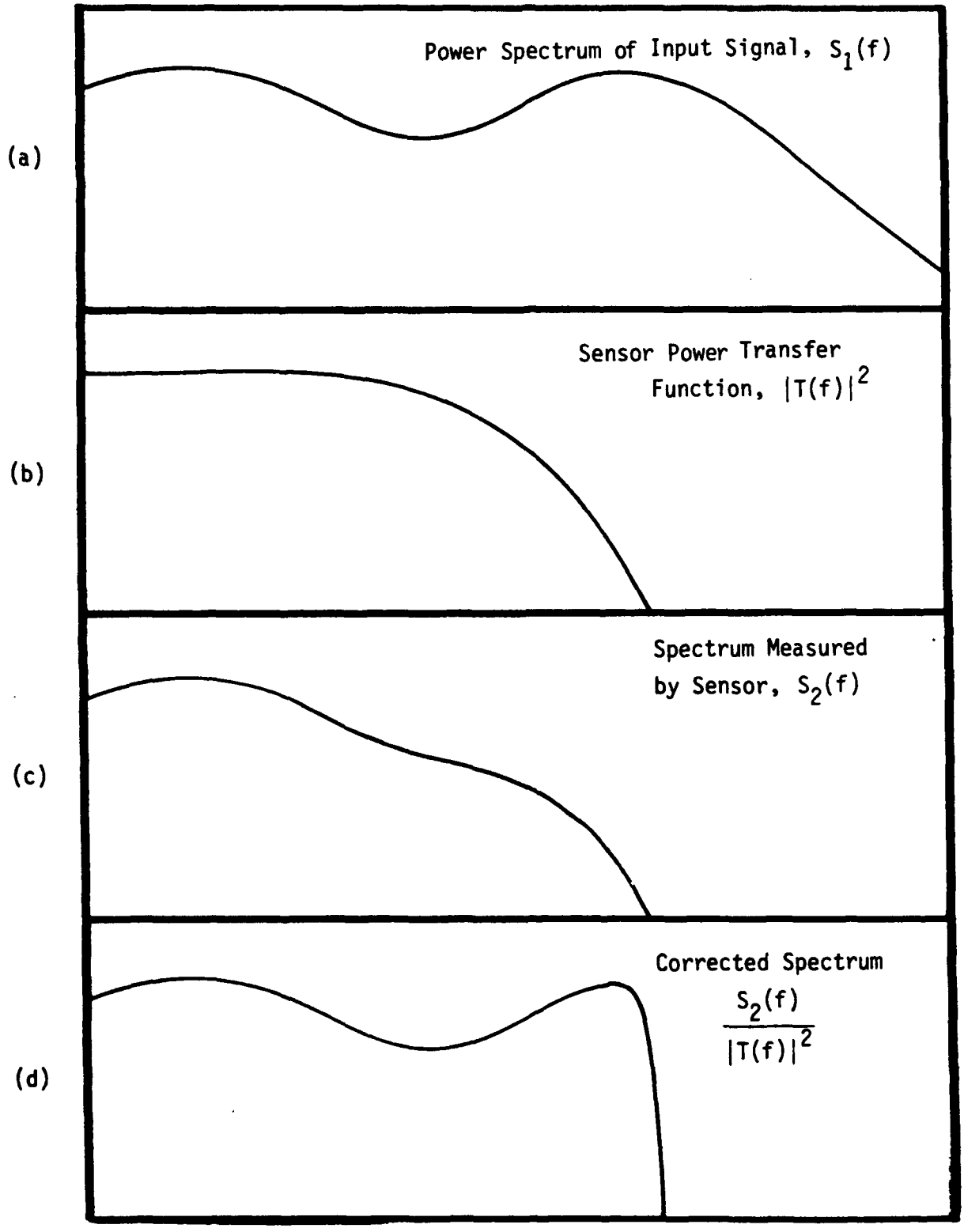

Figure 8. Comparison for a Hypothetical Measurement. (a) sensor input, (b) transfer function, (c) measured spectrum, and (d) corrected spectrum.

If information is present in the continuous time signal at any frequency greater than f_N, the power spectral density (PSD) associated with such information will appear in the discrete spectrum at a frequency

$$k\Delta f = 2f_N - f' \qquad (61)$$

if $f_N < f' \leq 2f_n$ and

$$k\Delta f = f'' - 2f_n \qquad (62)$$

for $2f_N < f'' \leq 3f_N$. Comparable relationships exist for frequencies higher than $3f_N$.

Figure (9b) shows the effect of aliasing in the hypothetical measured spectrum of fig. (8c) for a specific Nyquist frequency as shown. Note that since no information is present in the spectrum of fig. (8c) above $2f_N$, then only Eq. (61) will apply in predicting aliasing. The broken line shows the spectrum as it would have appeared without aliasing.

Figure (9a) repeats the measured spectrum from (8c), while fig. (9c) shows the effect of transfer correction on the aliased spectrum. Again, the broken line represents the corrected spectrum as it would have appeared in the absence of aliasing.

Aliasing in the Power Spectrum Quantified

As may be seen from the foregoing discussion, when a continuous physical signal is sensed and digitized, the potential for aliasing exists. However, aliasing will occur only if: 1) information is present in the signal at frequencies greater than the Nyquist frequency, and 2) the sensor response function is non-zero at these frequencies. In order to quantify the effect of aliasing, it is necessary to know both the transfer function and the true spectrum of the measured process.

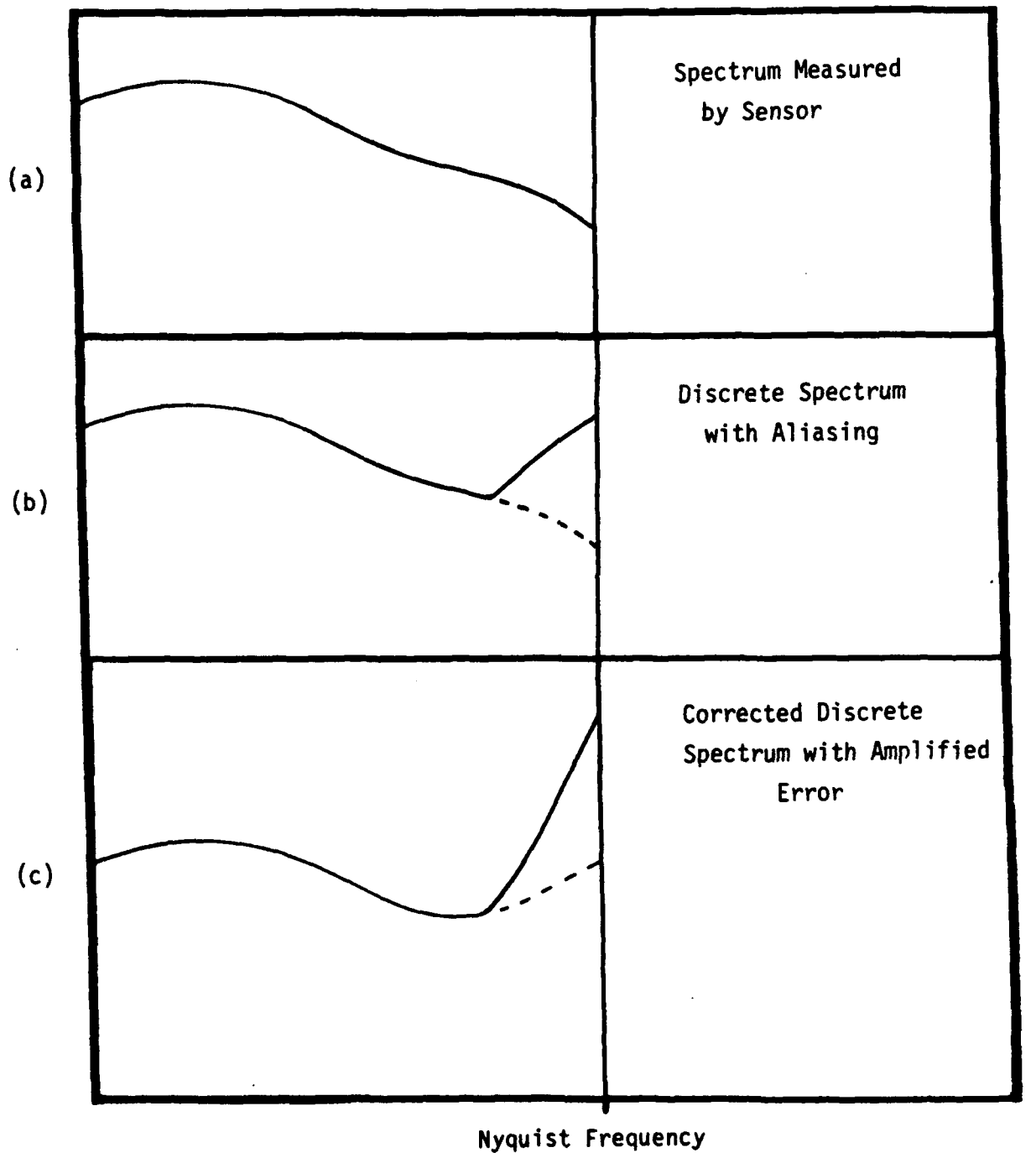

Figure 9. Effect of aliasing on the discrete spectrum. Broken line shows spectrum without aliasing from higher frequencies. Hypothetical spectrum from Figure 8c is used.

When aliasing occurs, the measured spectral estimate includes terms from higher frequencies in addition to the fundamental term which is desired. The aliased spectral estimate is

$$\hat{S}_2'(k\Delta f) = \hat{S}_2(k\Delta f) + \hat{S}_2(f') + \hat{S}_2(f'') + \ldots , \tag{63}$$

where f', f", ... represent frequencies from which aliasing has occurred. From Eq. (63), substituting for f' and f" from Eqs. (61) and (62), and substituting for $\hat{S}_2$ from Eq. (59), we have

$$\begin{aligned}\hat{S}_2'(k\Delta f) = {} & |\hat{T}(k\Delta f)|^2\hat{S}_1(k\Delta f) + |\hat{T}(2f_N-k\Delta f)|^2\hat{S}_1(2f_N-k\Delta f) + \\ & + |\hat{T}(k\Delta f - 2f_N)|^2\hat{S}_1(k\Delta f - 2f_N) + \ldots\end{aligned} \tag{64}$$

If this aliased spectral estimate is treated as an accurate one and is corrected for the sensor transfer effect at the frequency $k\Delta f$ to obtain an estimate of the input spectrum, as in Eq. (59), we have

$$\begin{aligned}\hat{S}_1'(k\Delta f) = {} & \hat{S}_1(k\Delta f) + \frac{|\hat{T}(2f_N-k\Delta f)|^2}{|\hat{T}(k\Delta f)|^2}\ \hat{S}_1(2f_N-k\Delta f) + \\ & + \frac{|\hat{T}(k\Delta f - 2f_N)|^2}{|\hat{T}(k\Delta f)|^2}\ \hat{S}_1(k\Delta f - 2f_N) + \ldots\end{aligned} \tag{65}$$

Because the spectral estimates are non-negative for all frequencies, the corrected spectral estimate will be biased larger due to the aliased spectral density by an amount

$$A(k\Delta f) = \hat{S}_1'(k\Delta f) - \hat{S}_1(k\Delta f) . \tag{66}$$

Whether this bias creates a significant error in the estimated PSD depends upon the relative magnitudes of $S_1(k\ f)$ and $A(k\ f)$. The relative error within a frequency band is then

$$E_S(k\Delta f) = \frac{A(k\Delta f)}{\hat{S}_1(k\Delta f)} \quad . \tag{67}$$

Because only the LHS of Eq. (63) is produced as a result of the digitization and spectral analysis, it is impossible to know the amount of error which will be introduced by the higher frequency terms in any given circumstance. Various techniques are available to prevent contamination of a measurement by aliased data, but a discussion of these is beyond the scope of this investigation. If none of these techniques is applied to the CTD data, then aliasing may occur. It is possible to gain an understanding of the magnitude of the problem by assuming a form for the measured spectral estimate $\hat{S}_1(k\Delta f)$. In fact, a quantitative prediction of $E_S(k\Delta f)$ may be made if we assume that the input spectrum takes some specific analytical form, $\alpha(f)$, when f is one of the discrete frequencies present in the spectral estimate. The relative error is then

$$E_S(k\Delta f) = \frac{|\hat{T}(2f_N - k\Delta f)|^2}{|\hat{T}(k\Delta f)|^2} \cdot \frac{\alpha(2f_N - k\Delta f)}{\alpha(k\Delta f)} + \tag{68}$$

$$+ \frac{|\hat{T}(k\Delta f - 2f_N)|^2}{|\hat{T}(k\Delta f)|^2} \cdot \frac{\alpha(k\Delta f - 2f_N)}{\alpha(k\Delta f)} +$$

$$+ \ \ldots$$

Error in Variance Estimation Due to Aliasing

Parseval's energy theorem[18] permits the variance of a time series to be estimated from the power spectrum, assuming that the time series satisfies those properties which enable the spectrum to be estimated in the first place, i.e., stationary, zero-mean process. Then

$$\sigma^2 = \Delta f \sum_{\text{all } k} \hat{S}_x(k\Delta f) \ . \tag{69}$$

Equation (69) shows that the power spectrum of a time series, here approximated by its spectral estimate, is, in fact, a spectral decomposition of the time-series variance. This fact is useful, enabling the contribution to variance of specific frequencies in the spectrum to be estimated by summing $\hat{S}_x$ over just those frequency bands of interest.

Furthermore, conductivity and temperature time series are routinely low-pass filtered to remove high-frequency information which gives rise to spikes in a computed salinity time series. Energy aliased prior to filtering may still remain in the filtered data and will bias the estimate of variance within the passband. If a perfect low-pass filter transmits all information at frequencies below f_c and blocks all information above f_c, the variance of the filtered time series is

$$\sigma_c^2 = \Delta f \sum_{\text{all } k \leq k_c} \hat{S}_1(k\Delta f) \ , \tag{70}$$

where

$$k_c = \frac{f_c}{\Delta f} \ .$$

If aliased information has contaminated the filtered data, the biased computed variance will be

$$\sigma_c'^2 = \Delta f \sum_{k \leq k_c} \hat{S}_1'(k\Delta f) \quad . \tag{71}$$

The relative error in variance will then be

$$E_{\sigma^2} = \frac{\sigma_c'^2 - \sigma_c^2}{\sigma_c^2} \quad . \tag{72}$$

As before, we may quantify the relative error in variance by assuming a form for the input spectrum, $\alpha(f)$. Then Eq. (72) becomes

$$E_{\sigma^2} = \frac{\sum_{k \leq k_c} E_S(k\Delta f)\, \alpha(k\Delta f)}{\sum_{k \leq k_c} \alpha(k\Delta f)} \quad . \tag{73}$$

2.6 EXTENSION TO SALINITY

Absolute salinity is defined as the ratio of the mass of dissolved material in seawater to the mass of seawater, expressed in parts per thousand by weight.[19] In practice, field salinity is determiend from conductivity measurements. In 1978, a Practical Salinity Scale was established by the Joint Panel of Oceanographic Tables and Standards (JPOTS). Gieskes[11] presents the algorithm for implementing the Practical Salinity Scale to compute salinity from measurements of conductivity, temperature, and pressure. The relationship of salinity to the measured parameters is non-linear. Therefore, it is not possible to predict explicitly the relationship between the power spectra of temperature and conductivity at constant pressure and the power spectra of salinity, a relationship which would permit extending the results of the preceeding discussion on aliasing to predict errors in the salinity spectrum. An alternative approach is available, which allows approximation of the frequency domain relationship.

Since salinity, S, is a function of pressure, P, temperature, T, and conductivity, C; an infinitesimal change in salinity, dS, is linearly related to similar changes dP, dT, dC in any of the three parameters:

$$dS = \frac{\partial S}{\partial P} dP + \frac{\partial S}{\partial T} dT + \frac{\partial S}{\partial C} dC \ . \qquad (74)$$

The relationship is approximately true for finite but small changes, ΔC and ΔT, and, for constant pressure, may be written

$$\Delta S \cong \frac{\partial S}{\partial T} \Delta T + \frac{\partial S}{\partial C} \Delta C \qquad (75)$$

Expressions for $\frac{\partial S}{\partial T}$ and $\frac{\partial S}{\partial C}$ are derived from the JPOTS algorithm in Appendix B. An algorithm for computing these quantities will be presented.

Consider a time series of N samples of conductivity and temperature sampled simultaneously at constant pressure from which a time series of salinity may be constructed. Each of the sequences of samples may be expressed in the form

$$x_j = \bar{x} + \Delta x_j \ , \tag{76}$$

where $\bar{x}$ is the mean of the time series. If the two sampled time series are composed of values which are close to the mean value, then the Δx_j will be small for all j and Eq. (75) will be approximately correct.

The variance of each of these time series is

$$\begin{aligned} \sigma_x^2 &= \frac{1}{N} \sum_{j=1}^{N} (\bar{x} - x_j)^2 \\ &= \frac{1}{N} \sum_{j=1}^{N} \Delta x_j^2 \ , \end{aligned} \tag{77}$$

which we see from Eq. (69), may also be determined by summing the spectral estimate over all frequencies. It is shown in Appendix C that

$$\sigma_s^2 \cong \Theta_T^2(\bar{C},\bar{T})\sigma_T^2 + \Theta_c^2(\bar{C},\bar{T})\sigma_C^2 \ , \tag{78}$$

where

$$\Theta_T(\bar{C},\bar{T}) = \frac{\partial S}{\partial T}\Big|_{C=\bar{C},\ T=\bar{T}} \tag{79}$$

and

$$\Theta_C(\bar{C},\bar{T}) = \frac{\partial S}{\partial C}\Big|_{C=\bar{C},\ T=\bar{T}} \ . \tag{80}$$

Spectral Density

Substituting from Eq. (69) into Eq. (78), we have

$$\sum_{\text{all } k} \hat{S}_s(k\Delta f) \cong \Theta_T^2(\bar{C},\bar{T}) \sum_{\text{all } k} \hat{S}_T(k\Delta f) + \Theta_C^2(\bar{C},\bar{T}) \sum_{\text{all } k} \hat{S}_C(k\Delta f) \qquad (81)$$

By extending the linear relationship between ΔS, ΔT and ΔC expressed in Eq. (75), we may remove the summation from each of the terms in Eq. (81), to yield an order of magnitude estimate for the salinity spectrum.

$$\hat{S}_s(k\Delta f) \cong \Theta_T^2(\bar{C},\bar{T})\hat{S}_T(k\Delta f) + \Theta_C^2(\bar{C},\bar{T})\hat{S}_C(k\Delta f) \quad . \qquad (82)$$

Equation (82) is developed in Appendix D. Now, by the same derivation which produced Eq. (68), we may compute the relative spectral error in the salinity function

$$E_{S_s}(k\Delta f) \cong \frac{E_{S_T}(k\Delta f) \cdot \Theta_T^2(\bar{C},\bar{T}) + E_{S_C}(k\Delta f) \cdot \Theta_C^2(\bar{C},\bar{T})}{\Theta_T^2(\bar{C},\bar{T}) + \Theta_C^2(\bar{C},\bar{T})} \qquad (83)$$

with the spectral error in temperature and conductivity, E_{S_T} and E_{S_C}, respectively, given by Eq. (68).

Variance Error

Again, after the manner of Section 2.5, we may express the variance error in a passband due to low-pass filtering with a cutoff frequency f_c. The relative variance error in salinity will be

$$E_{\sigma_s} \cong \frac{\sigma_{C_T}^2 E_{\sigma_C} \Theta_T^2(\bar{C},\bar{T}) + \sigma_{C_C}^2 E_{\sigma_C} \Theta_C^2(\bar{C},\bar{T})}{\sigma_{C_T}^2 \Theta_T^2(\bar{C},\bar{T}) + \sigma_{C_C}^2 \Theta_C^2(\bar{C},\bar{T})} \qquad (84)$$

with E_{σ_C} and E_{σ_T} the relative variance error in conductivity and temperature, respectively calculated from Eq. (73), and σ_{C_C} and σ_{C_T} the true variance, in the passband, of conductivity and temperature, respectively, given by

$$\sigma_{C_x}^2 = \Delta f \sum_{k \leq k_C} \alpha(k\Delta f) \ . \tag{85}$$

In summary, by making the assumption that a quasi-linear relationship exists between changes in conductivity, temperature, and salinity and by assuming an analytical form for the spectra of the measured processes, conductivity and temperature, it is possible to develop expressions for the error due to aliasing in the salinity spectrum and in the variance within a frequency passband.

These expressions, while approximations, at least provide a means of estimating the errors due to aliasing. It should be noted that the corresponding expressions, developed in Section 2.5 for temperature and conductivity, are exact and are as accurate as the assumed input spectral form, while the validity of the expressions for salinity is dependent upon the assumption of quasi-linearity.

3.0 RESULTS

High-speed temperature-and conductivity-time series were acquired and analyzed to produce an estimate of spectral error for both measured parameters and salinity. A total of five temperature and seventeen conductivity-response-test time series were made for analysis.

For each parameter, the individual time series was first normalized to a unit step, fit to an exponential decay, and this fit was then used to estimate the variance of the timing errors, as described in Section 2.3. A mean variance of timing errors was taken over all response tests for a parameter. A periodogram of the unit step was computed for each time series using Eq. (40) and the periodograms of all response tests for a parameter were averaged to obtain the ensemble spectral estimate, $S(k\Delta f)$. An upper bound for the transfer-function estimate was obtained from the ensemble spectral estimate using Eq. (55) and the mean timing-error variance was used to estimate a lower bound for the sensor transfer function (Eq. (56)).

Use of the transfer upper bound, $|\hat{T}_h(k\Delta f)|^2$, for estimation of spectral error due to aliasing gives a worst case (upper limit) estimate. Therefore, this approach was followed throughout. The spectral error, $E_S(k\Delta f)$ was then estimated for several input spectral forms; an estimate of time series variance error, E_σ^2, was also obtained.

Results of these computations for both temperature and conductivity are presented in sections 3.1 and 3.2. Section 3.3 extends the results to estimate error for computed salinity.

3.1 TEMPERATURE

Five response tests of temperature were evaluated. Figure 10 is a logarithmic plot of the normalized time series with data plotted as though they were sampled at regular time intervals. In each case, plotting of

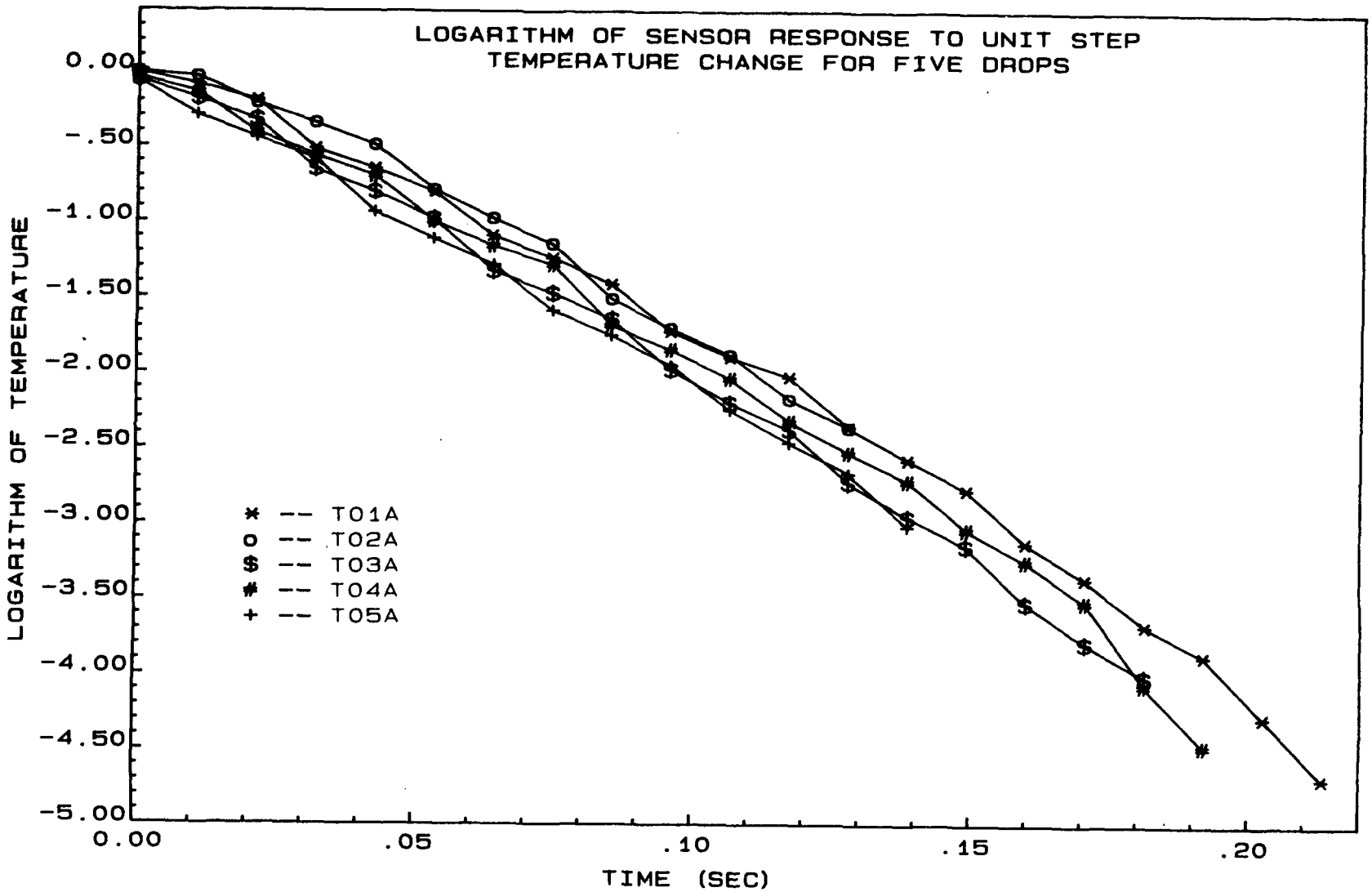

Figure 10. Logarithm of sensor response to a unit step temperature change for five tests. Data are plotted as though sampled at equal time intervals.

the curve began with the first point after an identifiable break in the curve. The repeatability of the sensor temperature response and its close approximation to an exponential decay are evident in fig. 10.

Figure 11 is a logarithmic plot of data from response test number four. Data are plotted as though acquired at equal intervals, $\Delta t = 0.01067$ sec. The best fit curve is also shown for comparison.

Table 1 presents results of the timing-error analysis for all five response tests. The identifier for each data run in this and all following tables uses the labeling scheme described in Appendix A. The second column lists the number of data points used in the curve fitting process and in the calculation of the timing-error variance. The error-analysis software which performed these calculations was set up to allow the operator to select a subset of the response-test time series for analysis by selecting the beginning and ending points of the subset. The subset of data that most closely fit the exponential curve was chosen for evaluation in each case. The constants α and t_o from Eq. (18) were calculated for each best-fit curve as was the time constant for the decay, given by the reciprocal of α. The timing-error variance is presented in column six of the table. Mean values for the time constant, for alpha, and for the timing-error variance, σ_e^2, are also tabulated.

A periodogram of each normalized step-response time series was computed in the manner described in Section 2.4. The software routine performing these calculations simply selected the first 32 data points for the spectral calculations. The time series was corrected for trend and offset using Eq. (46), transformed via a fast Fourier transform, and the periodogram was calculated via Eq. (49). Figure 12 shows the original time series, while fig. (13) shows the normalized, trend and offset corrected data prior to processing via FFT.

The individual step-response periodograms for temperature are presented in Table 2, as is the ensemble average spectrum. A comparison of PSDs between response tests emphasizes the consistency of results obtainable by this testing procedure.

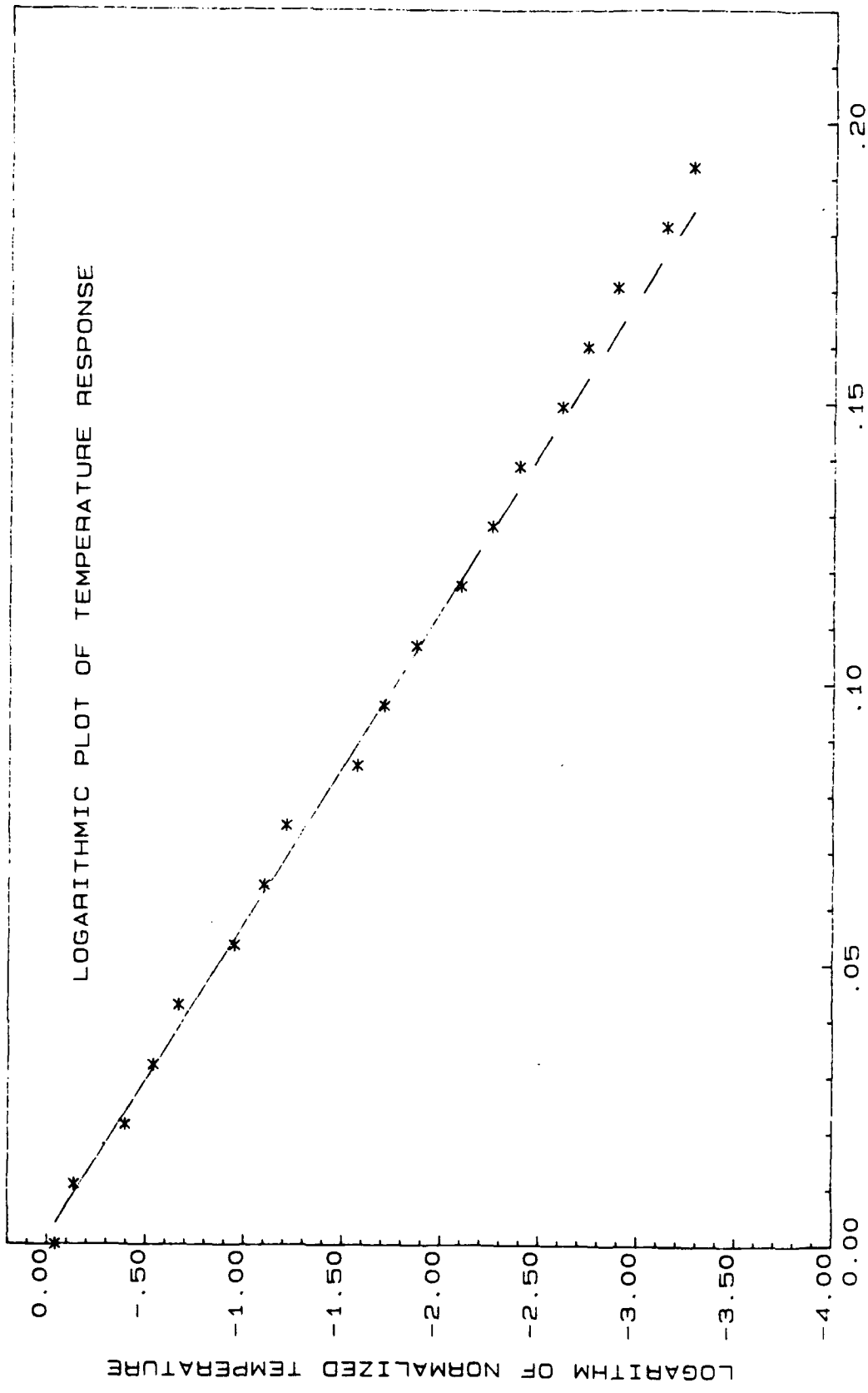

Figure 11. Logarithmic plot of temperature response test number 4.

Table 1. Results of Timing-Error Analysis for Temperature Response Tests.

Run Number	Number of Points	Alpha (s-1)	Time Constant (ms)	T_o (ms)	Timing Error Variance (ms^2)
T01A	18	17.02	58.7	4.93	6.5
T02A	13	17.95	55.7	1.25	6.5
T03A	15	18.70	53.4	0.30	5.9
T04A	12	17.89	55.9	1.34	7.2
T05A	13	17.43	57.4	-4.23	5.4
Mean		17.80	56.2		6.3

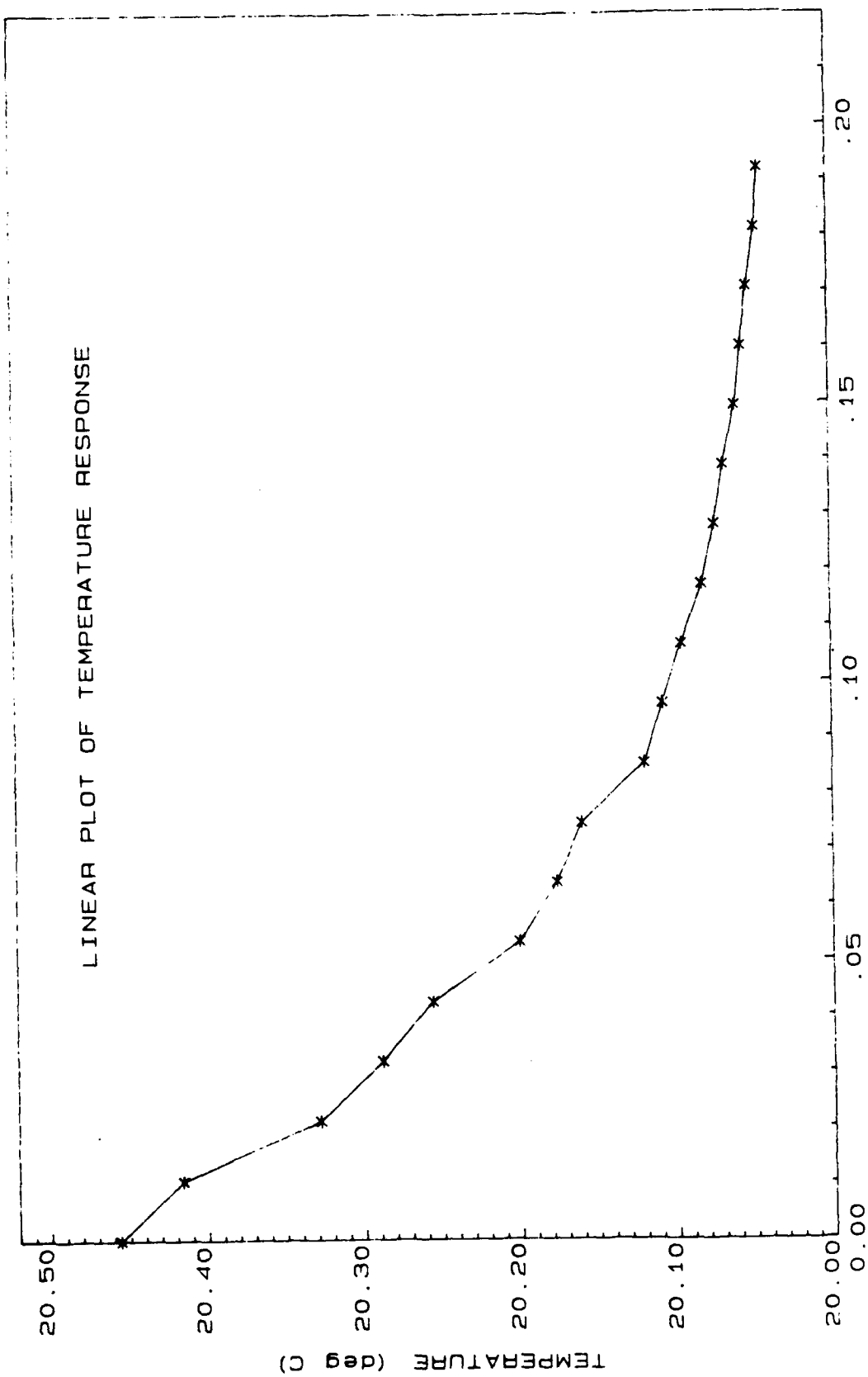

Figure 12. Linear plot of temperature response test number 4.

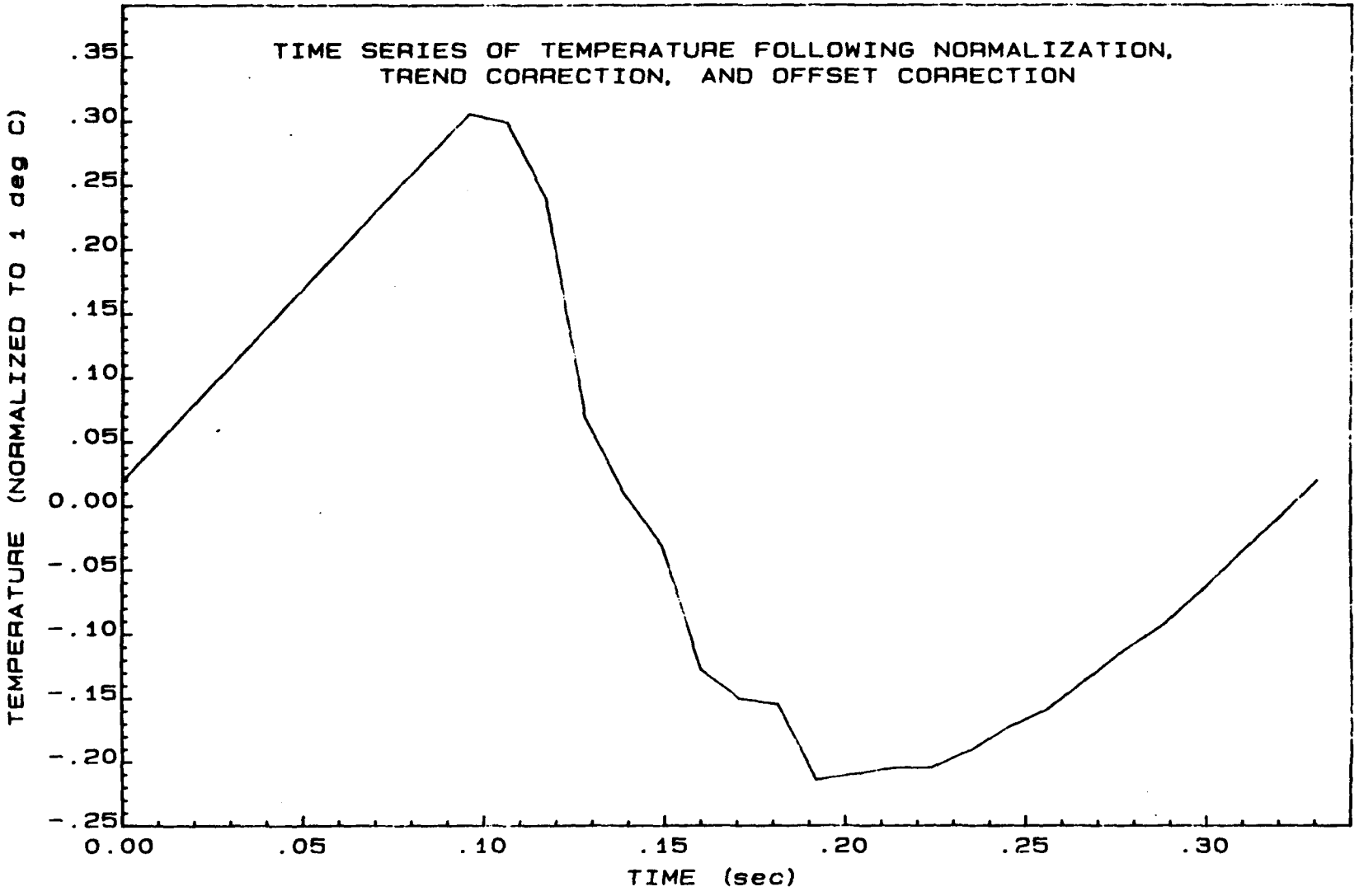

Figure 13. Plot of temperature response test number 4 after normalization and trend and offset correction.

Table 2. Individual Temperature-Step-Response Spectra and Ensemble Average Spectrum. Units are $^{\circ}C^2/Hz \times 10^2$.

Run Number	Center Frequency (Hz) 2.93	5.86	8.79	11.72	14.65	17.58	20.51	23.44	26.37	29.30	32.23	35.16	38.09	41.02	43.95
T01A	0.800	0.086	0.019	0.004	0.003	0.001	0.000	0.001	0.001	0.001	0.001	0.000	0.000	0.000	0.000
T02A	0.841	0.095	0.011	0.002	0.001	0.000	0.000	0.000	0.000	0.001	0.001	0.000	0.000	0.000	0.000
T03A	0.868	0.092	0.021	0.004	0.002	0.001	0.000	0.000	0.000	0.001	0.001	0.000	0.000	0.000	0.000
T04A	0.818	0.086	0.015	0.004	0.003	0.001	0.000	0.001	0.001	0.001	0.001	0.000	0.000	0.000	0.000
T05A	0.850	0.098	0.017	0.004	0.002	0.001	0.000	0.001	0.001	0.001	0.001	0.000	0.000	0.000	0.000
Average	0.835	0.091	0.017	0.004	0.002	0.001	0.000	0.001	0.001	0.001	0.001	0.000	0.000	0.000	0.000

Power transfer functions were computed from each of the temperature-response periodograms using Eq. (50). These appear in Table 3 as does the ensemble estimate, $|\hat{T}_h(k_\Delta f)|^2$, computed via Eq. (53). These data are plotted in fig. (14), the numbers corresponding to the run number shown in Table 3. The solid curve represents the estimated power transfer function.

Shaw's method was used to place bounds on the transfer function estimate, as described in Section 2.4. Upper and lower limits for the power and amplitude transfer functions are given in Table 4. The power transfer-function limits are plotted in fig. (15).

As described in Section 2.5, in order to quantify the extent to which aliasing will affect temperature (or other CTD) data acquired at the standard data rate, it is necessary to specify the spectral form of the input to the sensor. The particular shape of the spectrum, $\alpha(f)$, and the shape of the sensor transfer function completely determine the extent of aliasing; therefore the choice of $\alpha(f)$ has a strong effect as will be demonstrated below.

Physical considerations must play a role in the selection of a spectral form. Bracewell[14] has shown that if a function and its first n-1 derivatives are continuous, then the transform of the function dies away at least as rapidly as $f^{-(n+1)}$ for large f. Similarly, its power spectrum dies away at least as rapidly as $f^{-2(n+1)}$.

Real-world physical processes usually are assumed to be continuous. A less restrictive model for the input functions would be a signal which possesses, at most, a finite number of finite discontinuities, so that its first derivative is impulsive. Such a signal would possess a transform which behaves as f^{-1} for large f, and a power spectrum which decays as f^{-2}.

A worst-case model for the input functions which results in a poor signal-to-noise ratio is one whose spectrum is white noise for virtually all frequencies. Another class of signals would be those whose spectra decay as f^{-n} down to some constant noise level.

Table 3. Power Transfer Functions Computed from Individual Temperature Response Tests.

Run Number	Center Frequency (Hz)														
	2.93	5.86	8.79	11.72	14.65	17.58	20.51	23.44	26.37	29.30	32.23	35.16	38.09	41.02	43.95
T01A	0.463	0.199	0.101	0.036	0.041	0.030	0.010	0.019	0.025	0.049	0.078	0.036	0.047	0.036	0.025
T02A	0.486	0.219	0.060	0.021	0.019	0.006	0.003	0.012	0.023	0.052	0.089	0.031	0.024	0.003	0.004
T03A	0.502	0.212	0.110	0.035	0.024	0.017	0.003	0.007	0.012	0.037	0.079	0.031	0.046	0.018	0.009
T04A	0.473	0.200	0.077	0.033	0.044	0.026	0.007	0.027	0.038	0.064	0.091	0.030	0.026	0.002	0.005
T05A	0.492	0.226	0.090	0.033	0.027	0.012	0.009	0.033	0.041	0.070	0.099	0.033	0.036	0.002	0.005
Ensemble Estimate	0.483	0.211	0.088	0.032	0.031	0.018	0.006	0.020	0.028	0.054	0.087	0.032	0.036	0.012	0.006

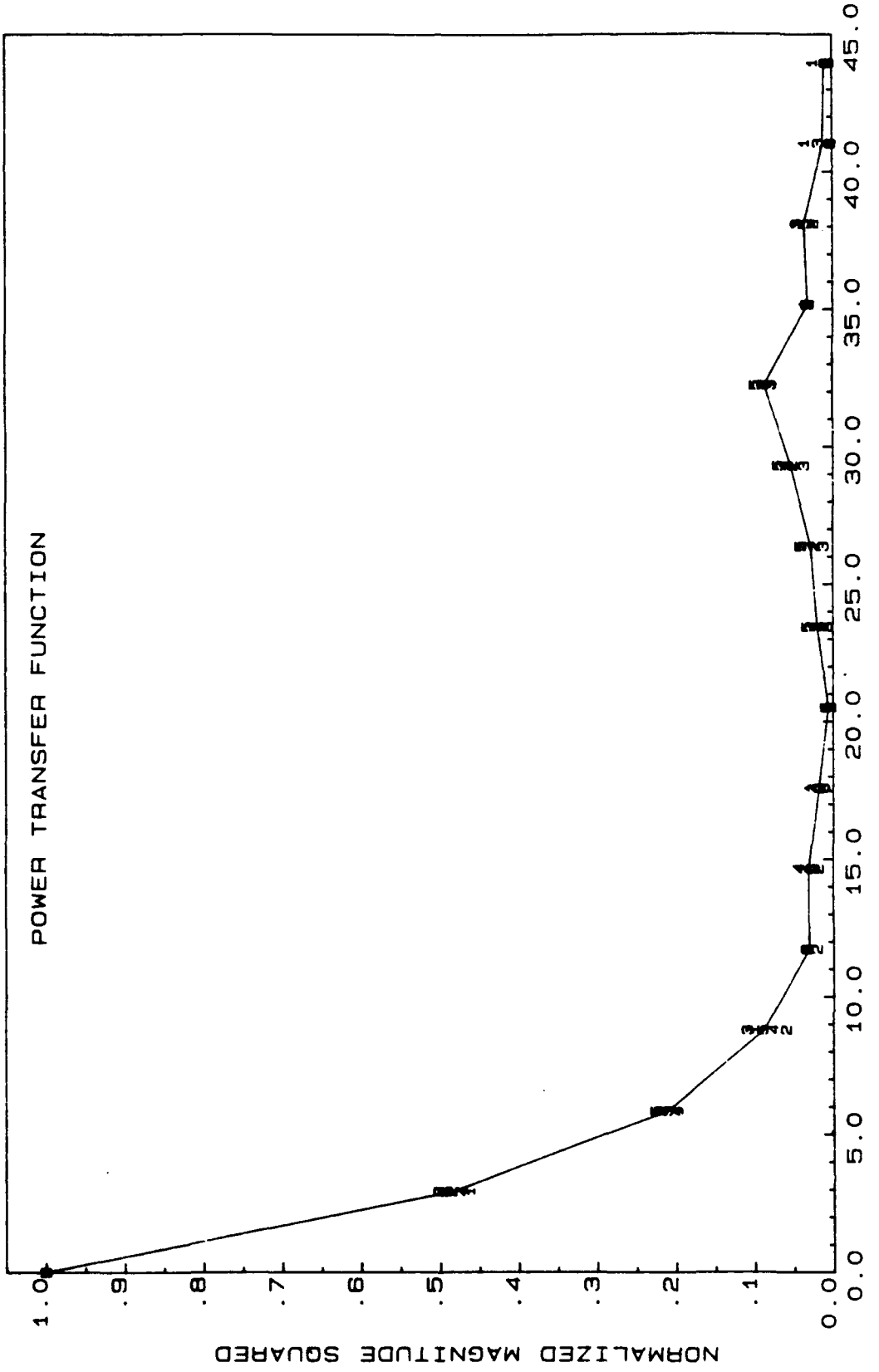

Figure 14. Power transfer functions for each of five temperature response tests. Ensemble average is plotted as solid line.

Table 4. Transfer-Function Limits for CTD Temperature Response. Wavelength corresponds to drop rate of 0.75 m/s.

Frequency (Hz)	Wavelength (m)	Power Transfer Function		Amplitude Transfer Function	
		Upper Limit	Lower Limit	Upper Limit	Lower Limit
0.00	-	1.000	1.000	1.000	1.000
2.93	0.256	0.483	0.482	0.695	0.694
5.86	0.127	0.211	0.196	0.459	0.443
8.79	0.085	0.088	0.072	0.297	0.268
11.72	0.064	0.032	0.017	0.180	0.131
14.65	0.051	0.030	0.017	0.174	0.131
17.58	0.043	0.019	0.006	0.137	0.075
20.51	0.037	0.006	0.000	0.075	0.000
23.44	0.032	0.026	0.010	0.161	0.098
26.37	0.028	0.028	0.003	0.168	0.051
29.30	0.026	0.052	0.018	0.228	0.133
32.23	0.023	0.084	0.051	0.290	0.225
35.16	0.021	0.033	0.000	0.183	0.000
38.09	0.020	0.039	0.007	0.198	0.086
41.02	0.018	0.011	0.000	0.106	0.000
43.95	0.017	0.000	0.000	0.000	0.000

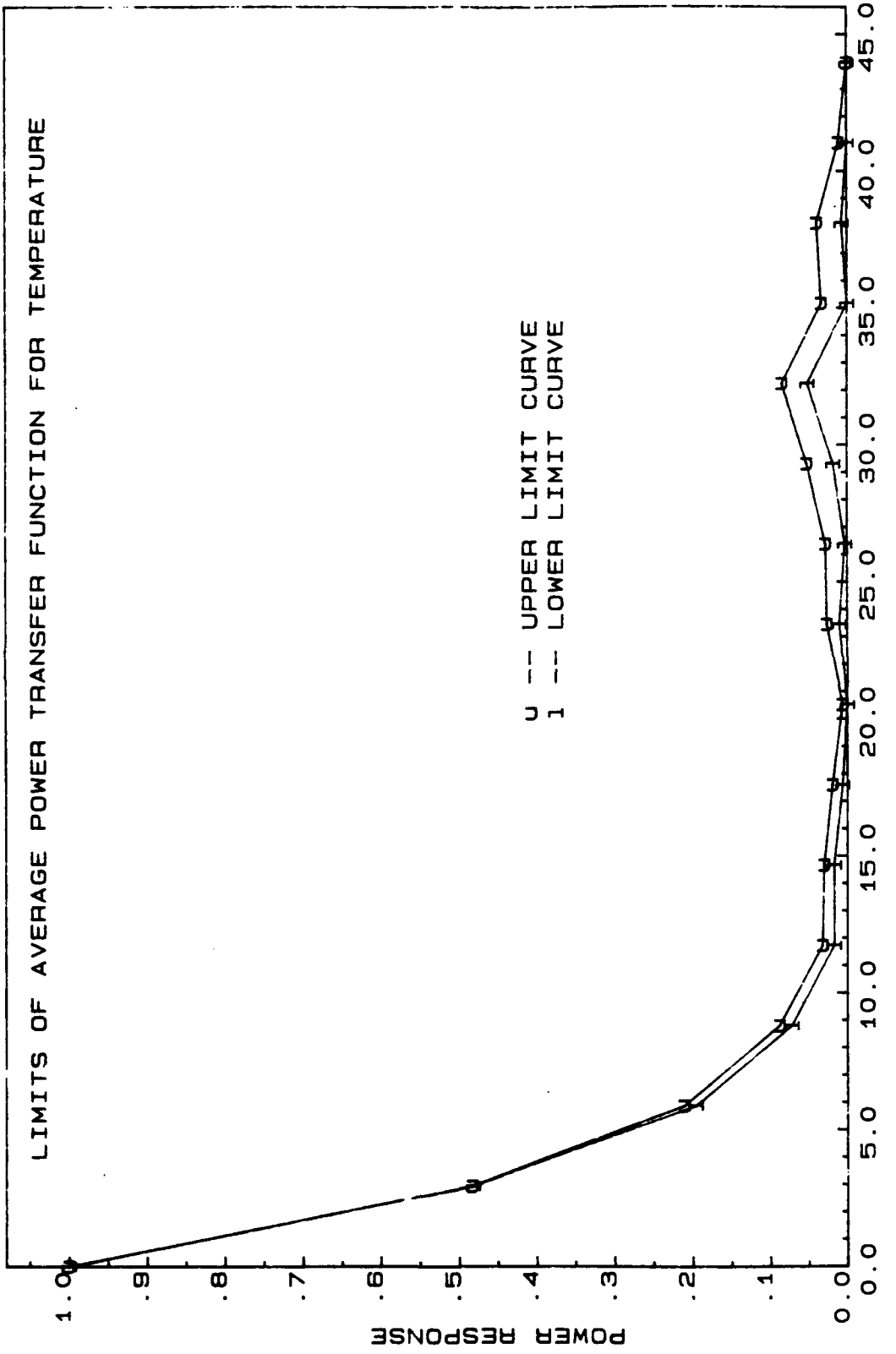

Figure 15. Upper and lower limits of ensemble average power transfer function for temperature.

The input spectral form for all these cases may be represented by

$$\alpha(f) = 1/f^n + 1/f_0^n \qquad (86)$$

with the second term being the constant-noise spectral density. Thus, f_0 represents the frequency at which the signal-to-noise power ratio is unity, the signal being given by $1/f^n$. The relative spectral error, given by Eq. (68), and relative variance error, given by Eq. (73), were calculated for three specific cases corresponding to those described above. Table 5 describes these three test cases. The relative spectral error in temperature for each of the test cases is shown in Table 6. The same data are plotted in fig. (16).

Recall that this parameter is the band-by-band ratio of aliased to unaliased spectral density, allowing for transfer function effects of the sensor prior to digitization and correction for transfer effects after aliasing occurs. The power-transfer-function upper limit from Table 4 was utilized for these calculations. The wavelength entry in the table is based upon the laboratory-response-test drop rate of 0.75 m/s and represents the spatial resolution corresponding to the particular frequency.

Test Case 1, white noise, is a pessimistic "worst case" which one might not expect to encounter in the real world. As shown in Table 6, spectral error is significant in all parts of the computed spectrum due to the fact that the sensor transfer function is non-zero beyond the Nyquist frequency, 15.63 Hz, for 32 ms sampling. Test Case 2, on the other hand, represents an optimistic case in which the spectral decay is not affected by instrumentation noise at any frequency. Clearly, aliasing does not present a problem except in that portion of the spectrum near the Nyquist frequency. Finally, Test Case 3 is an intermediate case more likely to be encountered than either of the other two cases in the course of real-world measurements. In examining the results of Test Case 3, it is seen that spectral error remains less than 10% until spatial resolution becomes less than 0.10 m. The qualifying assumption is that the S/N ratio equals 1 at the Nyquist frequency. Experience with this instrument has shown this to be a reasonable assumption.

Table 5. Test Cases Used for Computation of Spectral and Variance Error.

Test Case Number	Spectrum Description	Exponent, n	f_o (Hz)
1	White Noise	0	15.63
2	$1/f^2$	2.0	100.00
3	$1/f^2$ + white noise	2.0	15.63

Table 6. Relative Spectral Error in Temperature For Three Spectral Input Forms. Table entries are percentages.

Center Frequencies (Hz)	Wavelength (m)	Relative Spectral Error (Per Cent)		
		White Noise	$1/f^2$	$1/f^2$ + White Noise
0.00	-	7.4	0.0	0.0
2.93	0.256	19.5	0.1	0.4
5.86	0.127	28.1	0.9	3.7
8.79	0.085	40.9	3.8	11.9
11.72	0.064	61.3	13.1	29.5
14.65	0.051	103.4	58.7	78.5

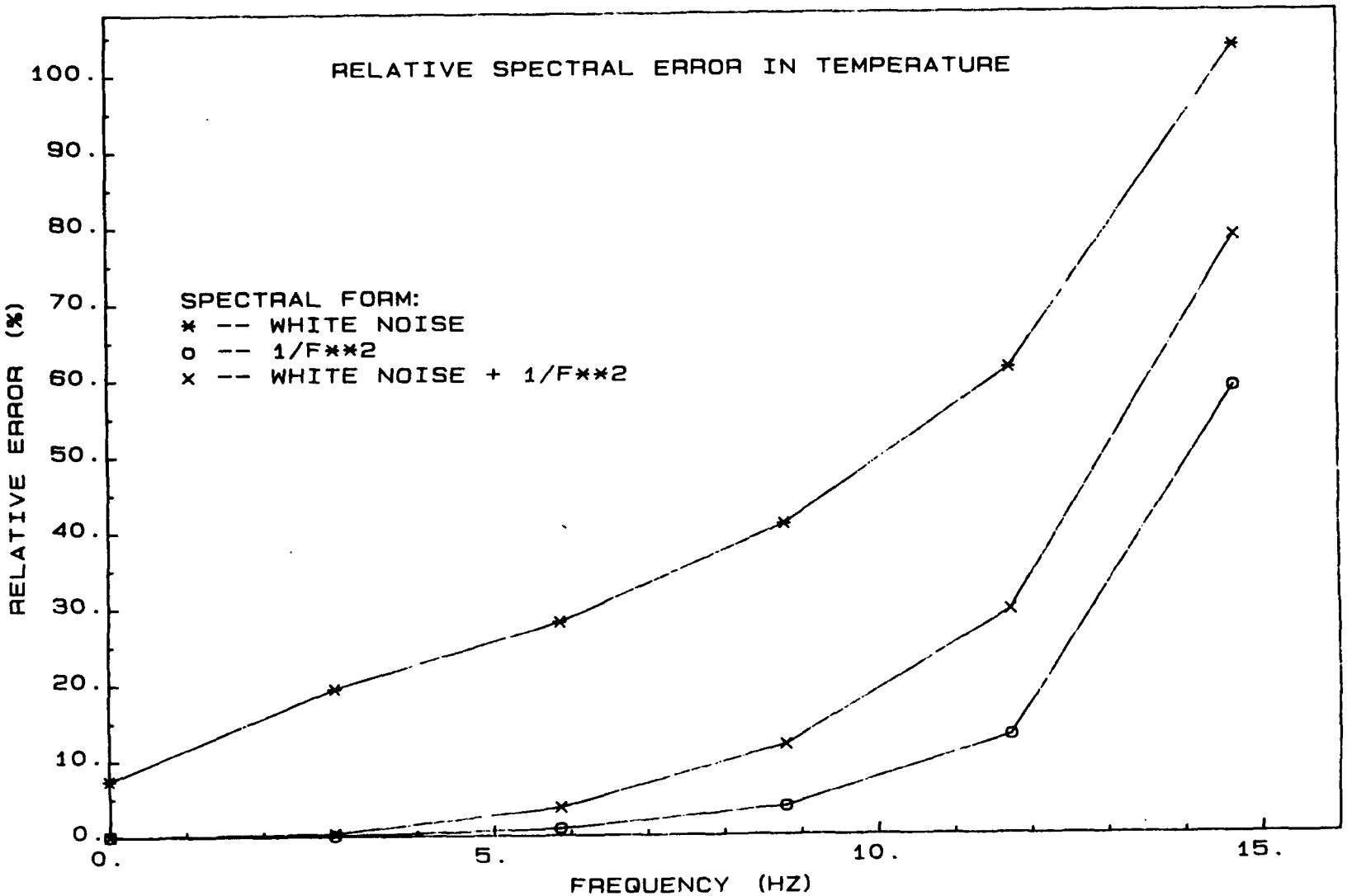

Figure 16. Relative spectral error in temperature. Three different input spectral forms are treated.

Cumulative error in variance also was computed. Recall that this represents the error which would be introduced by aliasing in a calculation of the time-series variance if the time series were numerically low-pass filtered after sampling, as is done with temperature and conductivity data to eliminate spikes in computed salinity. The cumulative error data are presented in Table 7 as a function of the low-pass-filter cutoff frequency for several different frequencies. These frequencies correspond to upper limits of the discrete frequency bands produced by the response-test spectral processing. Figure 17 is a graphical presentation of the same data for each of the three test cases.

In comparing the data of test cases 2 and 3 with corresponding results for relative spectral error, it is interesting to note that even though aliasing results in significant error in the spectrum at higher frequencies, the effect on computed variance is considerably less. Since the assumed temperature spectrum decays as $1/f^2$, the major contribution to the variance is at lower frequencies where aliasing error is relatively unimportant. Thus, even though the sensor responds to energy at frequencies above the Nyquist, the fraction of total signal energy available at those frequencies is small. Therefore, when this energy is aliased into the low frequency, high-energy region of the spectrum, its effect is relatively unimportant.

The white-noise case emphasizes the effect of the input spectrum. Since there is no decay in the spectrum at high frequencies, considerable energy is available to be aliased, the extent being determined by the transfer function. Therefore, the effect of aliasing on computed variance due to white noise is noticeably greater at all frequencies.

Table 7. Cumulative Aliasing-Induced Error in Temperature Variance after Low-Pass Filtering. Data presented are percentage error for various filter cutoff frequencies, calculated for three different input spectral forms.

Frequency Limit (Hz)	Variance Error (Per Cent)		
	White Noise	$1/f^2$	$1/f^2$ + White Noise
1.46	7.4	0.0	0.0
4.39	15.4	0.0	0.1
7.32	20.5	0.0	0.2
10.25	26.3	0.1	0.4
13.18	34.1	0.2	0.7
15.63	44.9	0.4	1.1

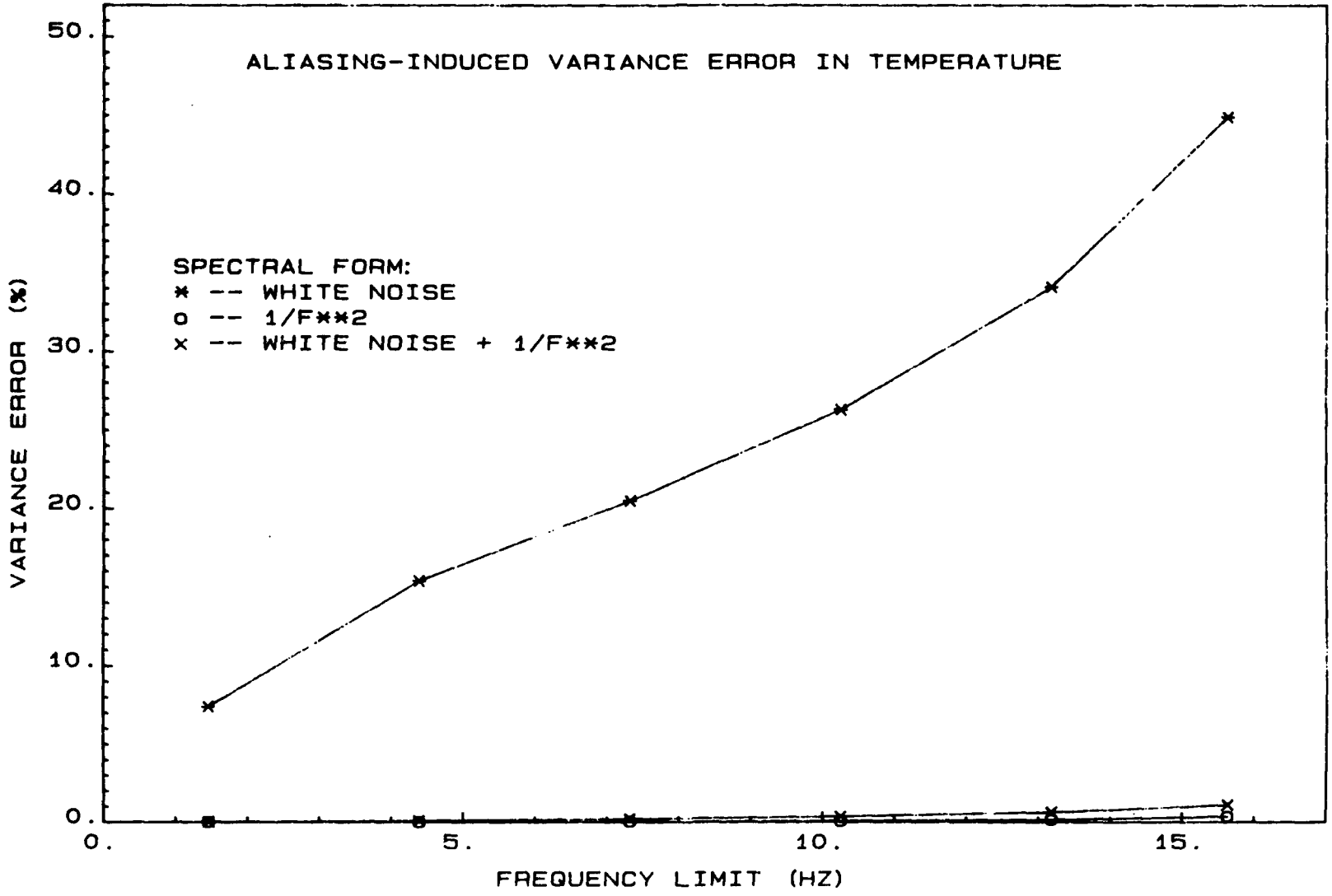

Figure 17. Cumulative aliasing-induced error in temperature variance after low-pass filtering. Data are percentage error in time-series variance for various filter cutoff frequencies, calculated for three different spectral forms.

3.2 CONDUCTIVITY

Evaluation of CTD conductivity response tests was conducted in the same manner as the temperature evaluations described in Section 3.1. Initially, five conductivity tests were performed. A preliminary evaluation of these data revealed substantially greater variation from one test to the next. Therefore, additional test data were acquired for the purpose of obtaining a more reliable estimate of the sensor's response. The five initial response tests are referred to as data set A, while the twelve additional response tests are referred to as set B. The same CTD unit and conductivity sensor were used in both tests. However, several weeks elapsed between performance of the two tests. Evaluations of the two sets were handled separately so that any variation in the data due to sensor changes or changes in test conditions could be identified. None were seen.

Figure 18 is a logarithmic plot of the five normalized time series of conductivity obtained during test A. Data are plotted as though acquired at equal intervals. Again, plotting of points begins with the first point after an identifiable break in the curve. Two features are obvious in this figure. First, as indicated above, the conductivity data are less consistent from test to test than were the temperature data. Secondly, instead of a simple logarithmic response, as in the case of the temperature sensor, the response of the conductivity sensor is clearly more complex. Although not plotted, data from Test B show the same features.

The conductivity response curve may be broken into two regions. Initial sensor response to the step change is sharp. On a logarithmic plot, such as figure 18, this portion of the curve is approximately linear; its duration is on the order of 40 - 50 ms. The slope of the logarithmic curve is steep, indicating a relatively short time constant, and is fairly consistent from test to test.

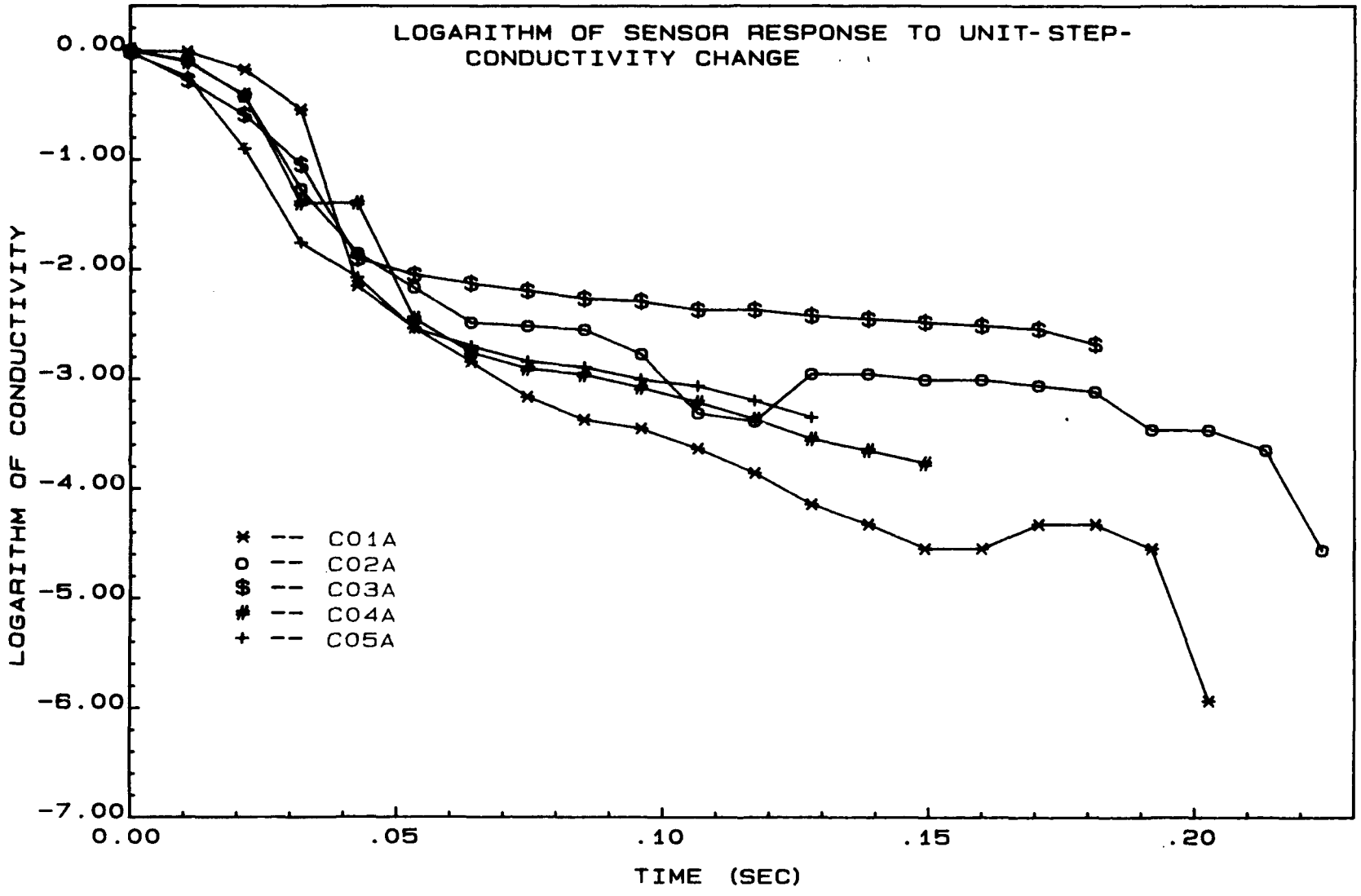

Figure 18. Logarithm of sensor response to a unit-step-function conductivity change for five tests - data Set A. Data are plotted as though sampled at equal time intervals.

The second region of the curve is even more linear than the first, suggestive of a more truly exponential response to the step change. The duration of this portion of the curve is greater, on the order of 80 - 120 ms. The time constant is substantially longer, but variation between tests is greater, as may be seen in figure 18. Figure 19 is a logarithmic plot of an individual response test, number three from set A. The delineation into two distinct regions is evident.

Previous researchers have noted this feature of the Neil Brown conductivity sensor. Gregg, et al.,[13] have developed a computerized model of the physical behavior of the cell which accurately predicts the sensor response to a step input. The initial sharp response is associated with the initial encounter between the sensor and the conductivity interface, as the water of "new" conductivity first enters the cell. The slower response is attributed to a flushing action which takes place as "old" water is gradually washed from the region of the sensor walls, both interior and exterior. Since the flow of water through and around the sensor is essentially laminar, flushing of residual water is described approximately by an exponential decay.

The observed variability in the flushing region of the curve is probably due to variation in the drop rate of the CTD unit through the conductivity interface. A higher drop rate would result in more rapid flusing and a steeper logarithmic response curve, while the opposite is true for a slow drop rate. From figure 18, we see that test C01A has a steeper slope, while the other four have slopes which are approximately the same and are shallower than the first. Since no means was available for controlling the drop rate of each individual test, some variation is expected.

Timing-error analysis of conductivity data was conducted, as described previously, by fitting an exponential decay to any desired region of the time series. Table 8 presents results of the analysis for data set A, with the curve fit performed only over the initial, steep region of each

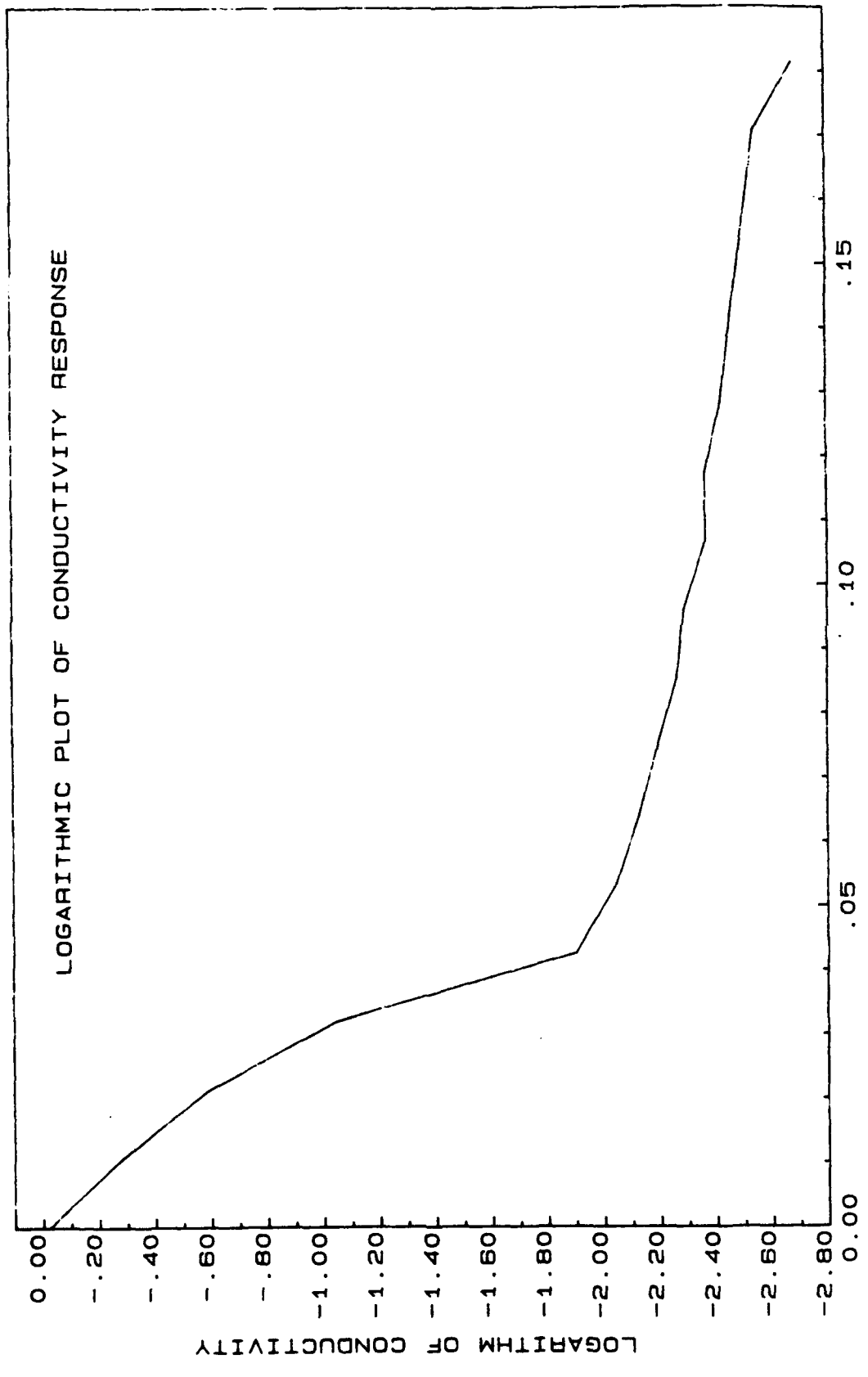

Figure 19. Logarithmic plot of conductivity response test number 3 from data Set A.

Table 8. Results of Timing-Error Analysis for Conductivity Response Tests, Data Set A. Exponential decay was fit to the steep portion of each response curve.

Run Number	Number of Points	Alpha (s^{-1})	Time Constant (ms)	T_o (ms)	Timing-Error Variance (ms^2)
C01A	4	87.93	11.4	0.7	10.7
C02A	6	54.65	18.3	-1.1	7.5
C03A	5	60.01	16.7	-1.6	10.6
C04A	5	56.11	17.8	1.0	15.1
C05A	6	54.52	18.3	2.2	6.9
Average		62.64	16.5		10.2

curve. A much greater variation in curve parameters from test-to-test is evident, relative to the equivalent data for temperature. A similar curve fit was conducted for the slow response portions of these same curves and results are presented in Table 9.

Again, the time constant for the first test is significantly less than the other four. Note that the mean timing-error variance, σ_e^2 is considerably greater than for the temperature tests. This increase in variance of conductivity is thought to be a measure of the poorness of fit of either region of the response curve to an exponential decay. Table 10 presents results of the timing analysis for data set B. The steep region of the curve was fit in all twelve of these tests. Variability of all parameters is again evident.

Since the sample timing error is determined solely by the data sampling circuitry and not by any characteristic of the sensor or the sensed parameter, the true timing error should be the same for both temperature and conductivity. Since the greater variance for conductivity is attributed to the larger residuals of the exponential fit as well as to the timing error, σ_e^2 for temperature, the smaller of the computed timing-error variances, was used in all subsequent calculations of spectral error for conductivity.

A periodogram of each normalized conductivity step-response-time series was computed in the manner described for temperature response. The periodograms for data set A are presented in Table 11, while Table 12 contains periodogram PSDs for conductivity data set B.

Power transfer functions for conductivity were computed using Eq. (50). For data set A these are presented in Table 13, and for data set B in Table 14. Ensemble average transfer functions are presented for each data set. Plots of these data appear in figs. 20 and 21. The ensemble average for each set is plotted as the solid curve in each case. These data also display considerable variation from one run to the next.

Table 9. Results of Timing-Error Analysis for Conductivity Response Tests, Data Set A. Exponential decay was fit to the shallow portion of each response curve.

Run Number	Number of Points	Alpha (s^{-1})	Time Constant (ms)	T_o (ms)	Timing-Error Variance (ms^2)
C01A	10	20.12	49.7	-130.0	9.7
C02A	14	12.74	78.5	-185.2	806.6
C03A	11	8.74	114.4	-309.2	11.8
C04A	9	11.33	88.2	-237.7	6.1
C05A	8	9.59	104.3	-264.1	9.3
AVERAGE		12.50	87.0		168.7

Table 10. Results of Timing-Error Analysis for Conductivity Response Tests, Data Set B.

Run Number	Number of Points	Alpha (s^1)	Time Constant (ms)	To (ms)	Timing-Error Variance (ms^2)
C01B	6	58.01	17.2	3.2	29.6
C02B	5	59.76	16.7	-3.7	2.6
C03B	4	77.32	12.9	0.3	15.0
C04B	5	53.03	18.9	0.6	8.5
C05B	6	55.24	18.1	2.2	27.3
C06B	5	56.02	17.9	5.6	21.9
C07B	6	52.82	18.9	-2.4	22.8
C08B	5	56.23	17.8	-1.0	1.1
C09B	5	54.93	18.2	-4.3	2.1
C10B	6	53.84	18.6	-3.5	28.4
C11B	6	53.03	18.9	4.1	20.2
C12B	5	52.91	18.9	3.6	12.1
Average		56.93	17.8		16.0

Table 11. Individual Conductivity Step-Response Spectra and Ensemble Average Spectrum for Data Set A. Units are $(mS/cm)^2/Hz \times 10^2$

Run Number	Center Frequency (Hz)														
	2.93	5.86	8.79	11.72	14.65	17.58	20.51	23.44	26.37	29.30	32.23	35.16	38.09	41.02	43.95
C01A	1.420	0.320	0.129	0.054	0.029	0.017	0.007	0.005	0.003	0.002	0.002	0.001	0.002	0.002	0.002
C02A	1.287	0.270	0.094	0.052	0.022	0.009	0.005	0.003	0.002	0.001	0.001	0.000	0.000	0.000	0.000
C03A	1.156	0.265	0.078	0.025	0.016	0.003	0.000	0.000	0.001	0.002	0.001	0.001	0.001	0.000	0.000
C04A	1.354	0.278	0.095	0.044	0.013	0.005	0.005	0.003	0.003	0.002	0.003	0.002	0.002	0.004	0.003
C05A	1.323	0.286	0.109	0.050	0.019	0.010	0.007	0.003	0.001	0.001	0.000	0.000	0.000	0.000	0.000
Ensemble Average	1.308	0.284	0.101	0.045	0.020	0.009	0.005	0.003	0.002	0.002	0.001	0.001	0.001	0.001	0.001

Table 12. Individual Conductivity Step-Response Spectra and Ensemble Average Spectrum, Data Set B. Units are $(mS/cm)^2/Hz \times 10^2$.

Run Number	Center Frequency (Hz)														
	2.93	5.86	8.79	11.72	14.65	17.58	20.51	23.44	26.37	29.30	32.23	35.16	38.09	41.02	43.95
C01B	1.355	0.277	0.092	0.038	0.014	0.003	0.002	0.001	0.002	0.003	0.004	0.002	0.002	0.003	0.002
C02B	1.401	0.292	0.122	0.052	0.022	0.013	0.008	0.004	0.002	0.002	0.001	0.000	0.000	0.000	0.000
C03B	1.284	0.290	0.115	0.046	0.026	0.014	0.006	0.004	0.002	0.002	0.002	0.002	0.003	0.003	0.003
C04B	1.357	0.278	0.100	0.045	0.017	0.010	0.007	0.004	0.002	0.001	0.001	0.001	0.001	0.001	0.001
C05B	1.325	0.261	0.089	0.038	0.013	0.003	0.001	0.000	0.000	0.002	0.003	0.002	0.002	0.003	0.003
C06B	1.274	0.261	0.096	0.032	0.011	0.004	0.001	0.000	0.000	0.001	0.002	0.001	0.001	0.001	0.000
C07B	1.291	0.271	0.114	0.056	0.021	0.012	0.008	0.004	0.002	0.002	0.001	0.001	0.001	0.001	0.001
C08B	1.309	0.280	0.108	0.045	0.015	0.008	0.004	0.001	0.001	0.001	0.001	0.001	0.000	0.001	0.001
C09B	1.275	0.279	0.106	0.048	0.017	0.010	0.006	0.003	0.001	0.001	0.001	0.000	0.000	0.000	0.000
C10B	1.353	0.276	0.104	0.051	0.022	0.010	0.007	0.004	0.001	0.001	0.002	0.001	0.002	0.002	0.002
C11B	1.363	0.248	0.101	0.043	0.016	0.006	0.003	0.002	0.001	0.002	0.002	0.001	0.001	0.002	0.002
C12B	1.280	0.265	0.087	0.034	0.009	0.004	0.001	0.000	0.000	0.001	0.001	0.001	0.000	0.001	0.000
Ensemble	1.322	0.273	0.103	0.044	0.017	0.011	0.004	0.002	0.001	0.002	0.002	0.001	0.001	0.002	0.001

Table 13. Power Transfer Functions Computed from Individual Conductivity Response Spectra for Data Set A.

Run Number	Center Frequency (Hz)														
	2.93	5.86	8.79	11.72	14.65	17.58	20.51	23.44	26.37	29.30	32.23	35.16	38.09	41.02	43.95
C01A	0.821	0.741	0.670	0.503	0.414	0.352	0.212	0.203	0.130	0.092	0.127	0.088	0.171	0.184	0.214
C02A	0.744	0.624	0.487	0.481	0.315	0.189	0.154	0.125	0.084	0.054	0.044	0.020	0.035	0.024	0.020
C03A	0.669	0.613	0.405	0.232	0.226	0.071	0.002	0.011	0.026	0.124	0.046	0.070	0.052	0.040	0.021
C04A	0.783	0.644	0.494	0.406	0.190	0.113	0.137	0.103	0.124	0.095	0.185	0.185	0.175	0.425	0.352
C05A	0.765	0.661	0.568	0.467	0.270	0.217	0.197	0.126	0.048	0.082	0.025	0.015	0.017	0.013	0.001
Ensemble Estimate	0.756	0.657	0.525	0.418	0.283	0.188	0.140	0.114	0.082	0.089	0.085	0.076	0.090	0.137	0.122

Table 14. Power Transfer Functions Computed from Individual Conductivity Response Tests, Data Set B.

Run Number	Center Frequency (Hz)														
	2.93	5.86	8.79	11.72	14.65	17.58	20.51	23.44	26.37	29.30	32.23	35.16	38.09	41.02	43.95
C01B	0.784	0.641	0.479	0.352	0.196	0.063	0.060	0.055	0.074	0.169	0.268	0.207	0.257	0.322	0.265
C02B	0.810	0.675	0.633	0.477	0.320	0.260	0.231	0.145	0.101	0.114	0.095	0.039	0.025	0.034	0.021
C03B	0.742	0.671	0.600	0.421	0.380	0.286	0.171	0.157	0.096	0.108	0.165	0.171	0.302	0.340	0.381
C04B	0.785	0.643	0.518	0.417	0.252	0.210	0.208	0.141	0.073	0.083	0.090	0.063	0.071	0.100	0.073
C05B	0.766	0.603	0.462	0.355	0.193	0.072	0.039	0.016	0.021	0.098	0.183	0.192	0.240	0.359	0.329
C06B	0.737	0.603	0.498	0.294	0.155	0.075	0.016	0.009	0.018	0.079	0.117	0.075	0.109	0.068	0.022
C07B	0.746	0.628	0.594	0.519	0.311	0.243	0.233	0.166	0.079	0.095	0.103	0.058	0.057	0.065	0.084
C08B	0.757	0.648	0.565	0.417	0.221	0.176	0.121	0.053	0.036	0.045	0.065	0.051	0.046	0.077	0.087
C09B	0.737	0.645	0.553	0.447	0.242	0.201	0.165	0.103	0.062	0.084	0.083	0.038	0.031	0.048	0.026
C10B	0.783	0.639	0.544	0.472	0.317	0.202	0.191	0.133	0.053	0.076	0.121	0.088	0.147	0.201	0.226
C11B	0.788	0.573	0.526	0.402	0.225	0.115	0.095	0.077	0.042	0.096	0.122	0.109	0.130	0.222	0.208
C12B	0.740	0.612	0.453	0.317	0.130	0.078	0.032	0.012	0.006	0.082	0.069	0.066	0.048	0.063	0.033
Ensemble Average	0.765	0.632	0.536	0.408	0.245	0.165	0.130	0.089	0.055	0.094	0.123	0.096	0.122	0.158	0.146

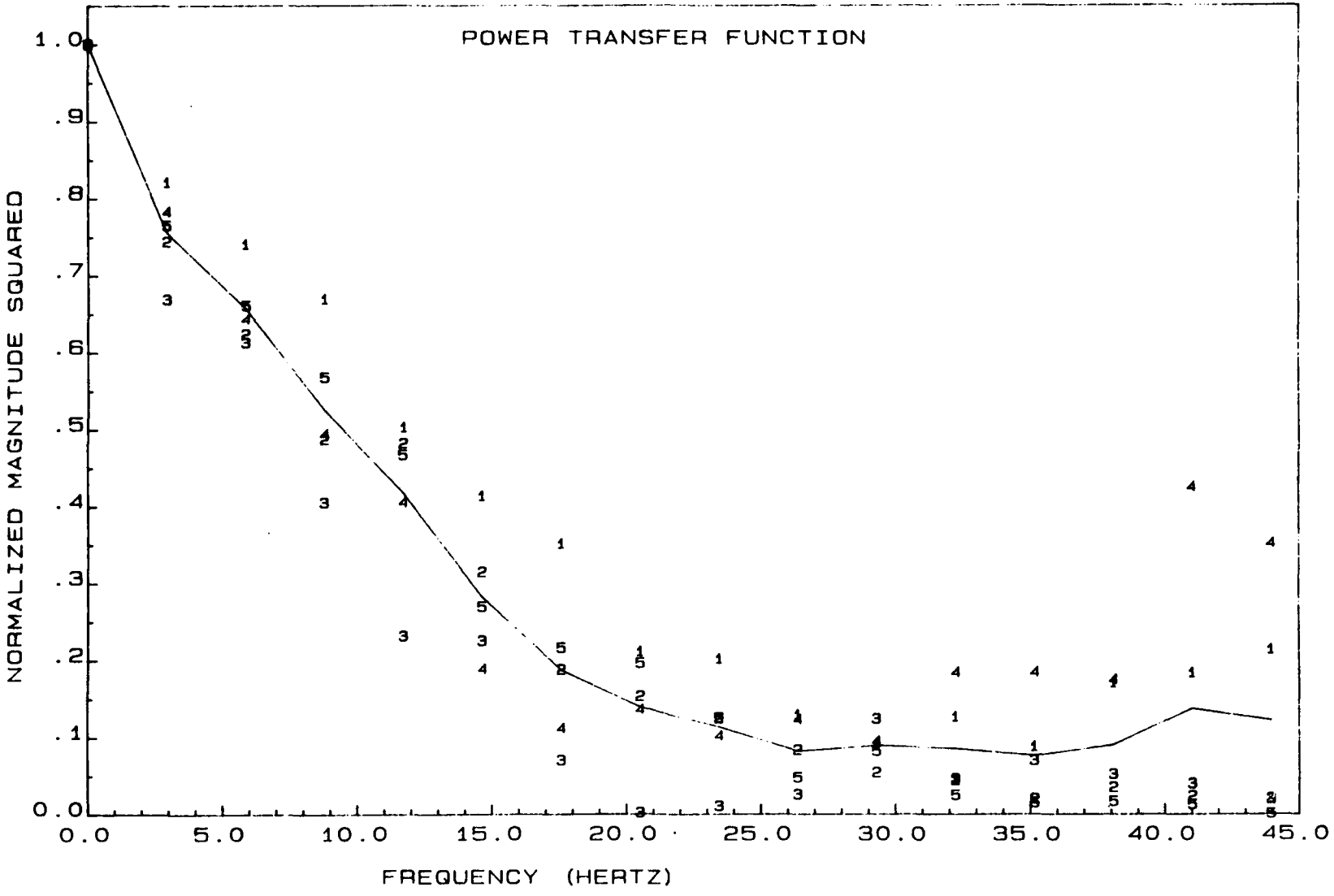

Figure 20. Power transfer functions for each of five conductivity response tests - data Set A. Ensemble average is solid line.

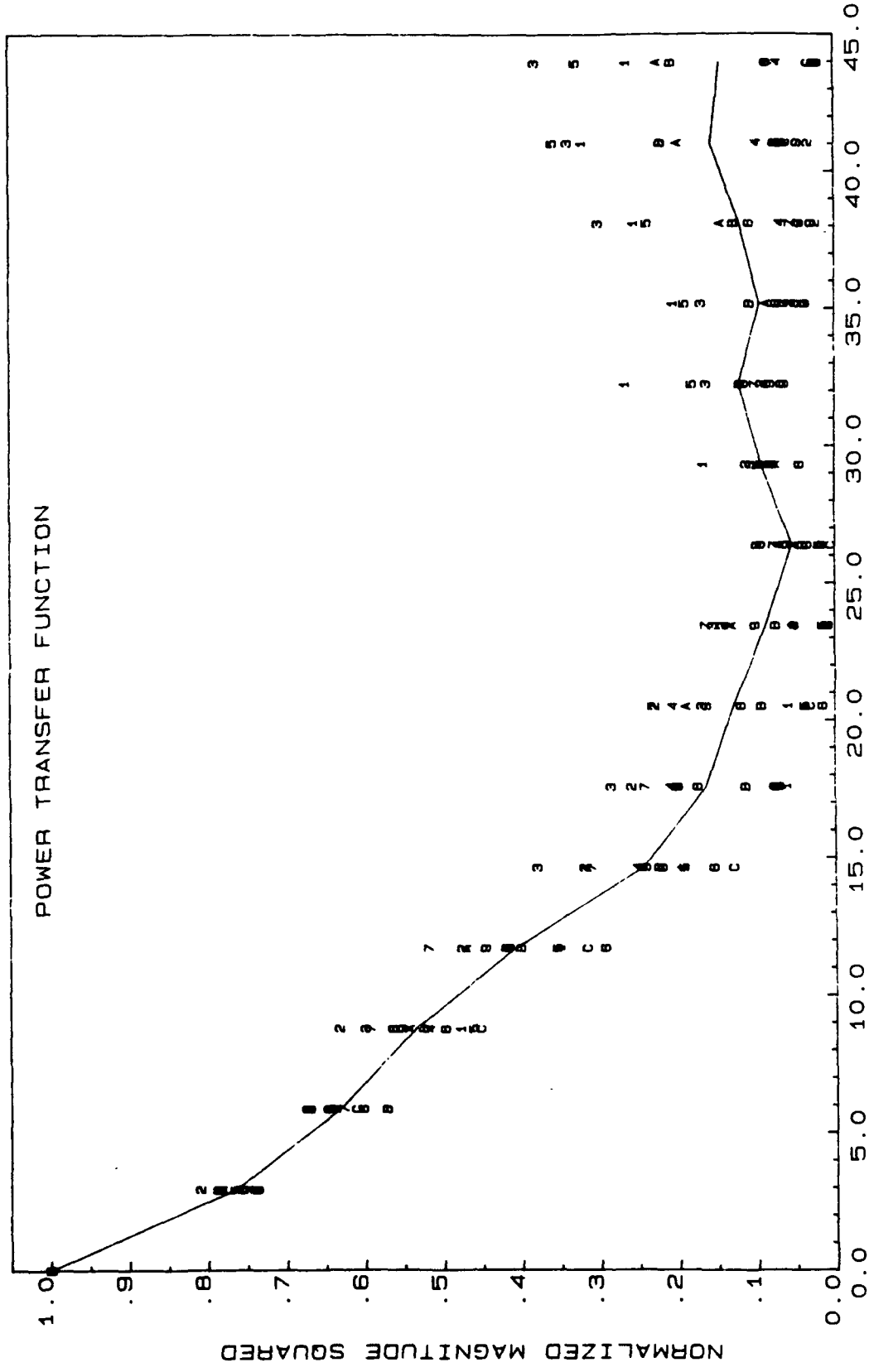

Figure 21. Power transfer functions for each of twelve conductivity response tests - data Set B. Ensemble average is solid line.

The ensemble average transfer functions are presented in Table 15 together with an average for all conductivity response tests. Upper and lower limits for both power and amplitude transfer functions obtained by using Shaw's method, as before, appear in Table 16. Transfer function limits are plotted in figure 22. As in the case of the temperature calculations, the upper-limit transfer function was used for computation of aliasing in order to obtain a "worst case" estimate.

Estimates of relative spectral error for conductivity were made employing the same three spectral forms and technique as was used for temperature. The results are tabulated in Table 17 and plotted in figure 23. Although the high-frequency response of the conductivity sensor is greater than for the CTD temperature sensor and the relative spectral error is somewhat greater in all frequency bands for conductivity, the results are not significantly different.

Cumulative, aliasing-induced error in the variance of conductivity was also computed and the results are presented in Table 18. As shown, the conductivity variance error differs only slightly from the temperature variance error. Results are plotted for each of the three cases in figure 24.

Table 15. Ensemble Average Power Transfer Functions for Conductivity Data Sets A and B and Weighted Average for All Conductivity Data.

Frequency (Hz)	Transfer Function		
	Set A (5 Runs)	Set B (12 Runs)	Average (17 Runs)
2.93	0.756	0.765	0.762
5.86	0.657	0.632	0.639
8.79	0.525	0.536	0.533
11.72	0.418	0.408	0.411
14.65	0.283	0.245	0.256
17.58	0.188	0.165	0.172
20.51	0.140	0.130	0.133
23.44	0.114	0.089	0.096
26.37	0.082	0.055	0.063
29.30	0.089	0.094	0.093
32.23	0.085	0.123	0.112
35.16	0.076	0.096	0.090
38.09	0.090	0.122	0.113
41.02	0.137	0.158	0.152
43.95	0.122	0.146	0.139

Table 16. Transfer Function Limits for CTD Conductivity Response. Wavelengths correspond to drop rate of 0.75 m/s.

Frequency (Hz)	Wavelength (m)	Power Transfer Function		Amplitude Transfer Function	
		Upper Limit	Lower Limit	Upper Limit	Lower Limit
0.00	-	1.000	1.000	1.000	1.000
2.93	0.256	0.762	0.759	0.873	0.871
5.86	0.127	0.639	0.609	0.799	0.781
8.79	0.085	0.533	0.487	0.730	0.698
11.72	0.064	0.411	0.352	0.641	0.594
14.65	0.051	0.256	0.189	0.506	0.435
17.58	0.043	0.173	0.105	0.416	0.325
20.51	0.037	0.133	0.067	0.365	0.260
23.44	0.032	0.096	0.031	0.310	0.175
26.37	0.028	0.061	0.000	0.247	0.000
29.30	0.026	0.093	0.016	0.304	0.125
32.23	0.023	0.112	0.024	0.335	0.154
35.16	0.021	0.092	0.000	0.303	0.000
38.09	0.020	0.117	0.000	0.342	0.000
41.02	0.018	0.147	0.009	0.384	0.095
43.95	0.017	0.143	0.035	0.378	0.187

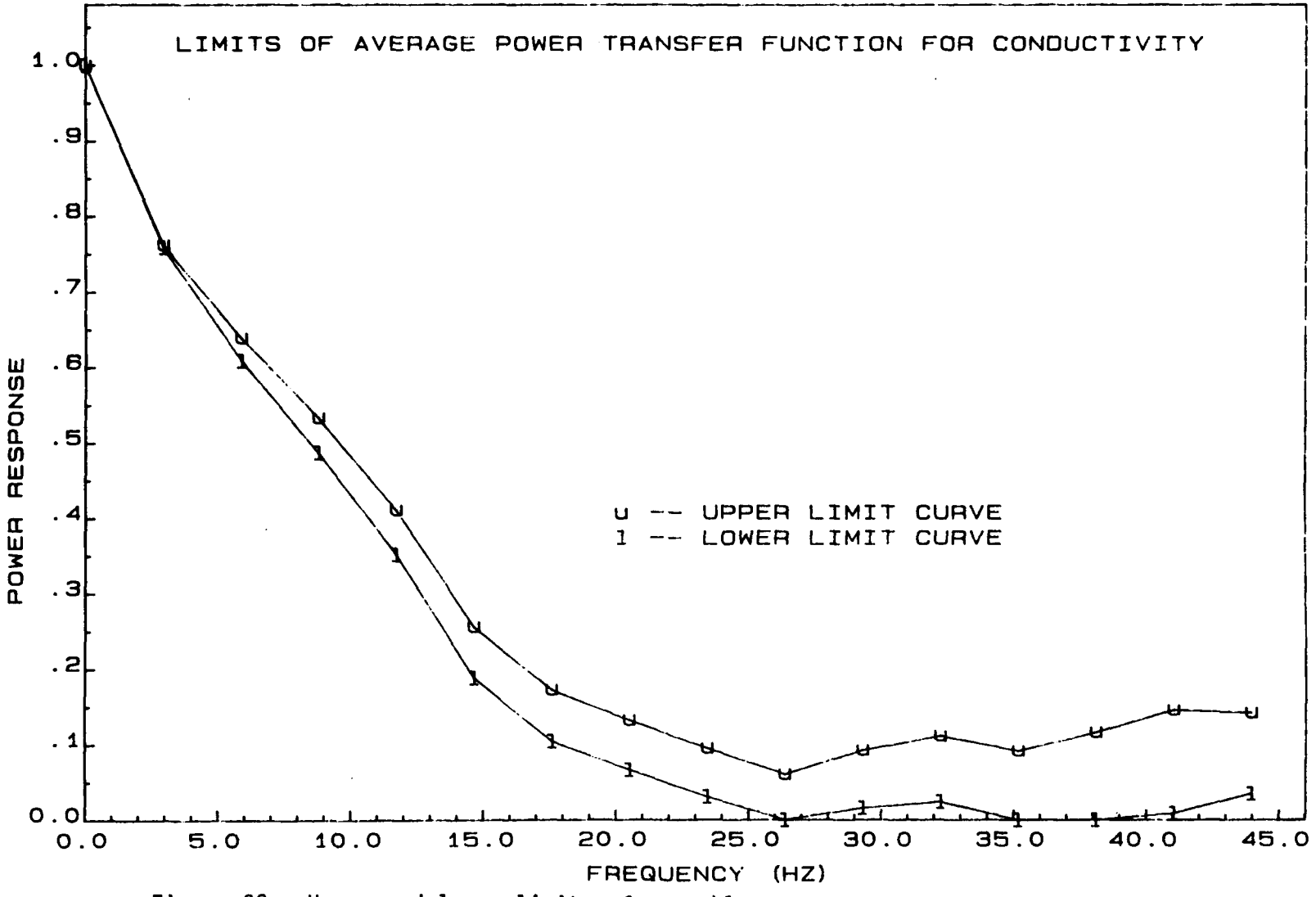

Figure 22. Upper and lower limits of ensemble average power transfer function for conductivity. Curves are a composite of results from data Sets A and B.

Table 17. Relative Spectral Error in Conductivity for Three Spectral Forms. Table entries are percentages.

Center Frequency (Hz)	Wavelength (m)	Relative Spectral Error (Per Cent)		
		White Noise	$1/f^2$	$1/f^2$ + White Noise
0.00	-	8.2	0.0	0.0
2.93	0.256	21.5	0.1	0.4
5.86	0.127	26.7	1.0	3.5
8.79	0.085	46.2	4.6	13.8
11.72	0.064	67.2	15.9	33.4
14.65	0.051	115.0	61.0	85.0

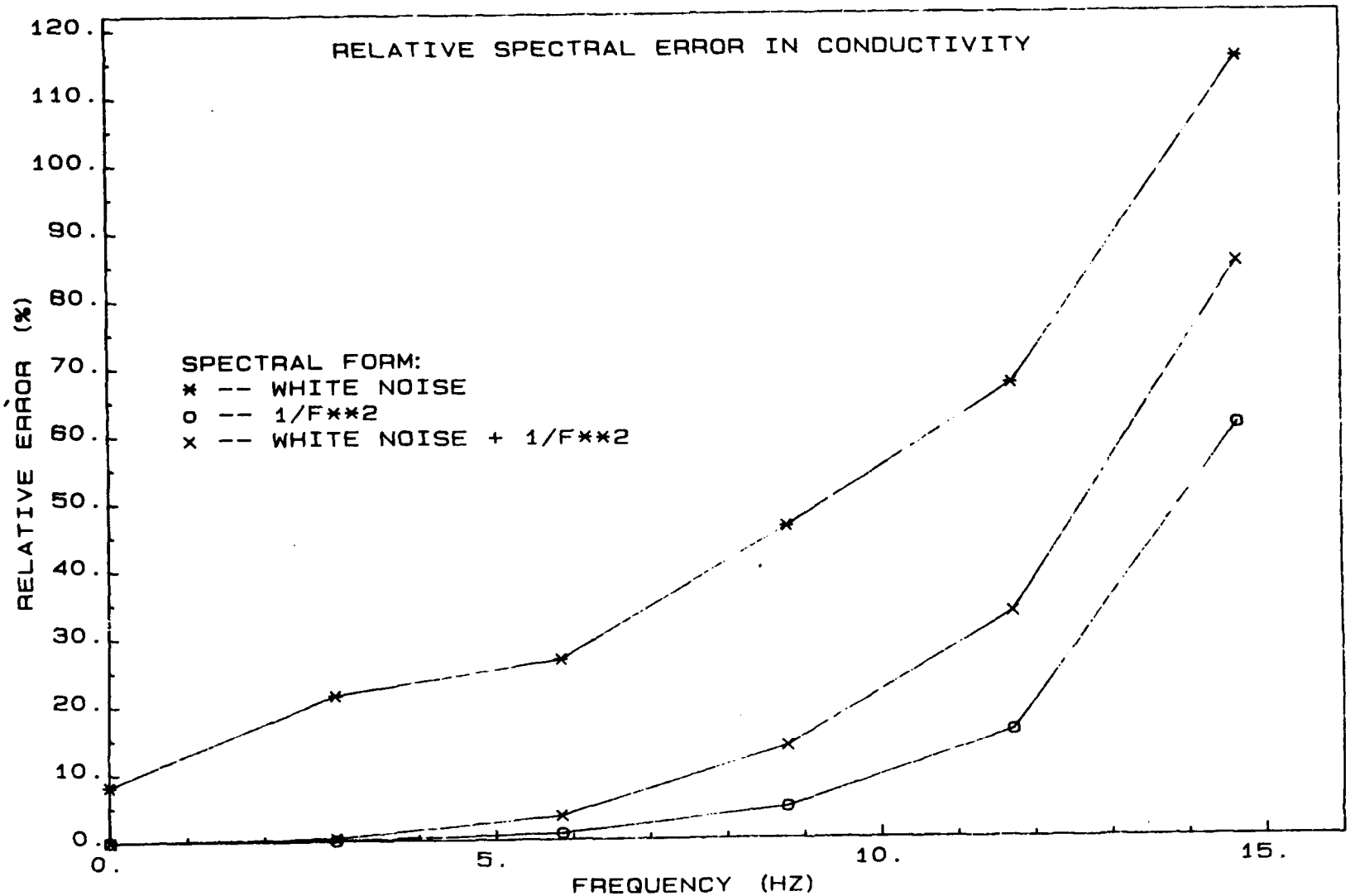

Figure 23. Relative spectral error in conductivity. Three different input spectral forms are treated.

Table 18. Cumulative, Aliasing-Induced Error in Conductivity Variance After Low-Pass Filtering. Data presented are percentage error for various filter cutoff frequencies, calculated for three different spectral forms.

Frequency Limit (Hz)	Variance Error (Per Cent)		
	White Noise	$1/f^2$	$1/f^2$ + White Noise
1.46	8.2	0.0	0.0
4.39	17.1	0.0	0.1
7.32	20.9	0.1	0.2
10.25	28.1	0.1	0.4
13.18	36.8	0.2	0.7
15.63	49.1	0.4	1.2

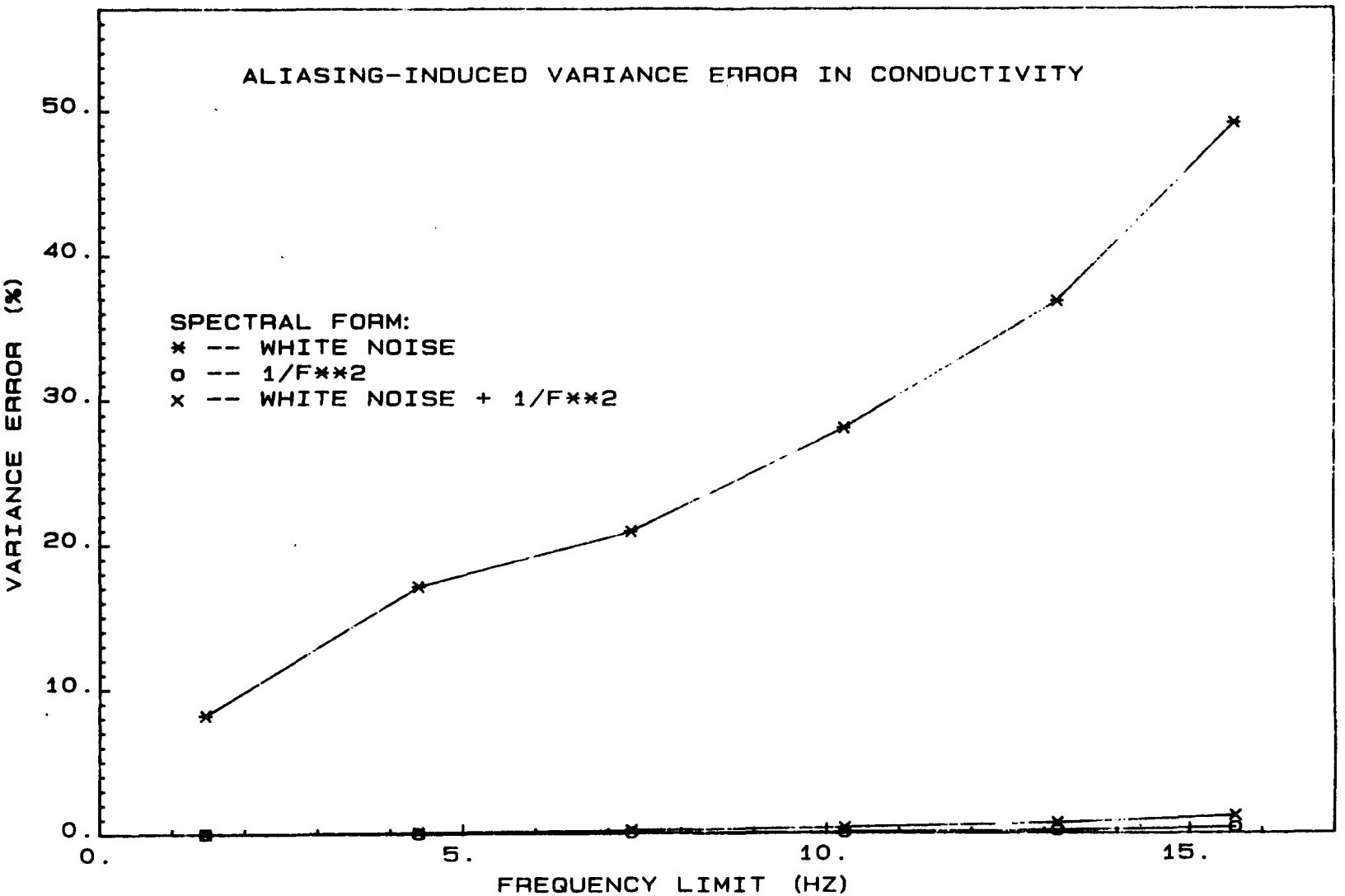

Figure 24. Aliasing-induced error in conductivity variance after low-pass filtering. Data are percentage error in time-series variance for various filter cutoff frequencies, calculated for three different input spectral forms.

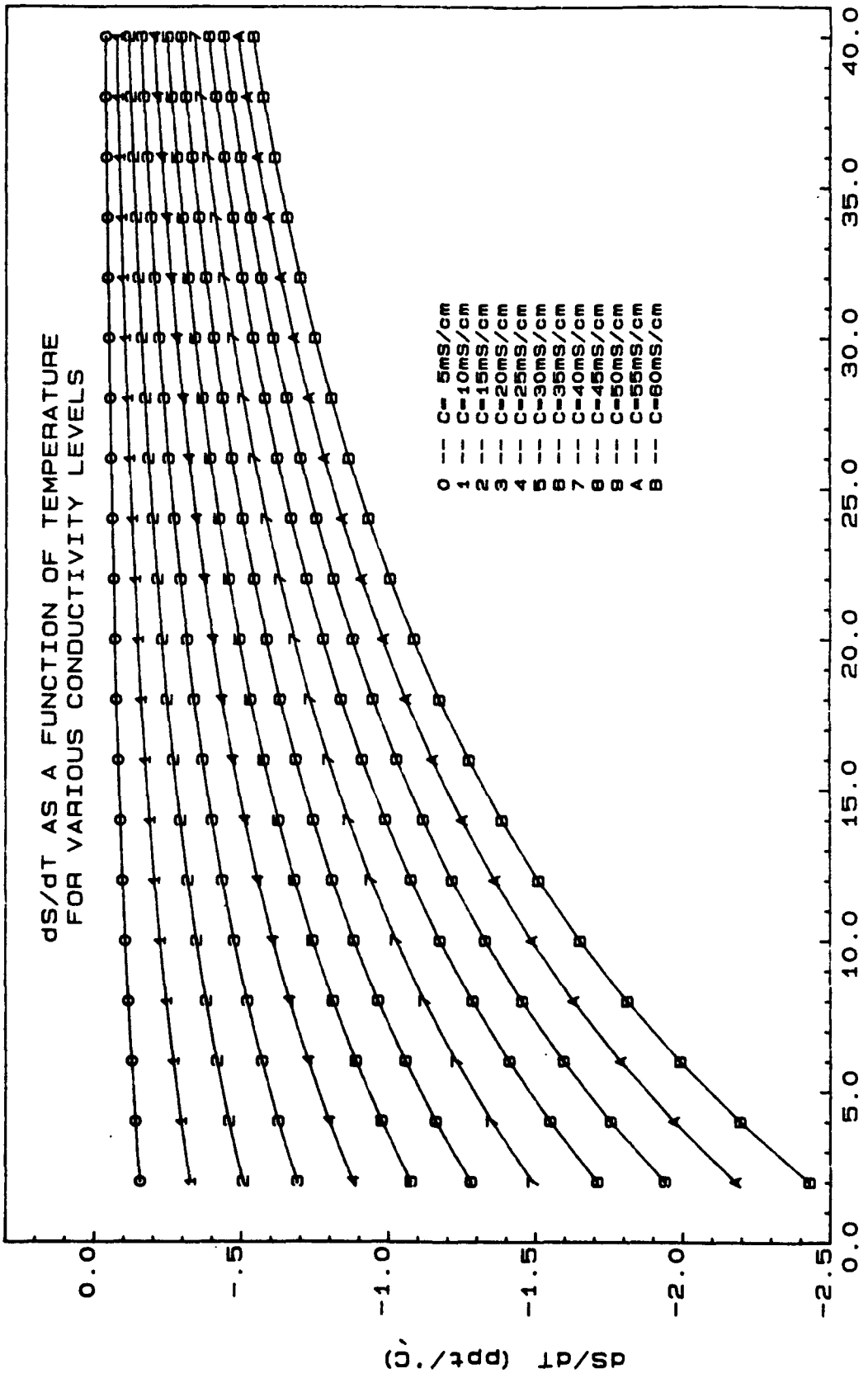

Figure 25. First partial derivative of salinity with respect to temperature.

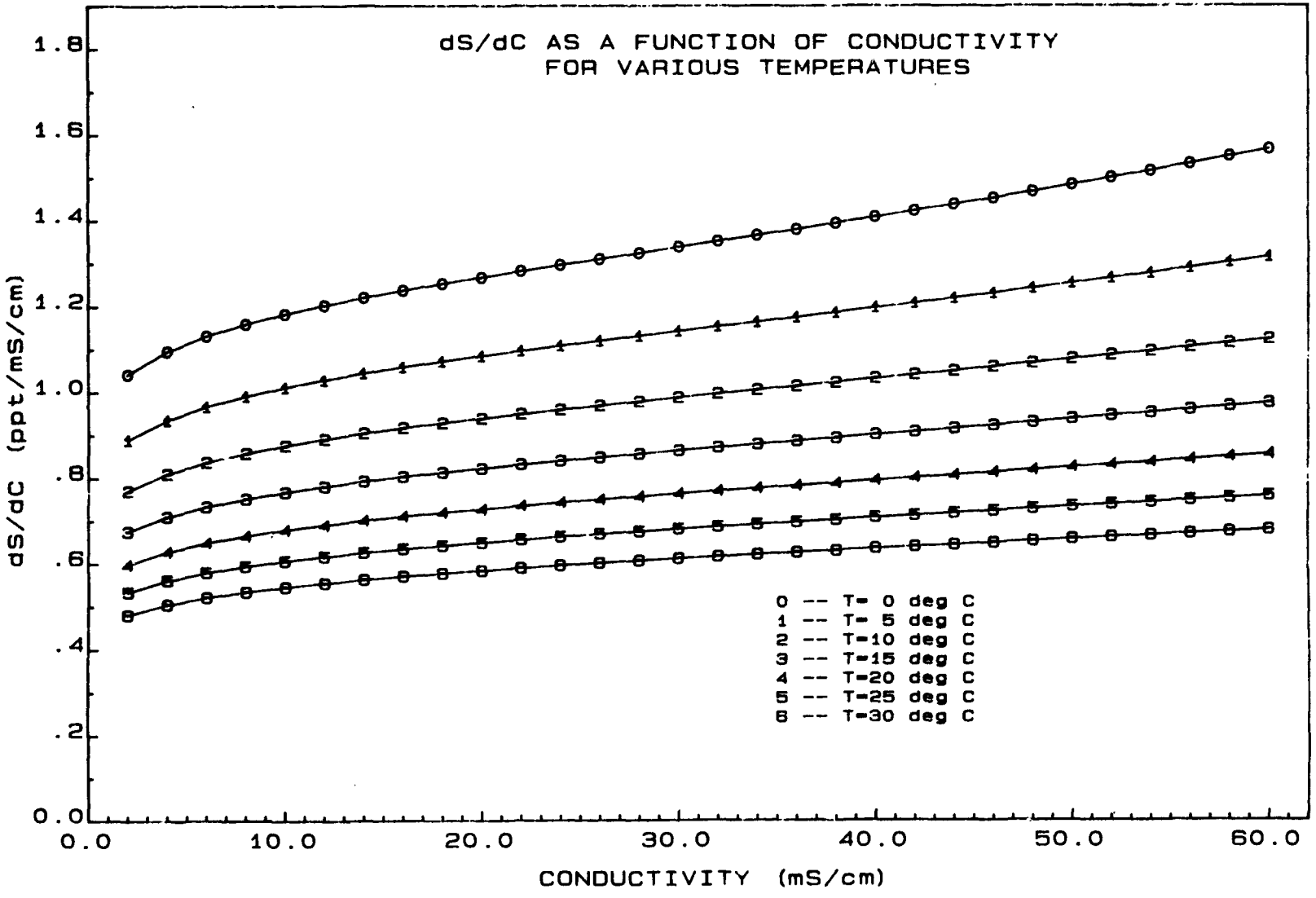

Figure 26. First partial derivative of salinity with respect to conductivity.

3.3 SALINITY

An approach for extending estimates of spectral error and variance error to error in salinity due to aliasing was developed in Section 2.6. As stressed previously, the expressions derived in that section and in Appendix C are approximate. However, the relationship between salinity, conductivity and temperature at constant pressure is nearly linear and, therefore, the accuracy of the approximate expressions is expected to be high.

The linearity question may be more definitively considered in the following way. If salinity were a linear function of temperature and conductivity, one could write

$$S(T,C) = c_1T + c_2C + c_3, \tag{87}$$

where c_1, c_2, and c_3 are constants. Then the total derivative of salinity would be

$$dS(T,C) = c_1dT + c_2dC. \tag{88}$$

But from Eq. (74), the exact expression for the total derivative of salinity is

$$dS(T,C) = \Theta_T(T,C)dT + \Theta_c(T,C)dC, \tag{89}$$

where $\Theta_T(T,C)$ and $\Theta_c(T,C)$ are the first partial derivatives of salinity with respect to temperature and conductivity, respectively.

An algorithm for computation of Θ_T and Θ_c is developed in Appendix B. This algorithm was implemented and used to compute Θ_T and Θ_c at zero pressure for a range of combinations of T and C. The results for Θ_T are plotted in fig. 25 as a family of curves which present Θ_T as a function of conductivity. Each curve corresponds to a single temperature. Figure 26 is an equivalent plot of Θ_c. Clearly, Θ_T and Θ_c are not constant.

However, review of these two plots shows that both Θ_T and Θ_C change relatively slowly with temperature and conductivity. Therefore, for small changes in T and C, salinity may be treated as linear and the correctness of previous assumptions to this effect is confirmed.

Equation (83) was used to compute the relative spectral error in salinity due to aliasing. As in the case of both conductivity and temperature, three different spectral cases were considered for purposes of the calculation. In each case the same spectral input was assumed for both temperature and conductivity. Table 19 is a tabulation of the results for the specific case of zero pressure, a temperature of 5.00°C, conductivity at 33.45 mS/cm, and salinity of 35.00 ppt. The data are presented graphically in fig. 27. As in the case of both temperature and conductivity, the extreme case of white noise shows significant error in all frequency bands, while the more realistic case of $1/f^2$ decay plus white noise shows error less than 10% while the wavelength (spatial resolution) is greater than 0.10 m.

The effect of different temperature and conductivity combinations at a constant salinity of 35.00 ppt was also considered. Results for an assumed input spectrum decaying as $1/f^2$ + white noise are tabulated in Table 20. The effect of changing temperature and conductivity conditions is almost undetectable. Comparing these results to those presented in Table 19 serves to emphasize the importance which is played by the input spectral form in determining the extent of aliasing in any parameter, including salinity.

The effect of aliasing on computed salinity variance was also evaluated using Eq. (84). The results were obtained for several cutoff frequencies, assuming that the digitized time series was idealy low-pass filtered prior to calculation of the variance. These are presented in tabular form in Table 21 and in graphical form in fig. 28. Three input spectral forms were considered and results were obtained for zero pressure, temperature of 5.00°C,

Table 19. Relative Spectral Error in Salinity for Three Input Spectral Forms. Salinity is computed for pressure = 0.00 dbars, temperature = 5.00 °C, conductivity = 33.45 mS/cm, salinity = 35.00 ppt.

Frequency (Hz)	Wavelength (m)	Relative Error (per cent)		
		White Noise	$1/f^2$	$1/f^2$ + White Noise
0.00	-	7.8	0.0	0.0
2.93	0.256	20.6	0.1	0.4
5.86	0.127	27.3	0.9	3.6
8.79	0.085	43.8	4.2	12.9
11.72	0.064	64.6	14.6	31.6
14.65	0.051	109.9	60.0	82.1

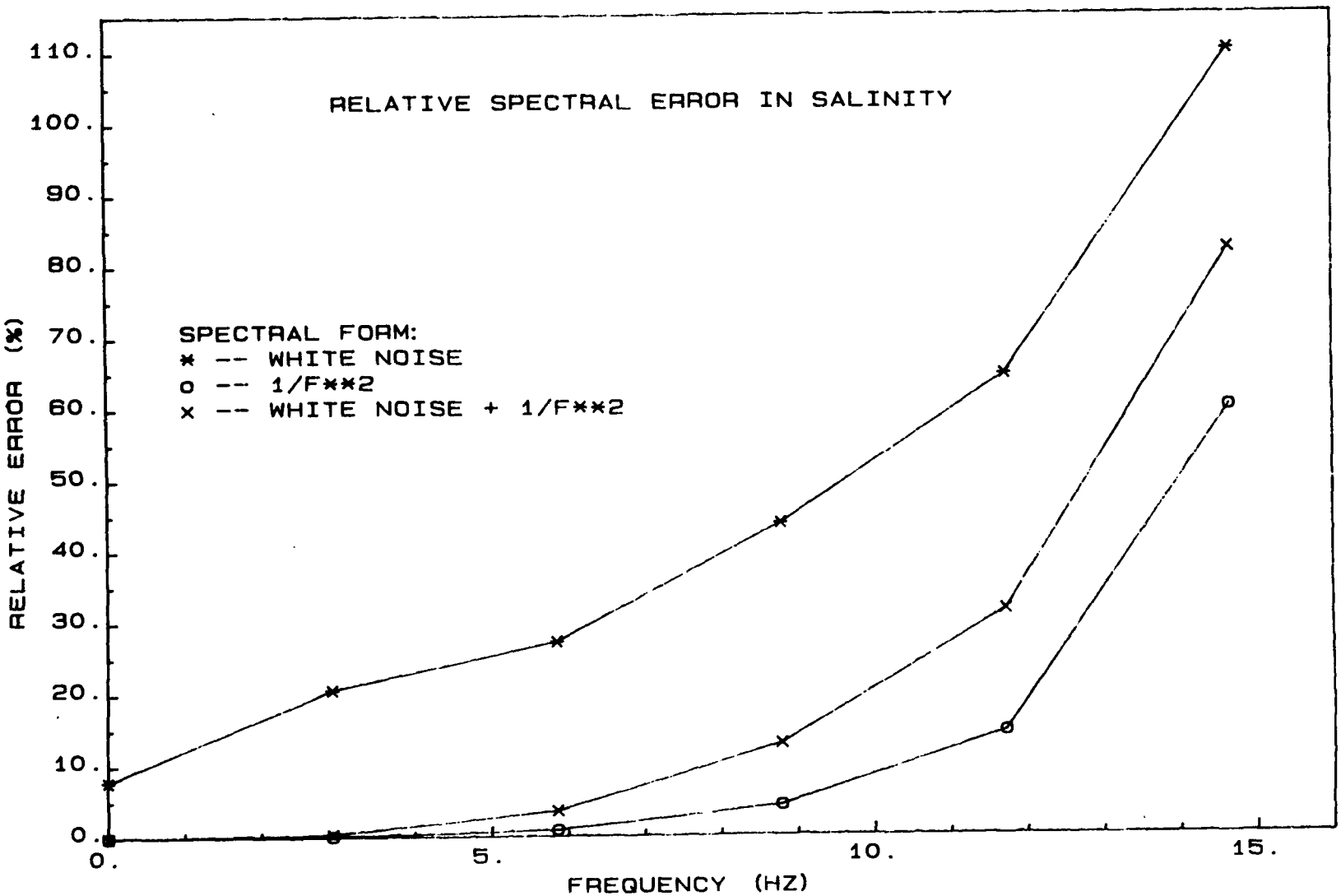

Figure 27. Relative spectral error in salinity. Three different input spectral forms are treated.

Table 20. Relative Spectral Error in Salinity for Assumed Input Spectral Form Behaving as $1/f^2$ + White Noise Tabulated As a Function of Temperature and Conductivity.

Frequency (Hz)	Wavelength (m)	Relative Error (per cent)			
		T = 5.00 °C C = 33.45mS/cm S = 35.00 ppt	T = 10.00 °C C = 38.09mS/cm S = 35.00 ppt	T = 15.00 °C C = 42.91mS/cm S = 35.00 ppt	T = 20.00 °C C = 47.91mS/cm S = 35.00 ppt
0.00	-	0.0	0.0	0.0	0.0
2.93	0.256	0.4	0.4	0.4	0.4
5.86	0.127	3.6	3.6	3.6	3.6
8.79	0.085	12.9	12.9	12.9	12.8
11.72	0.064	31.6	31.6	31.5	31.4
14.65	0.051	82.1	81.9	81.8	81.7

Table 21. Cumulative Aliasing-Induced Error in Salinity Variance After Low-Pass Filtering. Data presented are precentage errors for various filter cutoff frequencies, calculated for three different input spectral forms. Salinity is computed for pressure = 0.00 dbars, temperature = 5.00°C, conductivity = 33.45 mS/cm, and salinity = 35.00 ppt.

Frequency Limit (Hz)	Variance Error (Per Cent)		
	White Noise	$1/f^2$	$1/f^2$ + White Noise
1.46	7.8	0.0	0.0
4.39	16.3	0.0	0.1
7.32	20.7	0.0	0.2
10.25	27.3	0.1	0.4
13.18	35.6	0.2	0.7
15.63	47.2	0.4	1.2

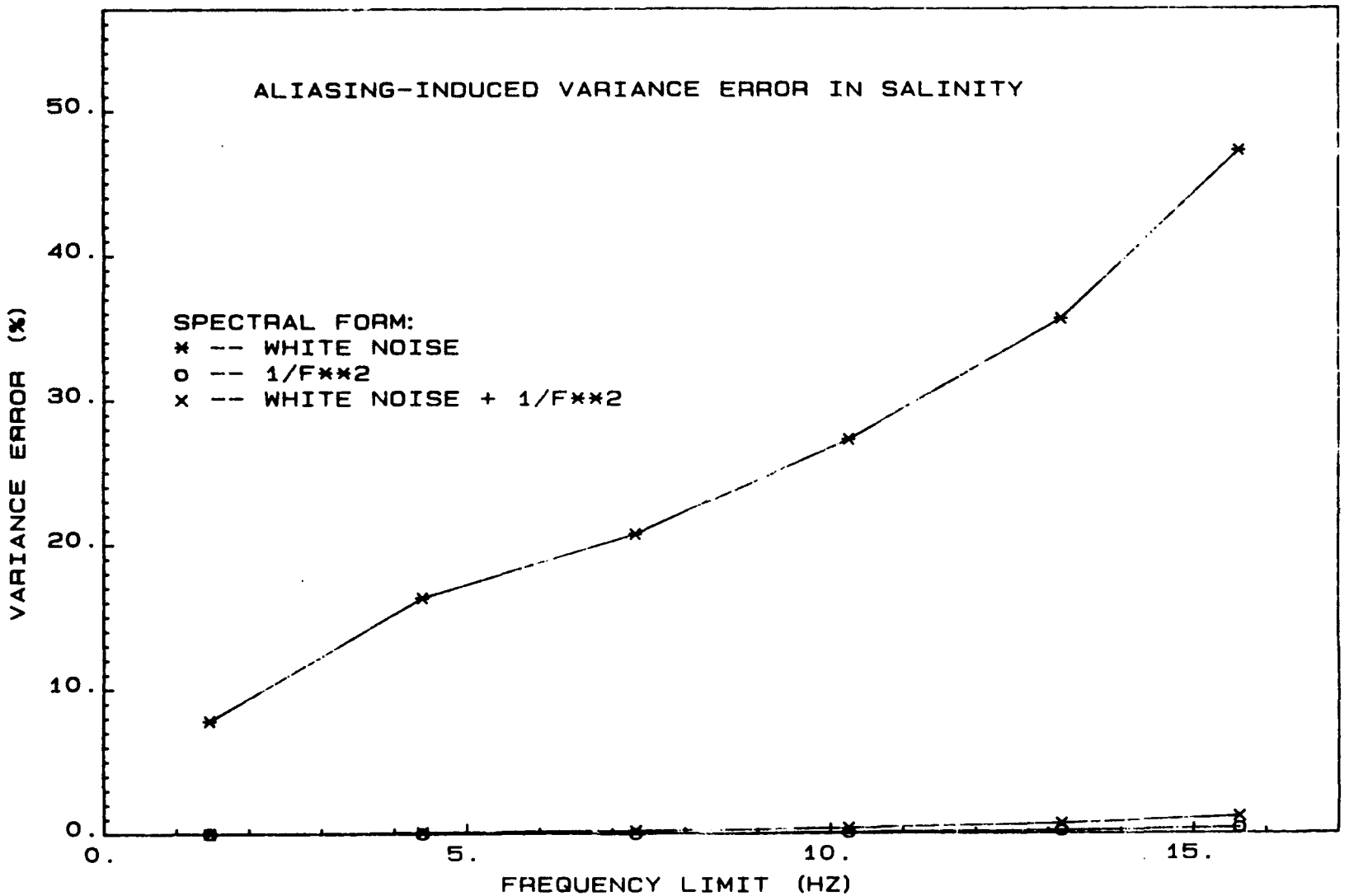

Figure 28. Aliasing - induced error in variance after low-pass filtering. Data are percentage error in time series variance for various filter cutoff frequencies, calculated for three different input spectral forms.

conductivity of 33.45 mS/cm, yielding a salinity of 35.00 ppt. The results obtained differ hardly at all from those of conductivity and temperature. Except for the white-noise case, variance error is very low for low-pass filtering schemes which one might employ.

4.0 COMPARISON WITH OTHER WORK

Gregg, et al., (1982)[13] describe an in-depth study of the transfer characteristics of the NBIS 3 cm conductivity cell. This definitive work discusses the physical basis for the observed effects and describes a physical model which incorporates these salient characteristics of the sensor and accurately predicts the measured transfer function.

The technique used by Gregg[20] for determining the conductivity–sensor transfer function utilizes a salt-stratified tank in which a stable, two-layer interface is maintained with the aid of stirring grids. Measurements of the interface show the transition region to be ∿2 cm thick. A small, two-electrode conductivity probe consisting of two 0.1 mm-diameter wires mounted 2 mm apart was used as a conductivity reference to which the test conductivity sensor was compared. Thus, assumptions regarding the thickness or other characteristics of the interface region were unnecessary. The test and reference sensors were mounted on a ram, the speed of which was controlled and measured as a digitally sampled parameter. The availability of simultaneously sampled time series of reference and test sensor data made possible the calculation of cross spectra from which the amplitude-squared and phase portions of the transfer function were computed. Time series data were acquired at a regular rate of 10,000 samples/s. Thus, the Nyquist frequency associated with the discrete spectra obtained in this fashion is well above any frequency to which the NBIS conductivity cell might be expected to respond.

From these experiments, power transfer functions were obtained for conductivity with much higher frequency resolution than reported herein for the NAVOCEANO CTD data aliasing study. The absence of jitter in the sampled data also contributed to a high level of confidence in the reported data.

The Gregg test data were acquired at various drop rates ranging from 0.05 m/s to over 3.1 m/s and the transfer function was shown to depend significantly upon the drop rate. One particular test conducted at a rate of 0.884 m/s was near the rate of 0.75 m/s used for the tests described in the NAVOCEANO study. The transfer function for this test is plotted in figure 29 together with the upper and lower limits of the conductivity power transfer function for purposes of comparison.

A comparison of Gregg's results with the NAVOCEANO study data shows: Good agreement at all frequencies; and that the transfer function estimate produced by this investigation tends to be slightly high relative to Gregg's results.

An explanation for the difference between the NAVOCEANO data and Gregg's results may be found in examining the power transfer function (PTF) for frequencies beyond the Nyquist frequency for high data rate sampling (f_N = 46.88 Hz). Plots of the PTF measured by Gregg's technique show significant, secondary side lobes centered at frequencies on the order of 40-60 Hz, depending upon sensor drop rate, and again at approximately 100 Hz. These peaks in the power transfer function, well above the high data rate Nyquist frequency, offer the opportunity for aliasing in the conductivity step response test data. Aliasing in the step response spectrum would then result in a bias of the estimated conductivity power transfer function. Use of this calculated biased transfer function for determination of error in conductivity due to aliasing will yield a biased high result. This biased result will be conservative in that the estimate of error due to aliasing will represent a worst case.

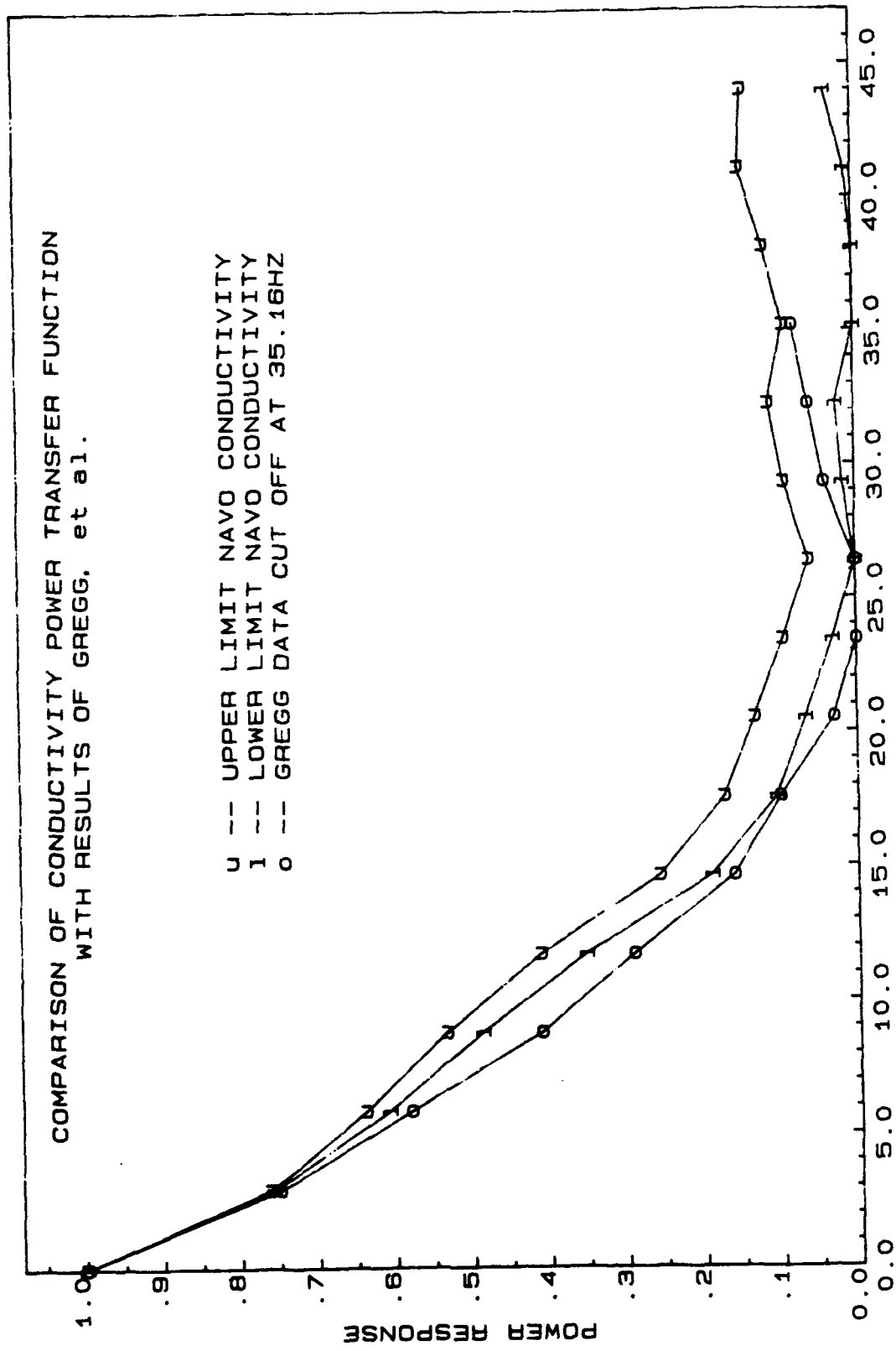

Figure 29. Comparison of conductivity power transfer function limits with results of Gregg et al.

5.0 CONCLUSIONS

The products of this investigation, described in Section 3.0, include estimates of the amplitude portion of the power transfer function for both the temperature and conductivity sensors of the NBIS Mark IIIb CTD. By assuming specific forms for the power spectrum of the input parameters, estimates for spectral error and variance error due to aliasing were derived for both conductivity and temperature and were extended, as approximations, to include the corresponding effects on calculated salinity. The conclusions which may be drawn from these results can be divided into two areas: Those relating to the methodology employed to obtain the results, and those relating to the results themselves. These two areas are discussed further in the following sections.

5.1 METHODOLOGY

The methods employed to obtain the results described in Section 3.0 include certain new techniques as well as adaptations of existing techniques for data analysis. For the purposes of this investigation, these techniques represent a product as well, since they are now made readily available to NAVOCEANO for further investigations of a similar nature and, with certain modifications as described in Section 6.0, for use in routine determination of CTD sensor transfer functions. A brief, summary description of each of the techniques used is provided below.

Transfer Function Estimation

A method of estimating the transfer functions of the NBIS CTD sensors has been developed which processes data obtained using existing NAVOCEANO laboratory and data acquisition equipment. The method does not produce the transfer function per se, but provides upper and lower bounds to the transfer function by using Shaw's method to estimate limits for the power spectrum of an unequally spaced sequence. The upper limit is adequate for

bounding the spectral effect of aliasing but a bounding approach does not produce a sufficiently accurate transfer function for use in deconvolution corrections to measured time series, such as operational CTD data. Recommendations regarding this problem are provided in Section 6.

Spectral Error Estimation

A procedure was also developed for estimating the error produced by aliasing in a spectrum of temperature or conductivity data sampled at the standard rate. The extent of aliasing in such sampled data is a direct function of the sensor transfer function and the true spectrum of the sampled process. The results presented in Section 3.0 are based on assumed input spectra, the shapes of which are derived from assumptions regarding basic physical characteristics of the data. Refined estimates could be obtained by using a more accurate representation for the spectral form, for example, actual measured data.

Variance Error Estimation

The approach used to estimate spectral error was extended to allow an estimate of aliasing-induced error in the calculated variance of a conductivity or temperature time series. Since these time series are presently low-pass filtered prior to calculation of salinity to reduce "spiking", the variance error was computed for various filter cutoff frequencies corresponding to upper limits of each of the frequency bands obtained in a spectrum of standard rate data. Parseval's relation was used to compute the variance and the variance error, so that the results are applicable to the case in which an ideal filter is used to low-pass the data.

Extensions to Salinity

On the assumption that changes in conductivity and temperature may be treated as perturbations from some mean value and are small (less than a few ^{o}C or mS/cm), a linearizing approximation was developed to extend the

spectral and variance error results to salinity. The results obtained are only approximations but are adequate to provide an estimate of the order of magnitude of the aliasing problem as it applies to salinity.

Validity of Results

The independent work of Gregg et al.,[13] described in Section 4.0, has provided a means of assessing the validity of the results of this study, at least insofar as the conductivity sensor power transfer function estimate is concerned. As indicated previously, the results of Gregg fell outside the upper and lower bounds obtained in this investigation for some frequencies. A possible explanation for this discrepancy, as discussed previously, is the presence in the step response spectrum of energy which has been aliased from frequencies higher than the high data rate Nyquist frequency. This aliased energy biases the spectral estimate and the transfer function, causing both to be higher than the correct value. The magnitude of the differences between the results of this investigation and those of Gregg is relatively small. Overall, the agreement is good, and serves to confirm the validity of the results obtained for the conductivity sensor power transfer function. Indirectly, this agreement confirms the correctness of the methodology used to obtain the transfer function.

5.2 DATA AND DATA PRODUCTS

Results beyond the conductivity transfer function have not been independently confirmed for this investigation. As pointed out previously, the validity of the specific results obtained for spectral error and variance error are dependent upon the correctness of the assumed input spectral forms. A discussion of the choice of those forms was presented in Section 3.1 and need not be repeated here. However, a discussion of the results of those calculations must be prefaced by a reminder that the choice of the spectral

forms used in this investigation was, in fact, an assumption made by the investigator. Assuming that the $1/f^2$ + white-noise model is a valid choice for the measured spectrum, the following specific conclusions may be drawn regarding the effect of aliasing upon data measured by the NBIS Mark IIIb CTD instrument.

Temperature

An extension of the temperature data product to a spatial resolution on the order of 0.10 m would not be limited by aliasing, assuming that spectral error less than or equal to 10% is acceptable. This may be seen by interpolating linearly in Table 17 to obtain an estimate of spectral error. At the laboratory drop rate of 0.75 m/sec, resolution of 0.1 m corresponds to a frequency of 7.5 Hz, for which the relative spectral error is approximately 9%. This frequency is also less than one-half the Nyquist frequency for standard data rate sampling. Lower spectral error results at lower frequencies.

An issue separate from that of aliasing is the signal-to-noise ratio in the data product itself. When a physical parameter is sensed by a transducer, an analog signal is typically produced, the level of which is proportional to the value of the sensed parameter. After sensing, the analog signal is contaminated by noise in the transducer itself and in the analog section of the data acquisition equipment. The process of conversion from an analog signal to a corresponding digital value introduces digitization noise. The spectral form of digitization noise is "white", meaning that it is evenly distributed over all portions of the frequency spectrum. Sensor and other analog noise have spectral forms which depend upon the specific sensor and circuitry involved. However, to a good approximation these may also be treated as white. It should be pointed out that the noise sources described here are internal to the system. External, or ambient, noise is not considered.

If an ideal sensor did not exhibit a frequency-dependent attenuation, then the signal-to-noise ratio (SNR) obtained would be

$$SNR(f) = S_2(f)/n$$

where $S_1(f)$ is the spectral density of the input process and n is the internal noise spectral density. Recall, however, that a real sensor possesses a power transfer function, $|T(f)|^2$, so that the measured spectral density is $S_2(f)$ given by Eq. (58). As described in Section 2.5, the measured spectrum may be corrected for transfer function effects. However, in so doing the signal-to-noise ratio is altered to

$$SNR'(f) = \frac{S_1(f)}{n} \cdot |T(f)|^2$$

Thus, in those portions of the spectrum for which the power transfer function is less than unity, the signal-to-noise ratio is reduced correspondingly. The SNR is poorest, i.e., has its lowest numerical value, in those regions where the transfer function has "rolled off" at the edge of the sensor passband. Extension of the resolution of any data products into this rolloff region of the spectrum will result in exaggeration of system noise in that frequency regime due to the transfer function correction process described in Eq. (58). A hard and fast rule cannot be established for determining the best cutoff frequency for a data product. This is especially true since both the sensor transfer function T(f) as well as the input signal level $S_1(f)$ vary during actual deployments.

If a cutoff frequency corresponding to the sensor transfer function half-power frequency is used (arbitrarily) as a rule, then the signal-to-noise power ratio will never be greater than twice the optimum value. The CTD temperature sensor transfer function reaches a half-power level at a frequency of approximately 2.8 Hz, corresponding to a spatial resolution of 0.26 m for the laboratory drop rate.

Because the temperature sensor is, to good approximation, a point sensor, its frequency response characteristics should be nearly independent of the sensor drop rate. This hypothesis is supported by the temperature data of fig. 10 which show virtually no variability from one response test to the next. Thus, the spatial frequency response of the sensor may be obtained by determining the spatial frequency k', corresponding to a particular temporal frequency f, via

$$k' = f/\nu$$

where ν is the drop rate. Spatial resolution, or wavelength, is given by

$$\lambda = 1/k' = \nu/f$$

Hence, for an operational drop rate of 1.0 m/s, the sensor half-power frequency is 0.36 m.

Thus, we conclude that the temperature data product could be extended to approximately 0.10 m without significant error due to *aliasing*. However, the signal-to-internal noise power ratio decreases below one-half the optimal value as spatial resolution becomes finer than 0.36 m and below one-fourth as resolution exceeds 0.18 m.

Conductivity

An extension of the conductivity data product to a spatial resolution on the order of 0.10 m would not be so limited. This resolution, equivalent to a frequency of 7.5 Hz at the laboratory drop rate, corresponds roughly to the half-power point for the conductivity sensor transfer function. This frequency is also less than half the Nyquist frequency for standard data rate sampling. As shown in Table 17, spectral error at a frequency of 7.5 Hz would be on the order of 10% and would be less for lower frequencies.

For the operational CTD downcast drop rate of 1.0 m/s, a spatial resolution of 0.10 m corresponds to a 10 Hz frequency. This is still substantially below the Nyquist frequency. Unlike the temperature sensor, the CTD conductivity sensor transfer function varies greatly with drop rate. Therefore, it is not possible to infer results from one drop rate to another. However, Gregg, et al.,[13] report results for several drop rates near 1.0 m/sec, showing that the power transfer function plotted in k' space does not change dramatically with drop rate. We may conclude that the value of the transfer function will be somewhat changed under operational conditions, but will still allow a good signal-to-noise ratio for the sensed signal.

Salinity

A review of Table 19 reveals that salinity is not adversely affected by aliasing for frequencies below 7.5 Hz and spatial resolutions coarser than 0.1 m. This is to be expected since a similar conclusion was reached for the two primary factors, conductivity and temperature. However, due to the restriction on extension of temperature beyond 2.8 Hz based on deterioration in the signal-to-noise ratio, a similar restriction should apply to salinity. In summary, we conclude that while aliasing does not prevent extension of data products to a spatial resolution on the order of 0.10 m, the rapid rolloff of the temperature sensor beyond 0.36 m does.

6.0 RECOMMENDATIONS

Sensor Performance

This study has shown that data products obtained from NBIS Mark IIIb CTD data are not significantly affected by aliasing at the present operational drop rate of 1.0 m/sec, as long as the products have a spatial resolution no finer than 1.0 m. In planning for extension of data products to finer resolution, the first barrier to be surmounted is that of the limited frequency response of the presently-used thermistor/platinum wire temperature sensor. It is recommended that an effort be undertaken to improve the high-frequency performance of this sensor, making its response comparable to that of the fast 3 cm conductivity cell.

If this improvement is realized, then an enhancement of data resolution to something on the order of 0.1 - 0.2 m should be possible without serious distortion due to aliasing. Improvement in resolution beyond 0.1 - 0.2 m will require an increase in the data sampling rate of the CTD so that the Nyquist frequency will be substantially higher than the frequencies of interest.

Data Correction

As improved resolution forces an expansion of the data frequency band, low-pass filtering of conductivity and temperature will no longer be a practicable means of eliminating salinity spikes. The most accurate alternative will be deconvolution correction of the individual sensor time series using the respective transfer functions. This will raise several problem areas which must be dealt with.

As indicated previously, deconvolution requires that both the amplitude and phase portions of the sensor transfer function be known. In addition, Gregg et al.[13] have pointed out that the relative phase of temperature and conductivity must also be known in order to produce a correct salinity.

Since the present drop rate procedure is not capable of directly determining the information, a significant modification of the testing procedure will be necessary. The changes required are:

1) Provide for variation, control, and measurement of the sensor drop rate,
2) Provide for data sampling at a fixed sampling frequency (without jitter) and at a sampling rate much greater than 100 Hz,
3) Provide for measurement of the salinity interface during the drop test with a reference probe.

A second problem is that of contamination of the data by noise which is amplified during the deconvolution process, as described in Section 5.2. Matsuyama[21] has discussed this problem in considrable depth. While Matsuyama presents a variation in the conventional deconvolution procedure to reduce contamination, a complete solution is not obvious and further investigation will be required.

A third problem which Gregg et al. [13] have also identified is that of data correction due to variation in the sensor drop rate. The variation in drop rate is primarily due to ship motion, particularly heave and roll. As has been discussed previously, the conductivity sensor transfer function changes with changes in the drop rate. This requires that conductivity be corrected via some form of dynamic deconvolution procedure in which both the data and the transfer function change with time. Such a correction procedure may be possible, but the existence of one is not known to the investigator. An alternative proposed by Gregg et al. would be mechanical compensation of the CTD drop rate via a controlled winch or other means so that vertical motion is nearly constant.

7.0 REFERENCES

1. Bowling, B. and T. Lai, "The Use of Linear Prediction for the Interpolation and Extrapolation of Missing Data and Data Gaps Prior to Spectral Analysis," Massachusetts Institute of Technology Lincoln Lab, Technical Report No. 1979-46. Lexington, MA, 18 June 1979.

2. Ackerman, C.L., "Effects of Non-Uniform Sampling and Limiting on Correlation Functions," Pennsylvania State University, Ordnance Research Lab., Technical Memorandum TM 676-2341-02, University Park, PA, 13 August 1969.

3. Jones, H. "Spectrum Estimation with Unequally Spaced Observations," Interim Report, AFOSR Contract No. F44620-69-C-0035, November 1970.

4. Singleton, R.C. and A.G. Larson, "Spectral Analysis of Unequally Spaced Data Samples," Stanford Research Institute, ONR Contract No. N00014-71-C-0380, Menlo Park, CA., April 1972.

5. Masry, E., "Discrete-Time Spectral Estimation of Continuous-Time Processes - the Orthogonal Series Method," The Annals of Statistics, Vol. 8, No. 5, 1980.

6. McClellan, J.H., "Multi-Dimensional Spectral Estimation for Unequally Spaced Data," Massachusetts Institute of Technology, Research Lab of Electronics, Army Research Office, Contract No. DAAG29-81-K-0073, June 1982.

7. Shaw, L., "Spectral Estimates from Nonuniform Samples," IEEE Trans. Audio and Electroacoustics, Vol. AU-19, No. 1, March 1971.

8. Jenkins, G.M. and D.G. Watts, Spectral Analysis and Its Applications, Holder - Day, San Francsico, 1968.

9. Mayoral, C.R., "Determination of CTD Sensor Responses for Use in Deconvolution Filtering," Proceedings of the International STD Conference and Workshop, La Jolla, CA, 8-11 February 1982.

10. Paige, M.A., "Response Characteristics of the Neil Brown Instrument Systems, Inc. Mark III CTD to Step Changes in Temperature and Conductivity," Naval Oceanographic Office Technical Report TR-259, Bay St. Louis, MS, October 1980.

11. Geiskes, J.M., "A New Definition of Salinity," Proceedings of the International STD Conference and Workshop, La Jolla, CA, 8-11 February 1982.

12. Neil Brown Instrument Systems, Inc., Operations Manual for the Mark III b CTD, Cataumet, MA.

13. Gregg, M.C., J.C. Schedvin, W.C. Hess, and T.B. Meagher, "Dynamic Response Calibration of the Neil Brown Conductivity Cell," J. of Physical Oceanography, Vol. 12, p. 720, July 1982.

14. Bracewell, R.N., The Fourier Transform and Its Applications, McGraw-Hill Book Co., New York, 1978.

15. Welch, P.D., "The Use of the Fast Fourier Transform for the Estimation of Power Spectra: A Method Based on Time Averaging Over Short Modified Periodograms," IEEE Transactions on Audio and Electroacoustics, Vol. AU-15, No. 2, June 1967.

16. Blackman, R.B., and J.W. Tukey, The Measurement of Power Spectra from the Point of View of Communications Engineering, Dover Publications, Inc., New York, 1959.

17. Brenner, N., "FOUR 1," MIT Lincoln Laboratory, (Unpublished program listing), July 1967.

18. Kay, S.M. and S.L. Marple, Jr., "Spectrum Analysis - A Modern Perspective," Proceedings of the IEEE, Vol. 69, No. 11, Nov. 1981.

19. Ross, D.A., Introduction to Oceanography, Appleton-Century-Crofts, New York, 1970.

20. Gregg, M.C., T.B. Meagher, E.E. Aagaard, and W.C. Hess, "A Salt-Stratified Tank for Measuring the Dynamic Response of Conductivity Probes," IEEE J. of Oceanic Eng., Vol. OE-6, No. 4, p. 113, Oct. 1981.

21. Matsuyama, B.M., Recovering Oceanic Signals by Means of Deconvolution and Equalization, Thesis (MSEE) University of Washington, Seattle, Washington, 1983.

APPENDIX A

PLOTS OF HIGH DATA RATE TIME SERIES

APPENDIX A

PLOTS OF HIGH-DATA-RATE TIME SERIES

Time series of each of the response test data sets are plotted in the following figures. Two sets of such data were acquired for analysis in this investigation. The initial set (data set A) consisted of five temperature response tests, T01A - T05A, and five conductivity response tests, C01A - C05A. A second set (data set B) consisted of twelve conductivity response tests, C01B - C12B. All data were acquired using the same CTD and sensors.

Data were acquired at a nominal sampling rate of 93.75 Hz. Due to the data acquisition procedure, sampling occurred with some jitter. The data of this appendix are plotted as though samples were acquired at intervals of 10 msec, 10 msec, and 12 msec, respectively.

Figures A-1 through A-5 and A-11 through A-22 are plots of conductivity vs. time with conductivity in mS/cm.

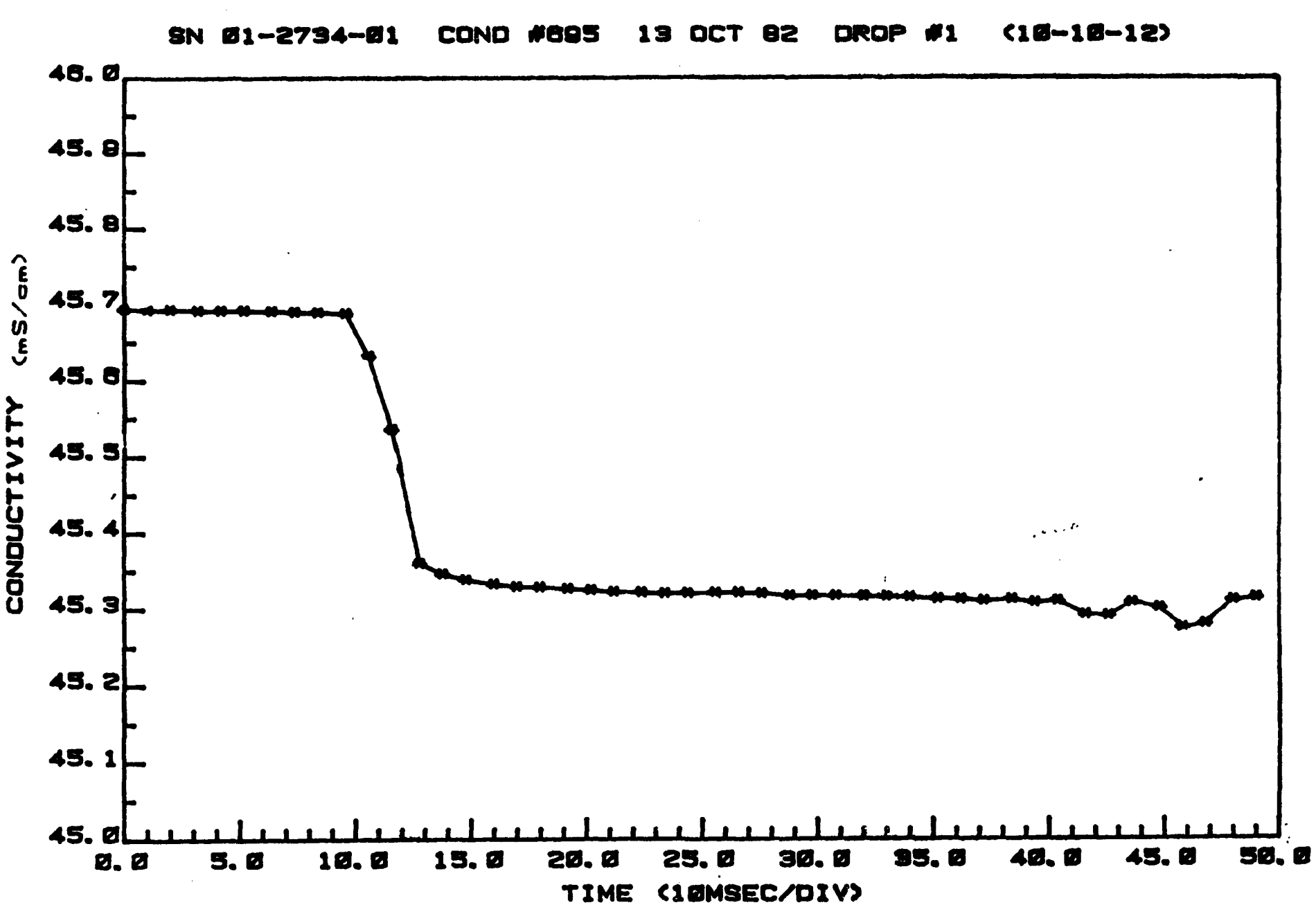

Figure A-1. Time Series of Conductivity Acquired During Response Test C01A.

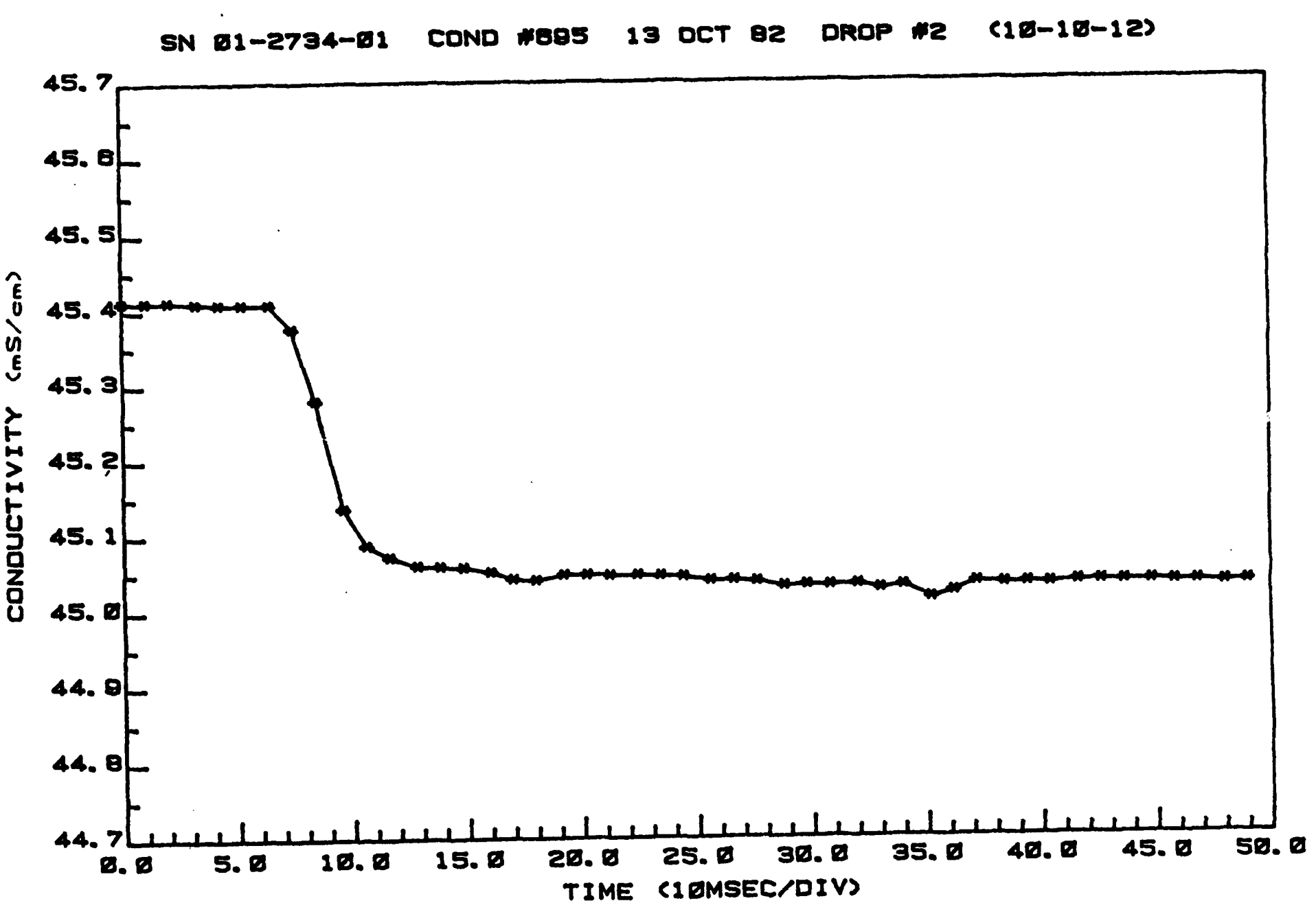

Figure A-2. Time Series of Conductivity Acquired During Response Test C02A.

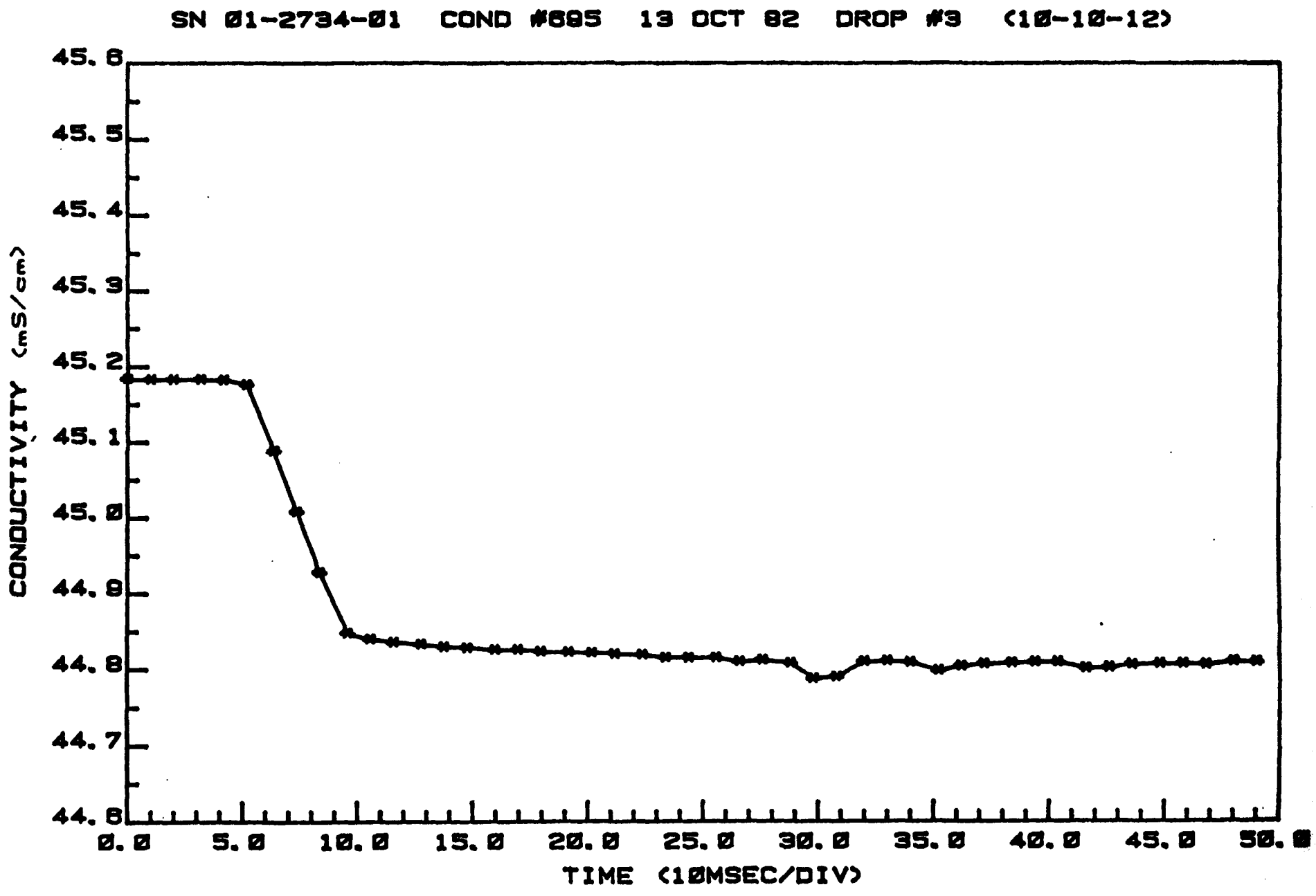

Figure A-3. Time Series of Conductivity Acquired During Response Test C03A.

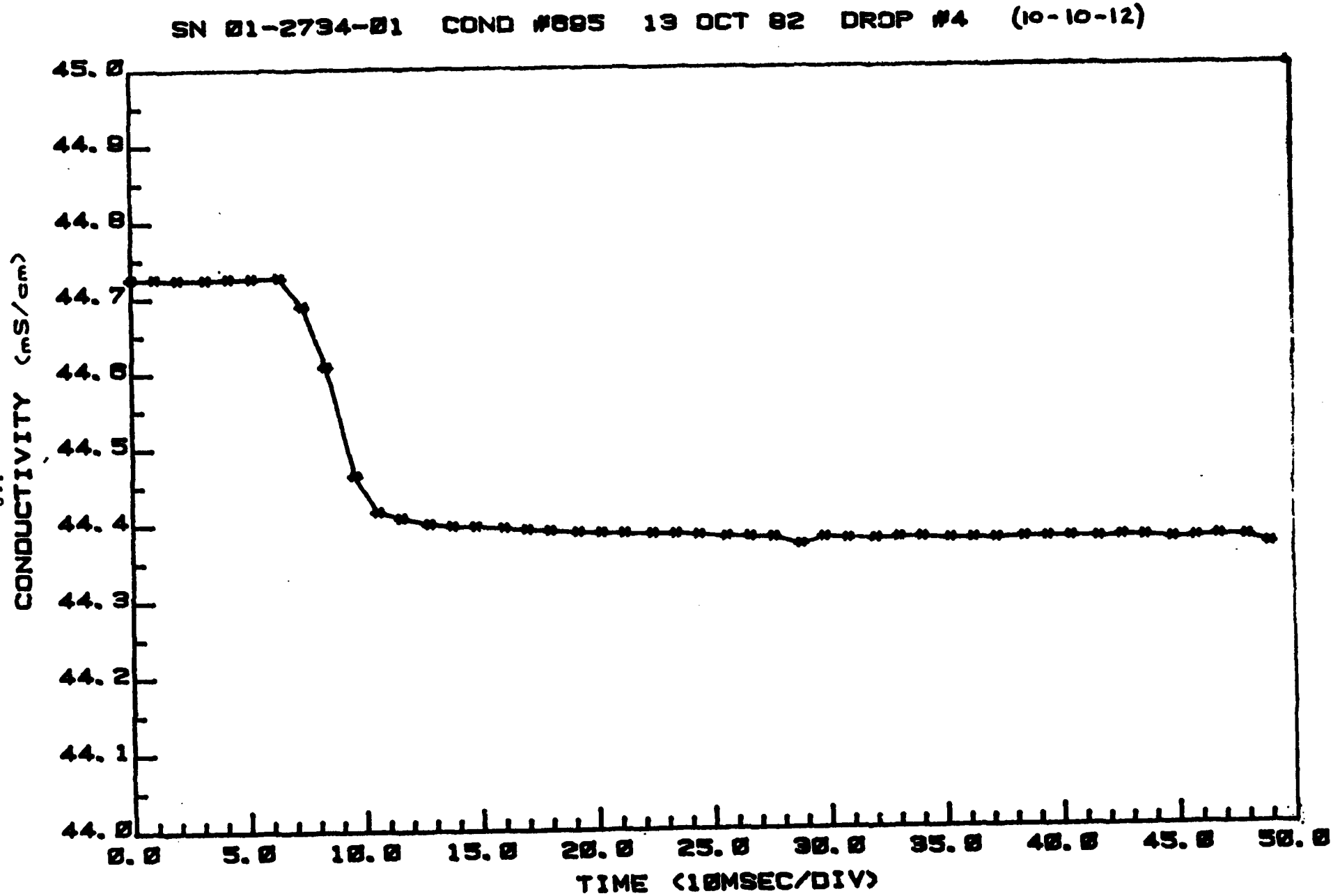

Figure A-4. Time Series of Conductivity Acquired During Response Test CO4A.

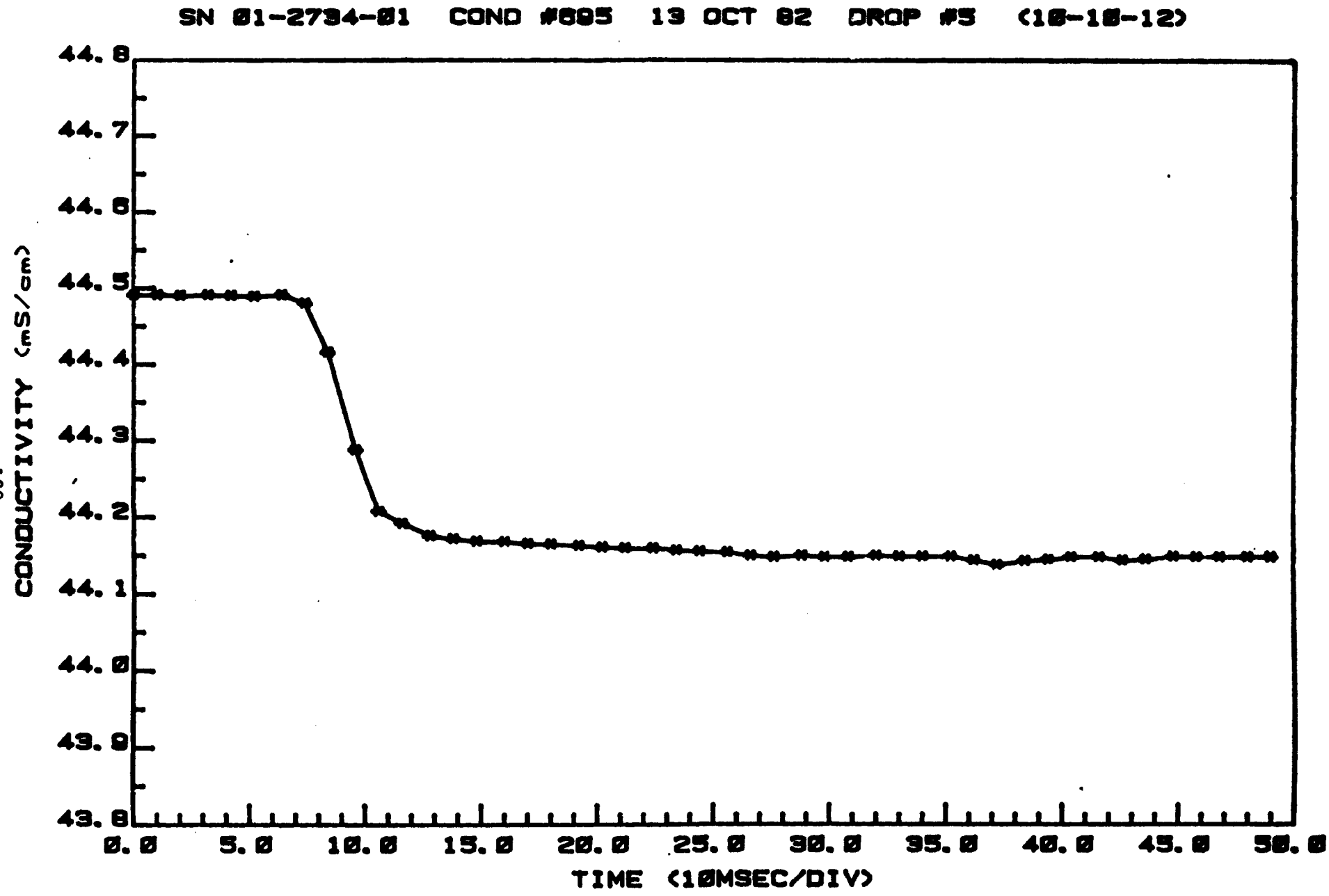

Figure A-5. Time Series of Conductivity Acquired During Response Test C05A.

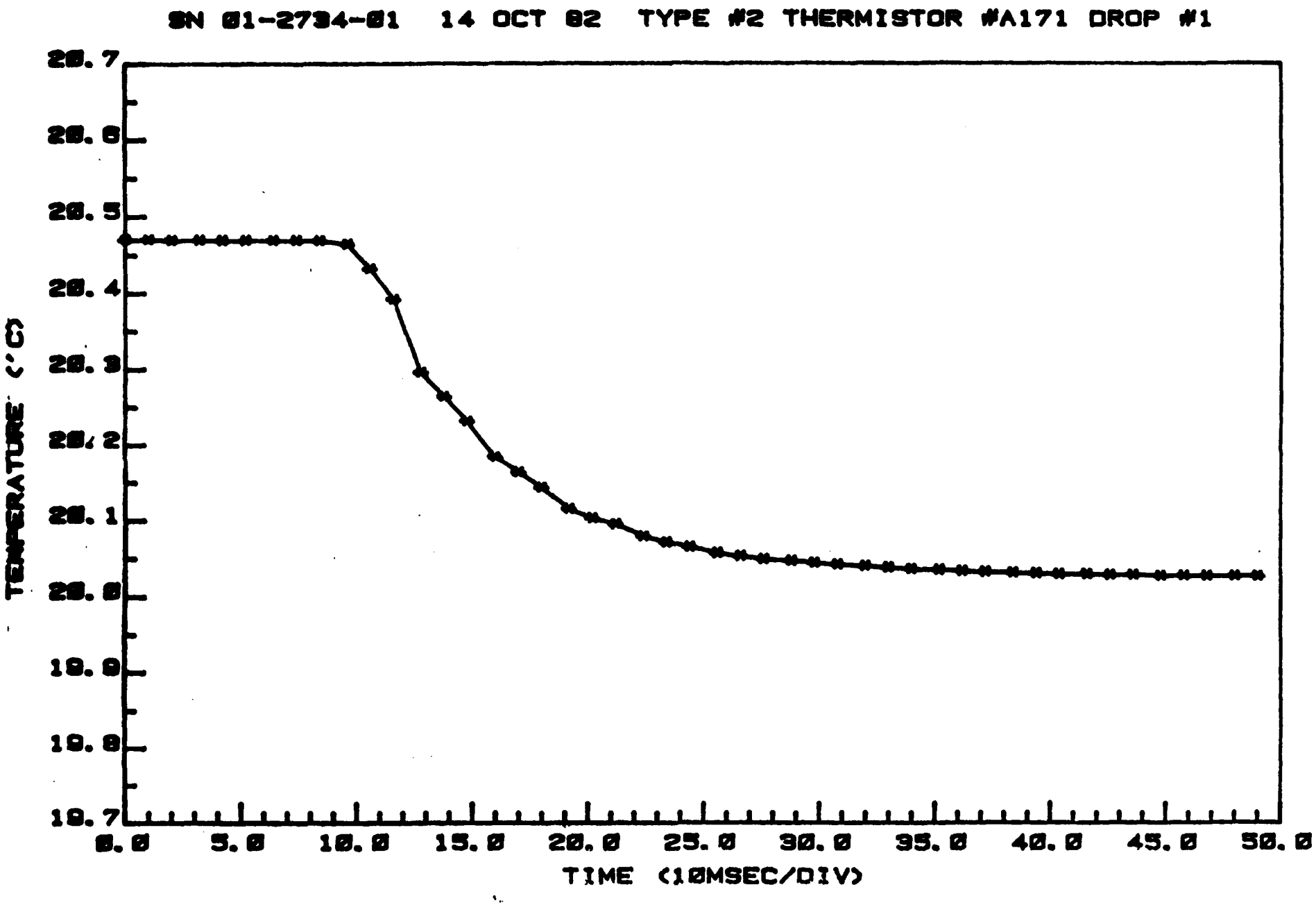

Figure A-6. Time Series of Temperature Acquired During Test T01A.

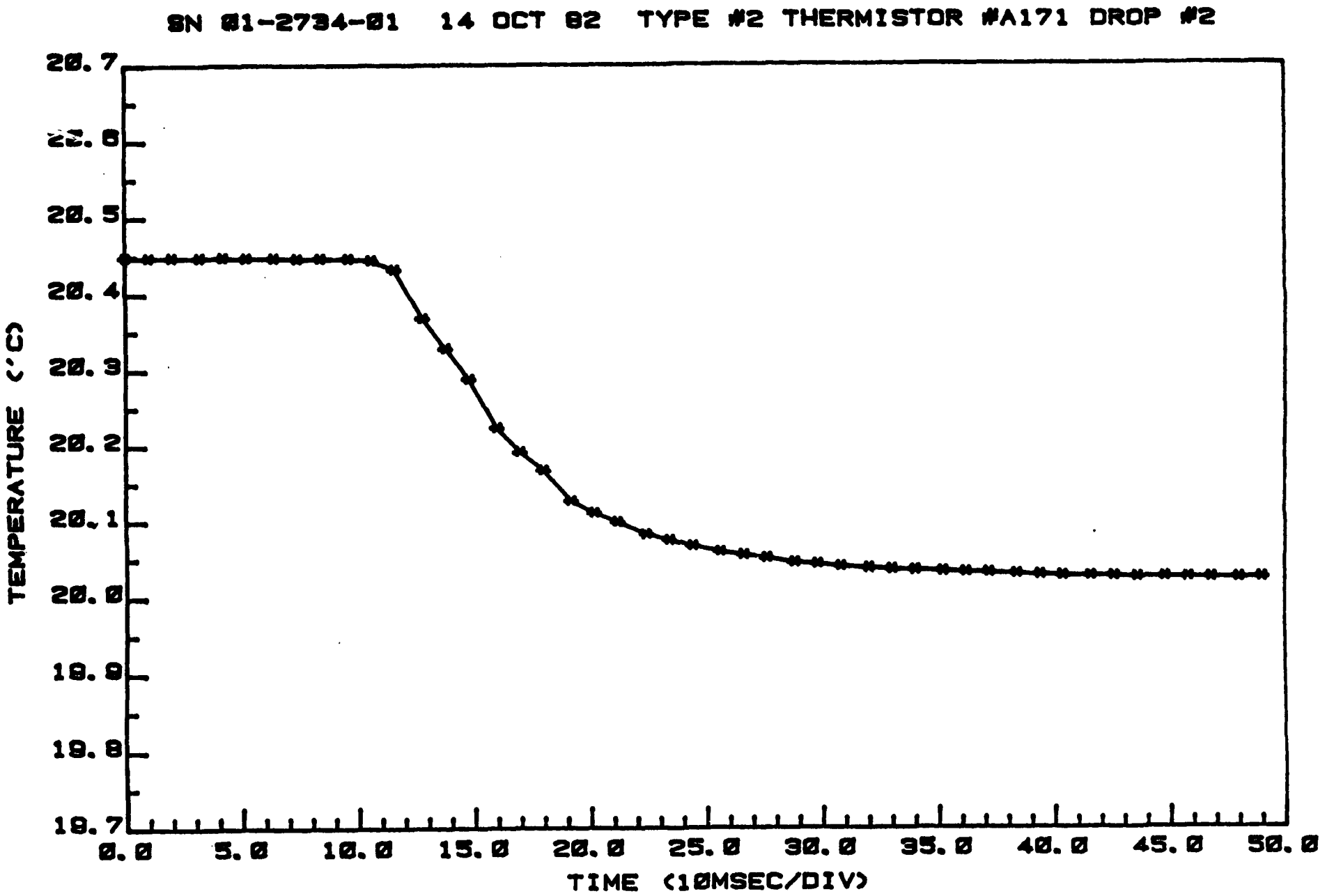

Figure A-7. Time Series of Temperature Acquired During Response Test T02A.

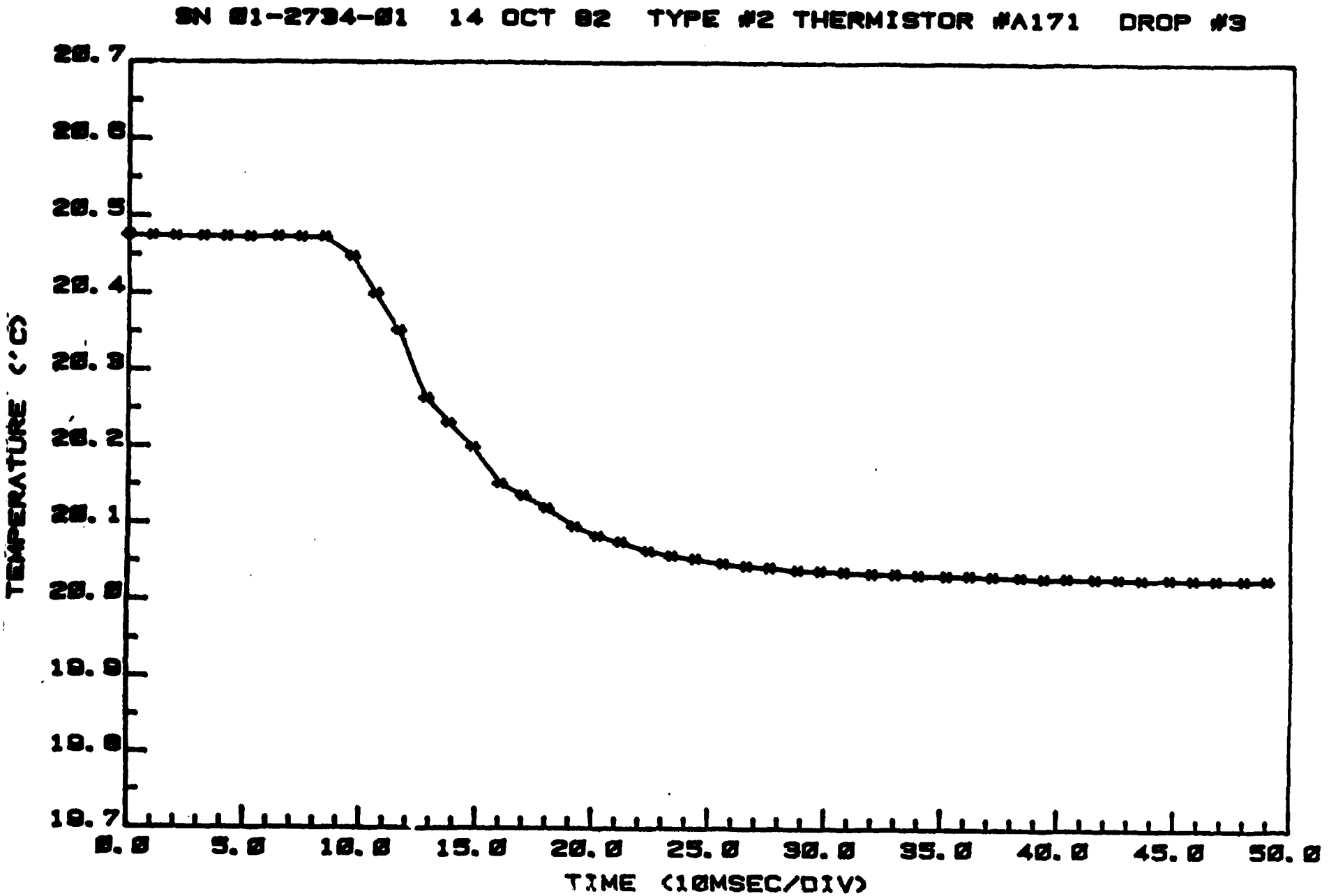

Figure A-8. Time Series of Temperature Acquired During Response Test T03A.

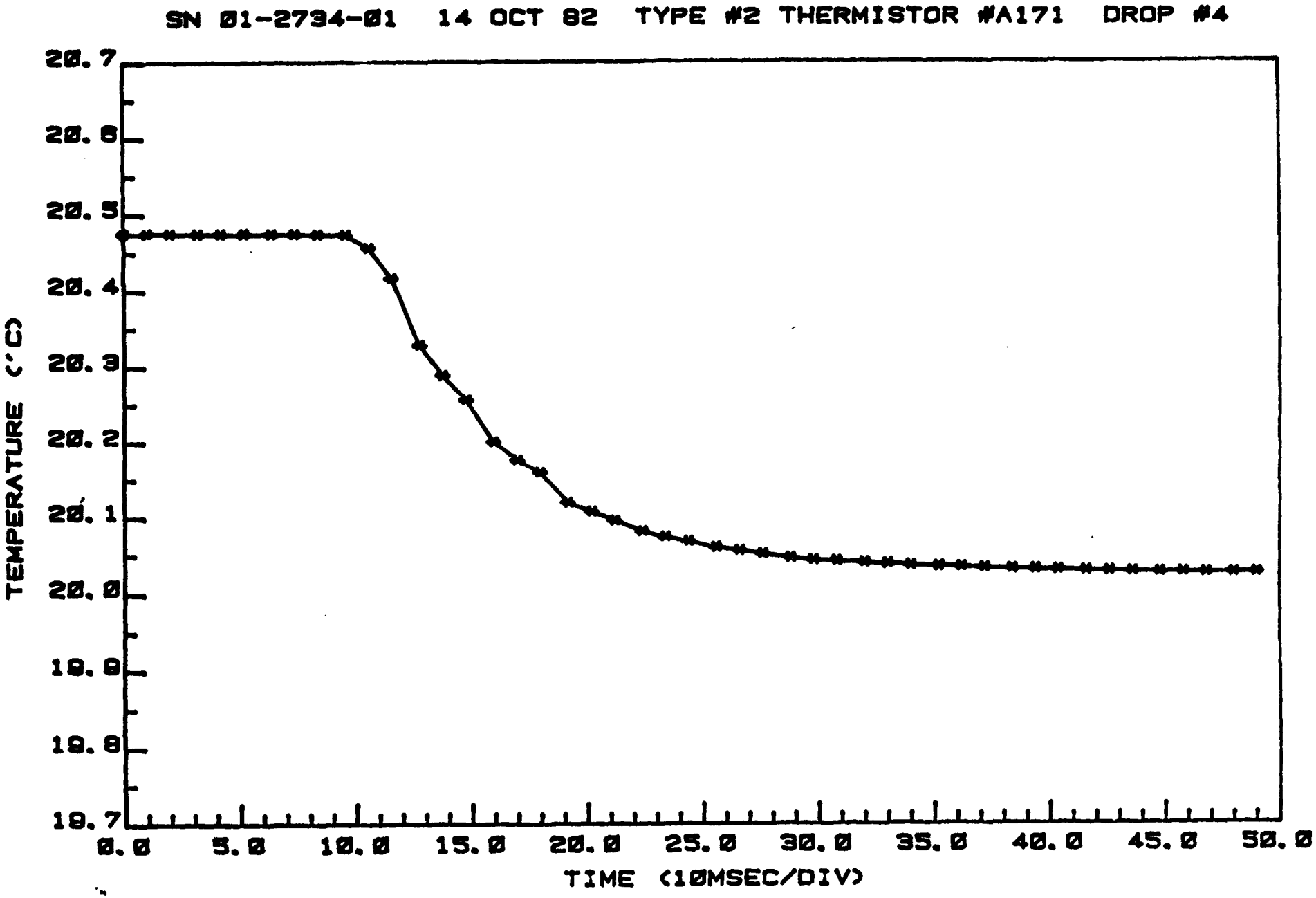

Figure A-9. Time Series of Temperature Acquired During Response Test T04A.

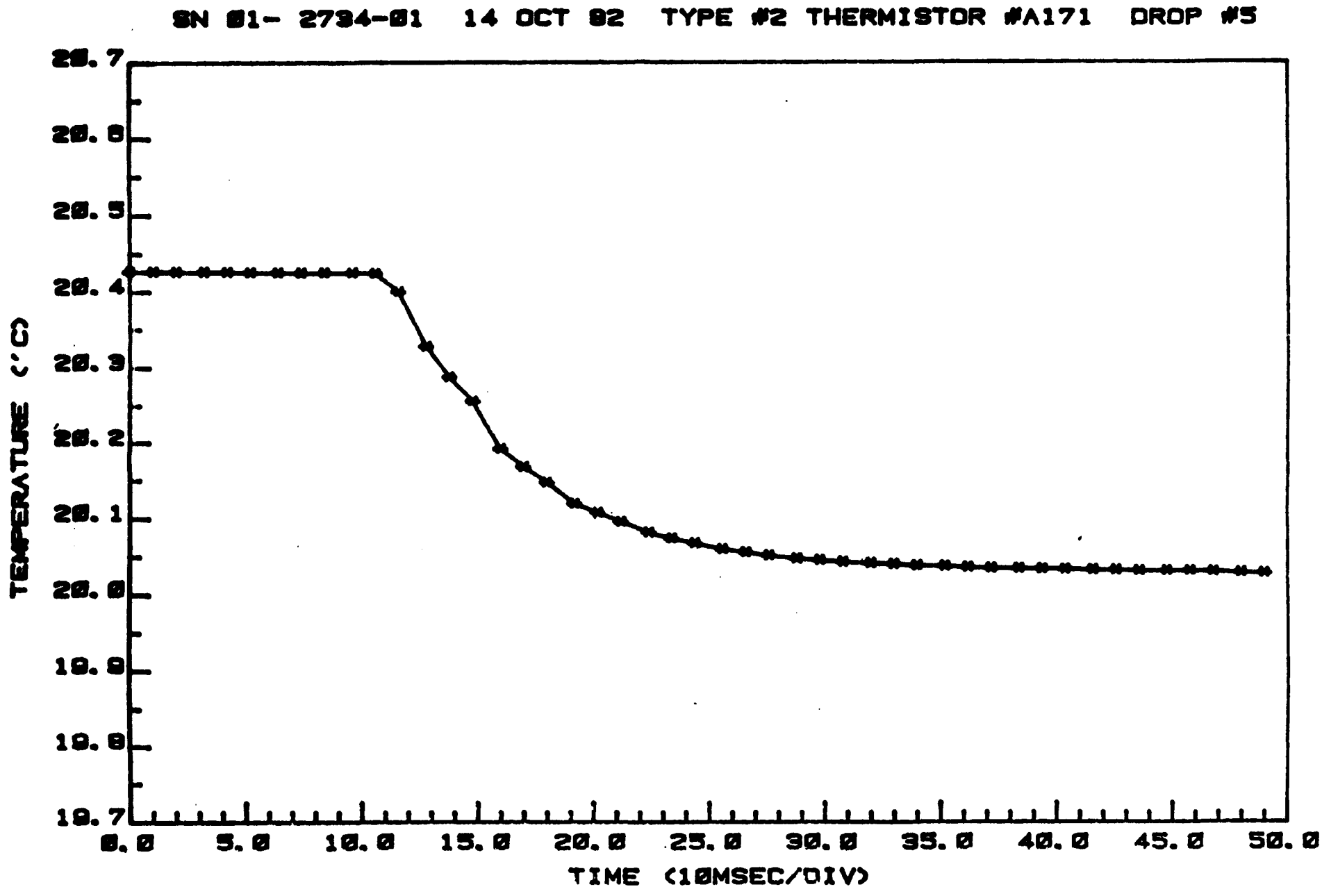

Figure A-10. Time Series of Temperature Acquired During Response Test T05A.

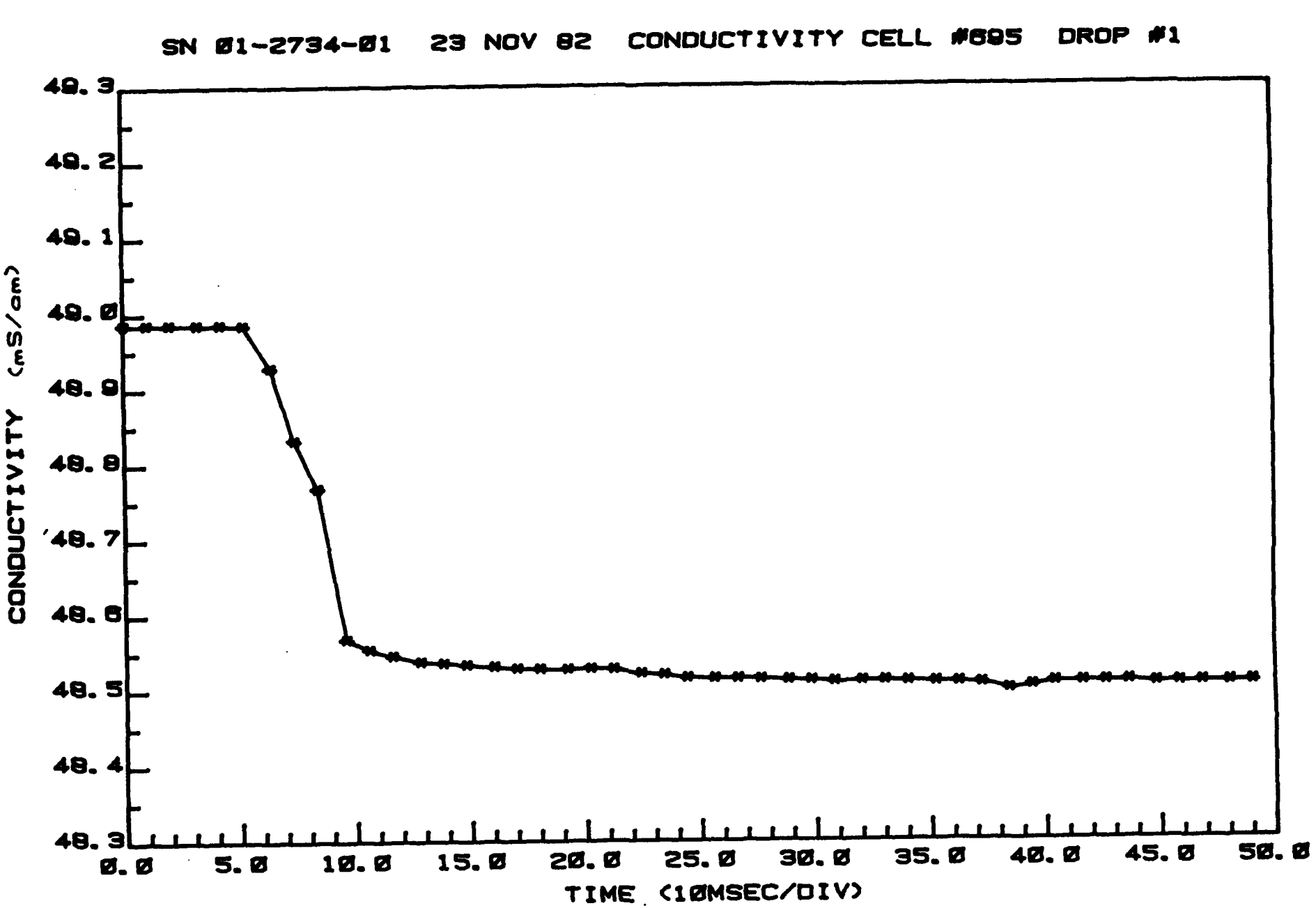

Figure A-11. Time Series of Conductivity Acquired During Response Test C01B.

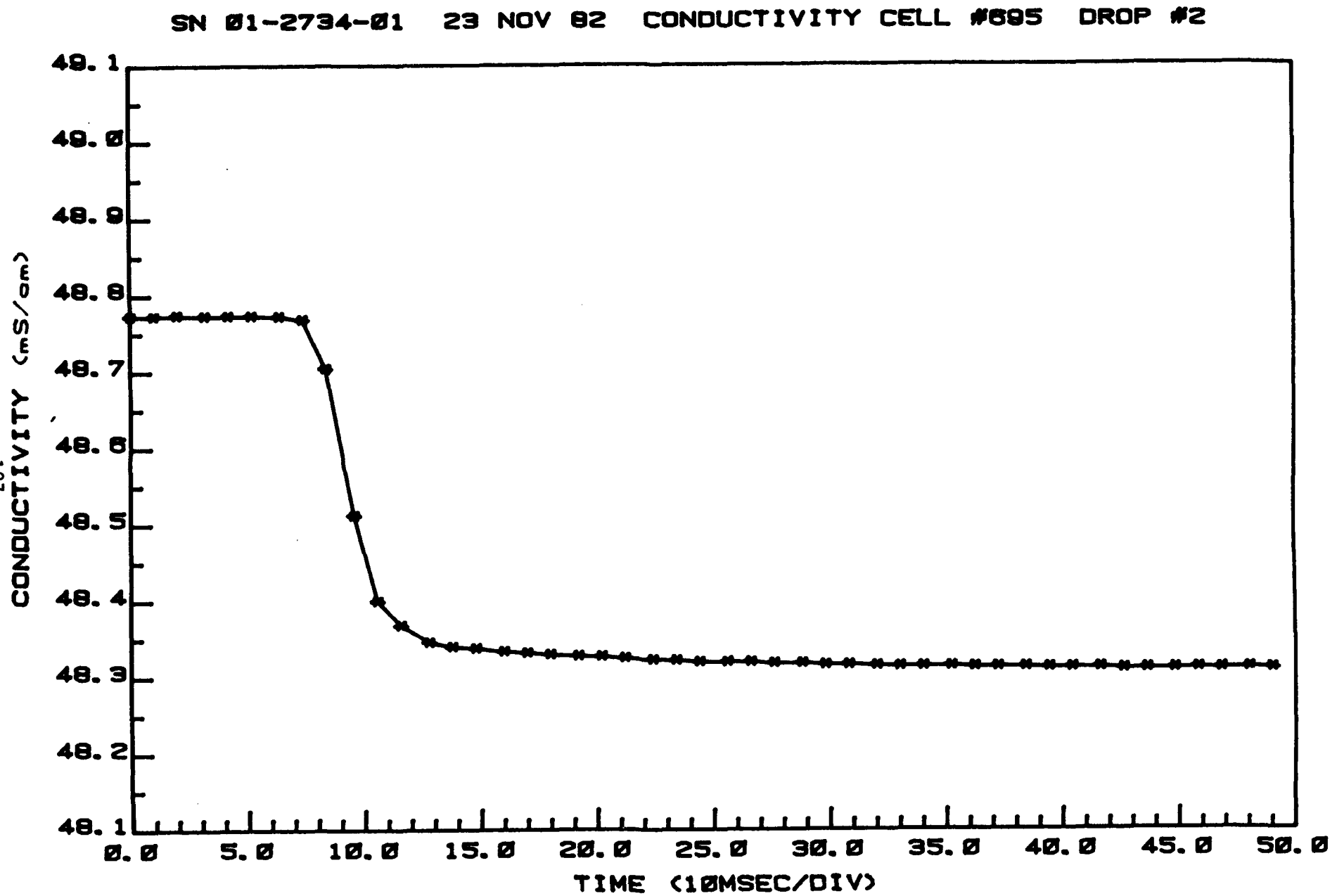

Figure A-12. Time Series of Conductivity Acquired During Response Test C02B.

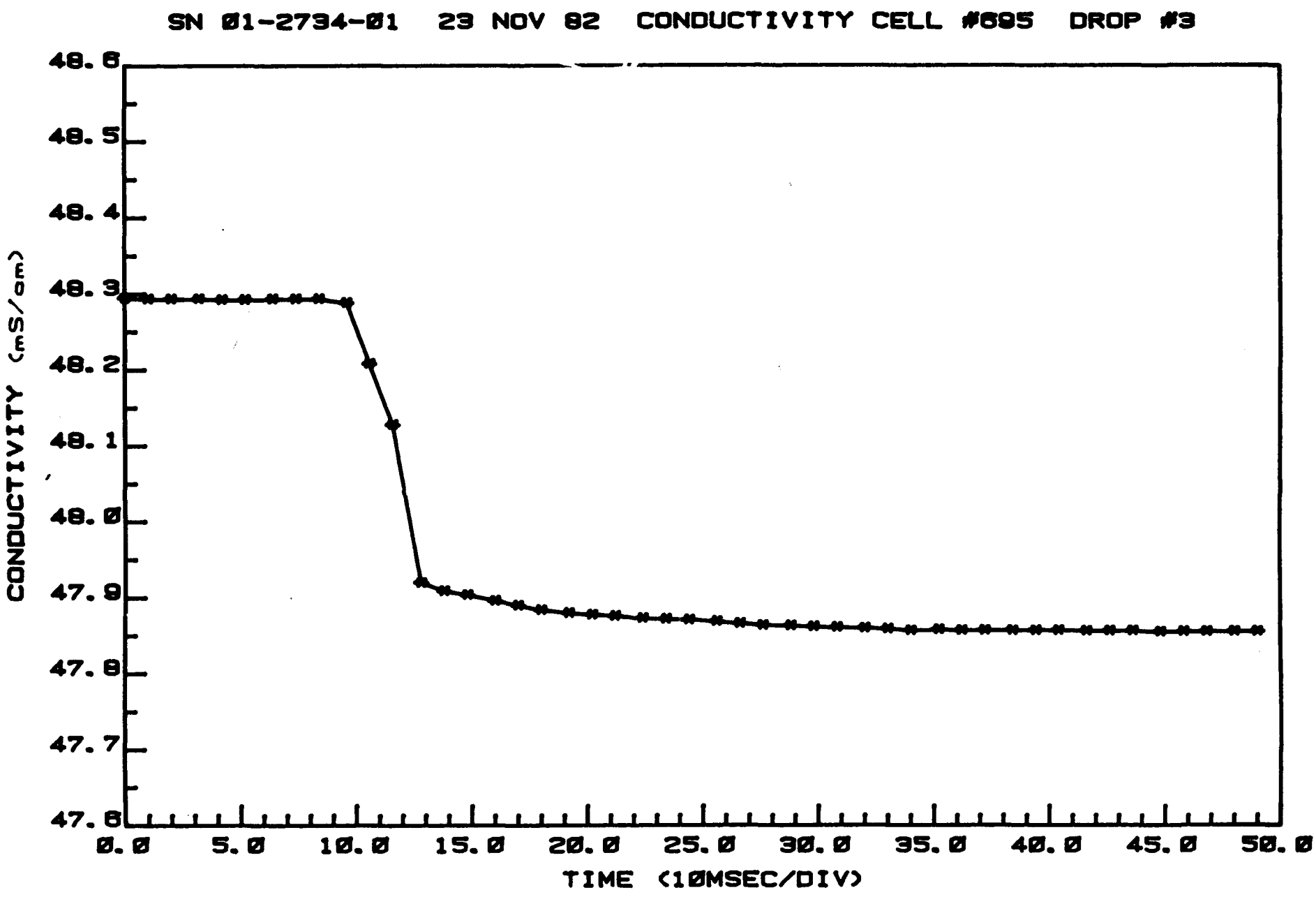

Figure A-13. Time Series of Conductivity Acquired During Response Test CO3B.

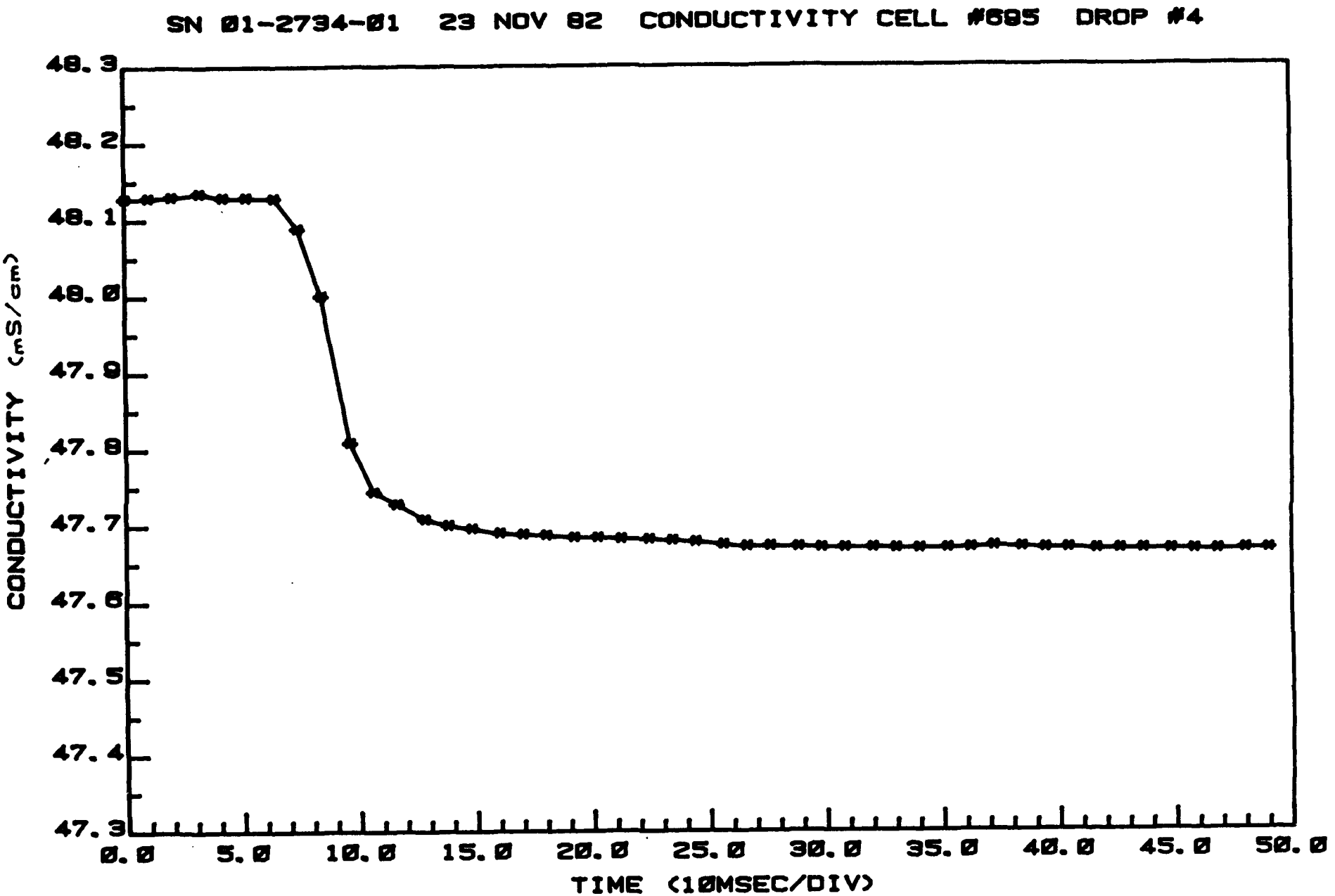

Figure A-14. Time Series of Conductivity Acquired During Response Test C04B.

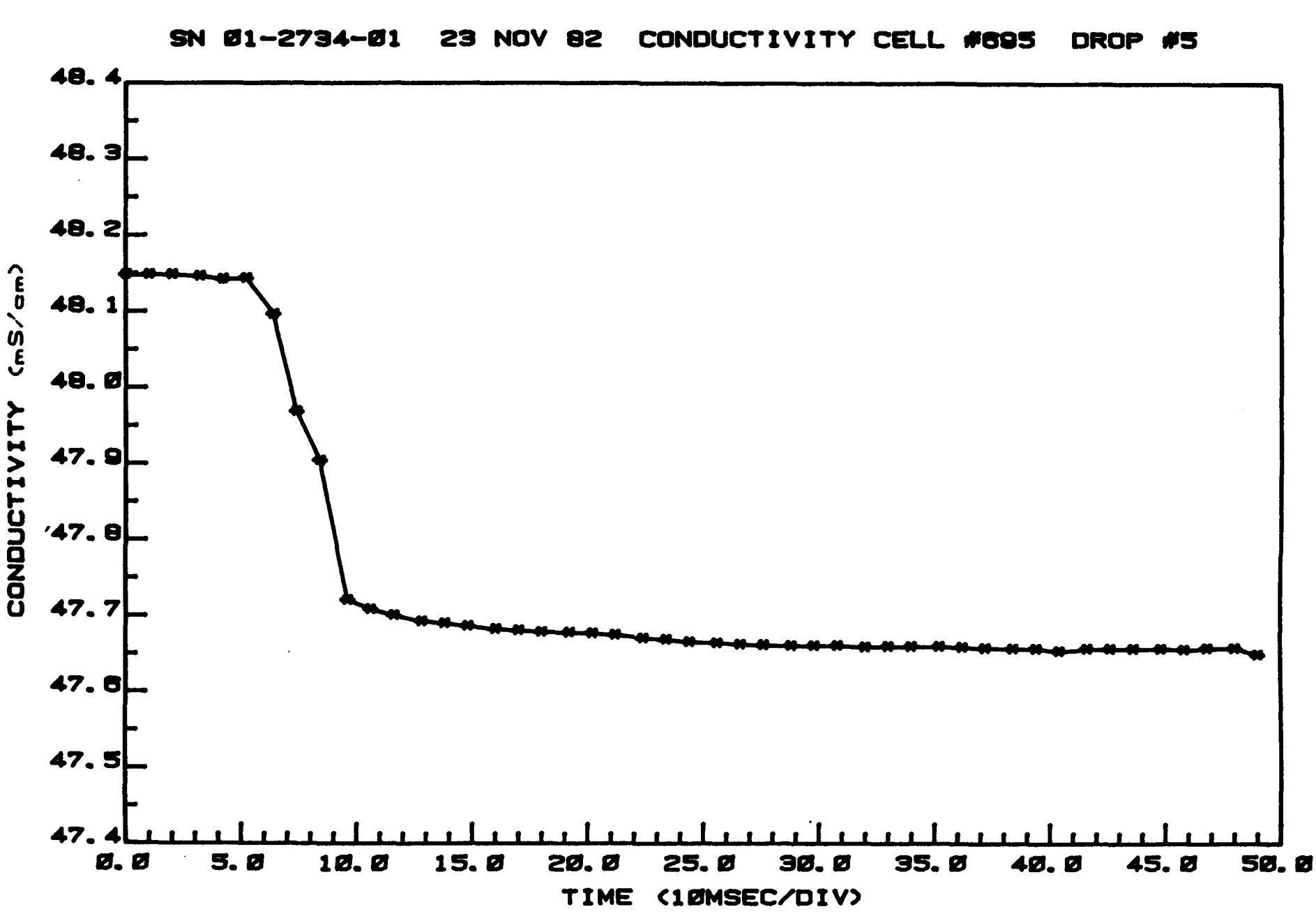

Figure A-15. Time Series of Conductivity Acquired During Response Test C05B.

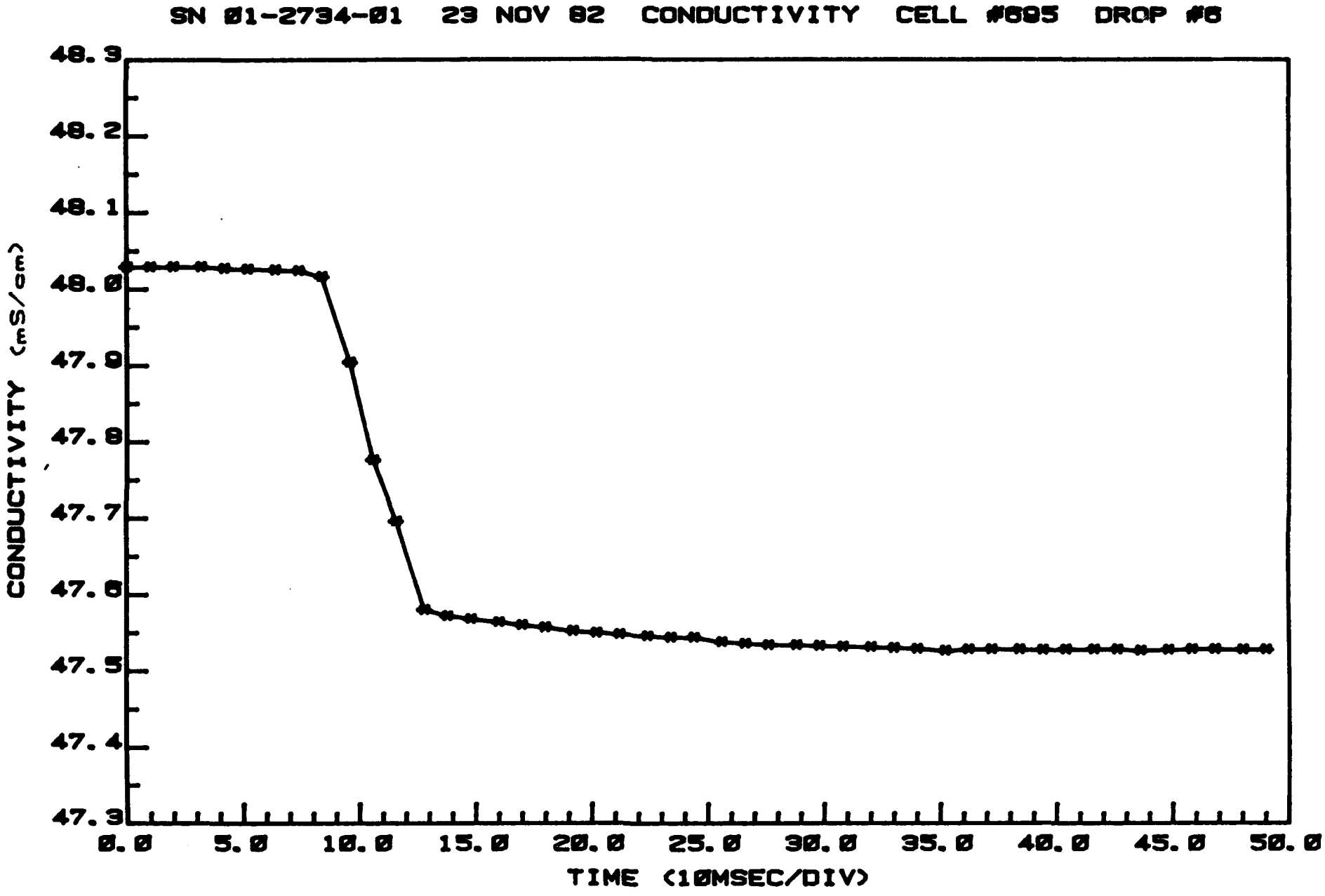

Figure A-16. Time Series of Conductivity Acquired During Response Test C06B.

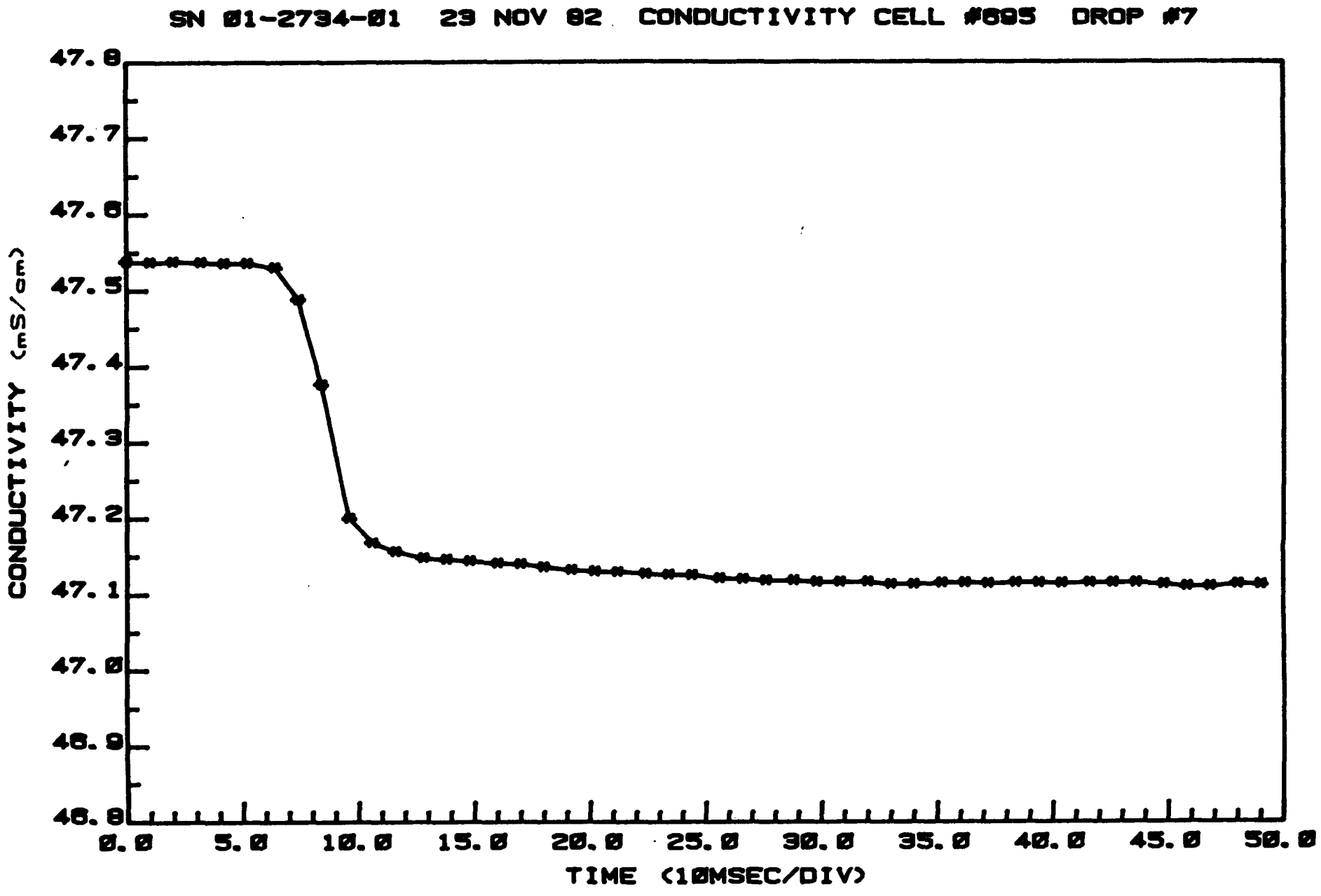

Figure A-17. Time Series of Conductivity Acquired During Response Test C07B.

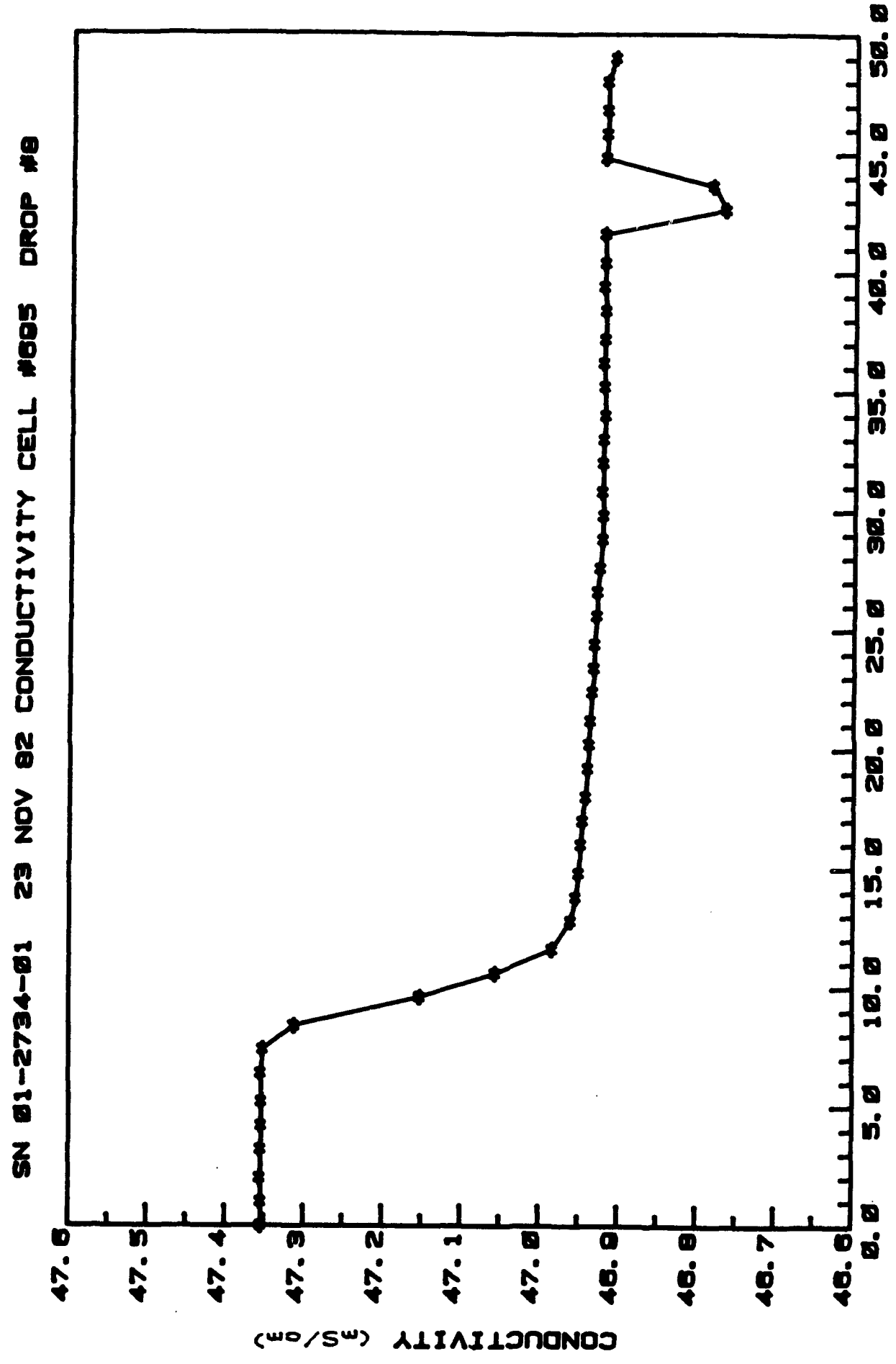

Figure A-18. Time Series of Conductivity Acquired During Response Test C08B.

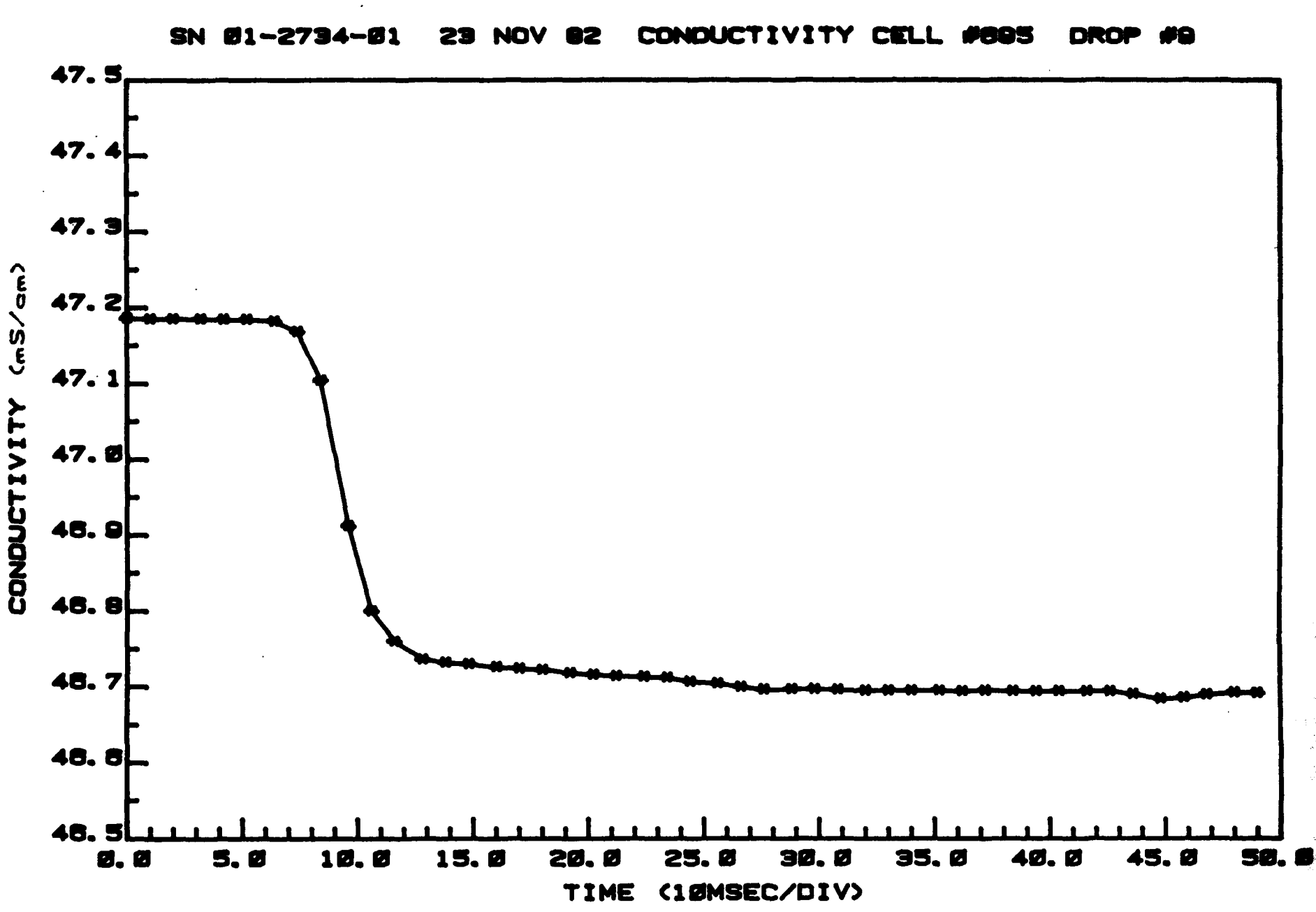

Figure A-19. Time Series of Conductivity Acquired During Response Test C09B.

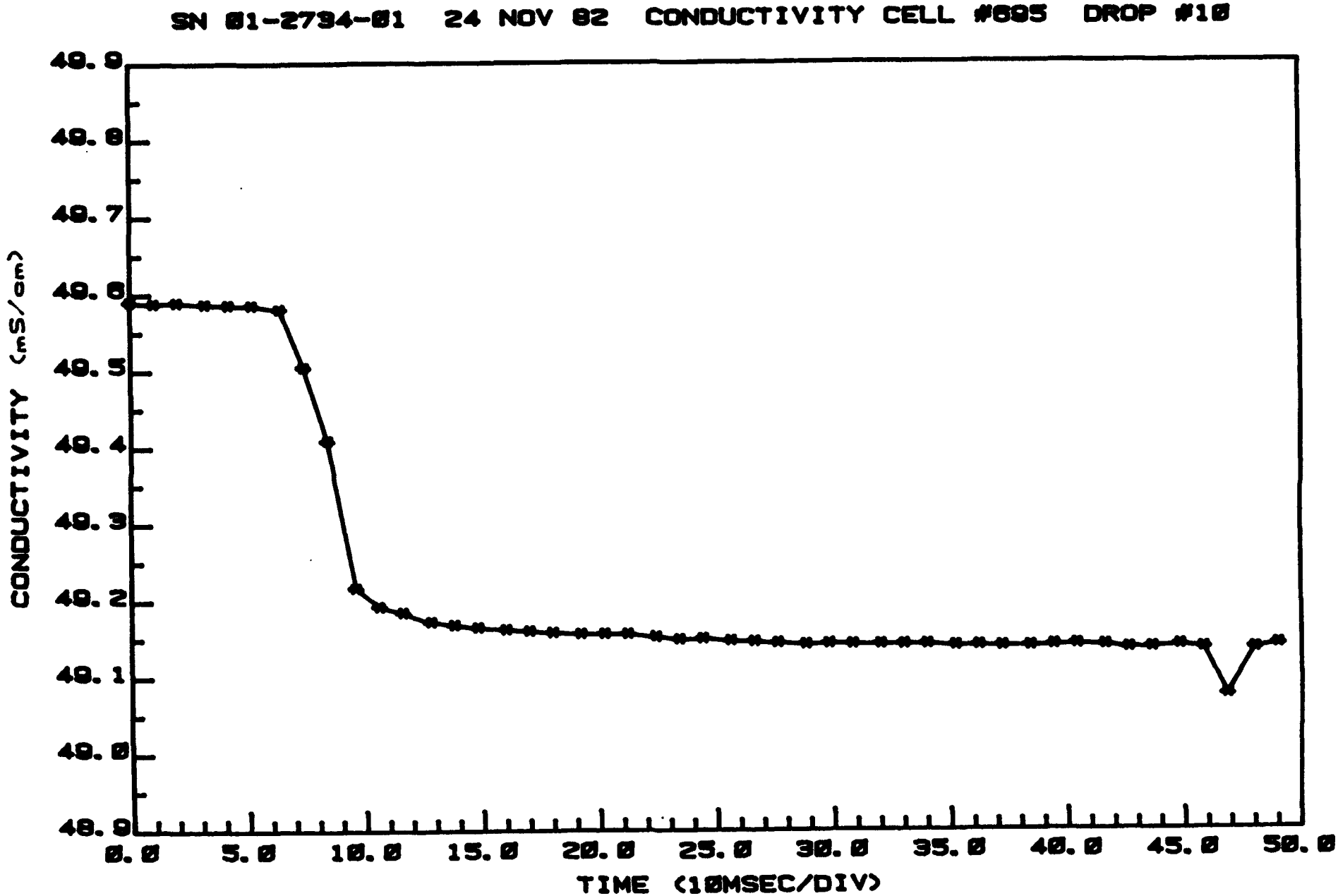

Figure A-20. Time Series of Conductivity Acquired During Response Test C10B.

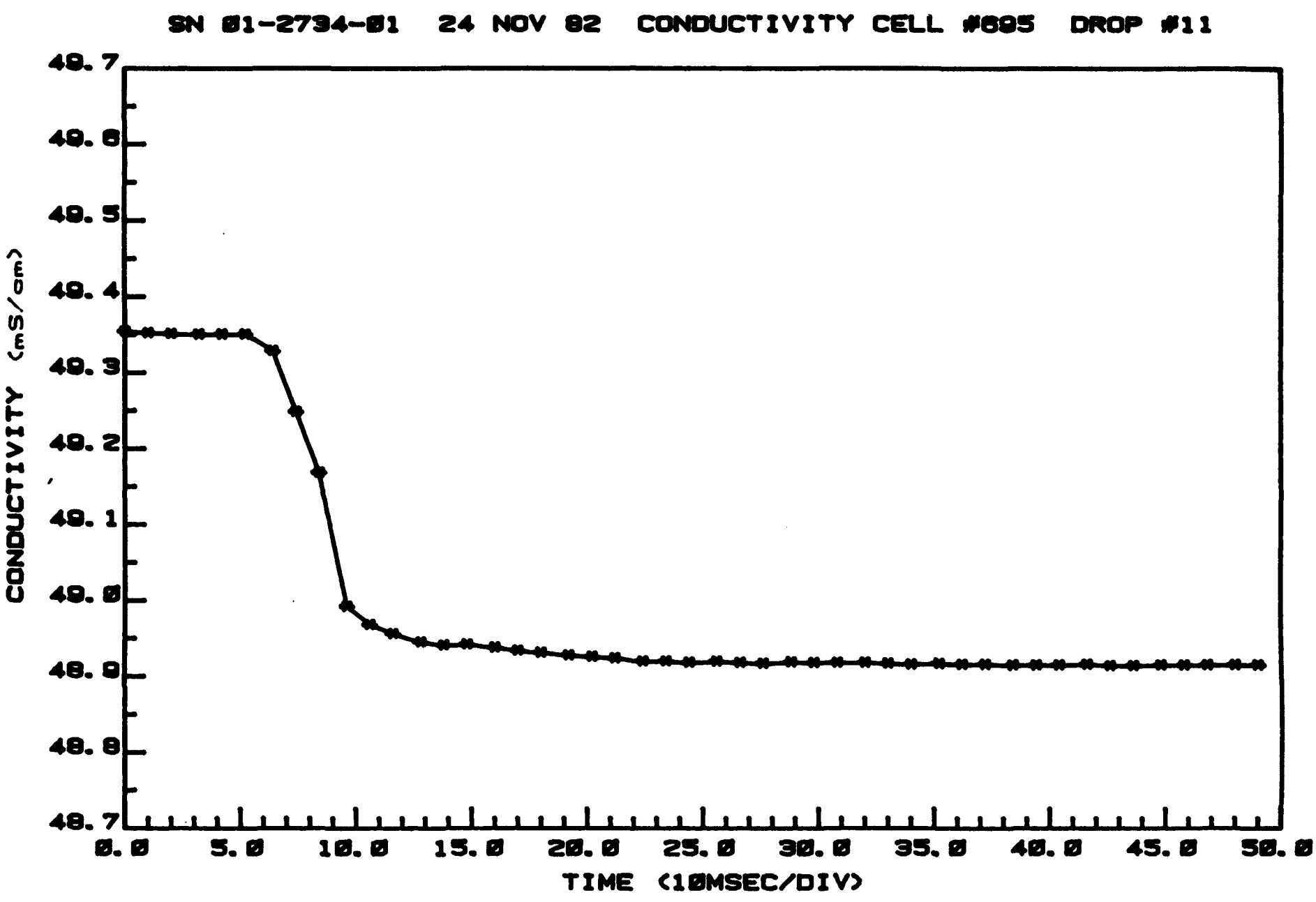

Figure A-21. Time Series of Conductivity Acquired During Response Test C11B.

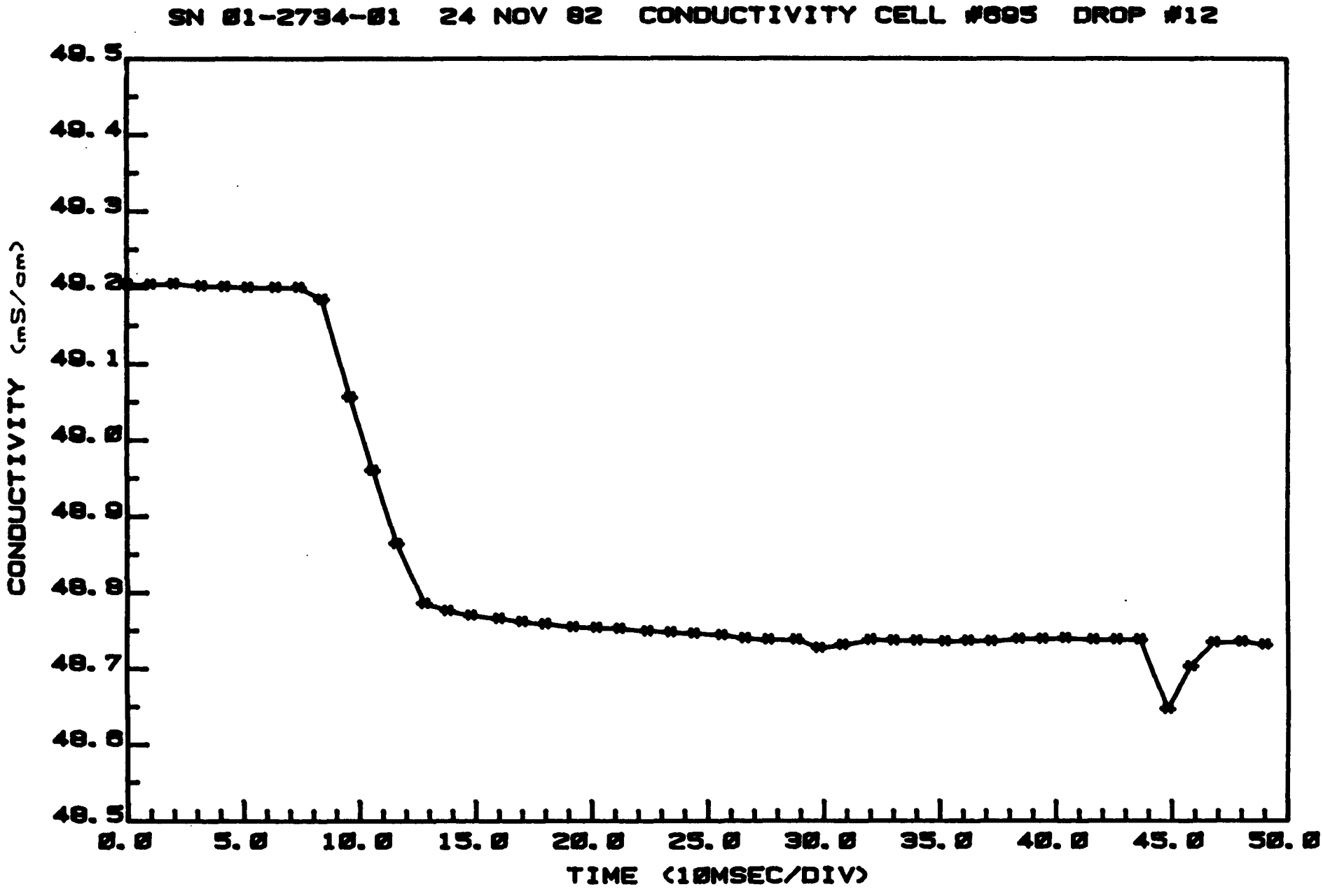

Figure A-22. Time Series of Conductivity Acquired During Response Test C12B.

APPENDIX B

COMPUTATION OF PARTIAL DERIVATIVES OF SALINITY

APPENDIX B

COMPUTATION OF PARTIAL DERIVATIVES OF SALINITY*

The Practical Salinity Scale adopted by the Joint Panel on Oceanographic Tables and Standards provides a means of relating temperature, T, conductivity, C, pressure, P, and salinity, S, of seawater. An algorithm for computing salinity from the other parameters is presented by Gieskes.[11] The following development results in an algorithm for computing the first partial derivatives of salinity with respect to temperature and conductivity at constant pressure for use in eq. (68) et seq. The notation of Geiskes is followed.

The salinity function S(P,T,C,) may be written

$$S = S_o + \Delta S \tag{B1}$$

where

$$S_o = \sum_{i=o}^{5} a_i R^{i/2} \tag{B2}$$

and

$$\Delta S = \frac{T - 15}{1 + k(T-15)} \sum_{i=o}^{5} b_i R^{i/2} \tag{B3}$$

$$= \tau(T) \sum_{i=o}^{5} b_i R^{i/2} \qquad = \tau(T)\sigma_b$$

The parameter R is given by

$$R = \frac{R}{R_p r_t} \tag{B4}$$

*Note that S is used to represent salinity in this appendix while θ is used in the main body of this report.

with

$$R = R(c) = \frac{C}{C_o} \quad , \quad C_o = 42.914 \text{ mS/cm}$$

and

$$R_p = R_p\,(T,P,C) = 1 + \frac{C(P)}{B(T) + A(T)R(C)}$$

$$r_t = r(T) = \sum_{i=o}^{4} C_i\, T^i$$

→(B6)

The differential of S is

$$dS = \frac{\partial S}{\partial P} \cdot dP + \frac{\partial S}{\partial T} \cdot dT + \frac{\partial S}{\partial C} \cdot dC \qquad (B7)$$

However neglecting the effect of pressure, we have $dP = 0$ so that

$$dS = \frac{\partial S}{\partial T} \cdot dT + \frac{\partial S}{\partial C} \cdot dC \qquad (B8)$$

We will evaluate these terms independently.

The temperature term is

$$\frac{\partial S}{\partial T} = \frac{\partial S_o}{\partial T} + \frac{\partial}{\partial T}(\Delta S) \qquad (B9)$$

Again, evaluating separately, we have

$$\frac{\partial S_o}{\partial T} = \frac{\partial}{\partial T}\left\{ \sum_{i=o}^{5} a_i\, R^{i/2} \right\} \qquad (B10)$$

$$= \frac{\partial}{\partial T}\left\{ a_o + \sum_{i=1}^{5} a_i\, R^{i/2} \right\}$$

$$= \sum_{i=1}^{5} \left\{ a_i \frac{\partial}{\partial T} R^{i/2} \right\}$$

$$= \sum_{i=1}^{5} a_i \left\{ R^{(i/2-1)} \cdot i/2 \cdot \frac{\partial}{\partial T} R \right\} = \alpha \frac{\partial}{\partial T} R$$

where

$$\alpha = \sum_{i=1}^{5} a_i \cdot i/2 \cdot R^{(i/2-1)} \tag{B11}$$

Then

$$\begin{aligned}\frac{\partial}{\partial T}(\Delta S) &= \left[\frac{\partial}{\partial T}\ \tau(T)\right] \cdot \sum_{i=0}^{5} b_i R^{i/2} \\ &\quad + \tau(T)\ \frac{\partial}{\partial T}\left[\sum_{i=0}^{5} b_i R^{i/2}\right] \\ &= \left[\frac{1}{1 + k(T-15)} - \frac{T - 15}{[1 + k(T-15)]^2}\right] \sum_{i=0}^{5} b_i R^{i/2} \\ &\quad + \tau(T)\left[\sum_{i=0}^{5} b_{i}\left(\frac{i}{2}\right) R^{(i/2-1)}\right] \frac{\partial R}{\partial T} \\ &= \left\{\frac{1}{[1 + k(T-15)]^2}\right\}\ \sigma_b + \tau(T)\ \beta\ \frac{\partial R}{\partial T}\end{aligned} \tag{B12}$$

Thus

$$\begin{aligned}\frac{\partial S}{\partial T} &= \alpha \frac{\partial R}{\partial T} + \beta\tau(T) \frac{\partial R}{\partial T} + \frac{\sigma_b}{[1 + k(T-15)]^2} \\ &= (\alpha + \beta\tau(T)) \frac{\partial R}{\partial T} + \frac{\sigma_b}{[1 + k(T-15)]^2}\end{aligned} \tag{B13}$$

Next we evaluate $\frac{\partial S}{\partial C}$

$$\frac{\partial S}{\partial C} = \frac{\partial S_o}{\partial C} + \frac{\partial}{\partial C}(\Delta S) \tag{B14}$$

Now

$$\frac{\partial S_o}{\partial C} = \alpha \frac{\partial R}{\partial C} \tag{B15}$$

as shown before for $\frac{\partial S_o}{\partial T}$. Likewise

$$\frac{\partial}{\partial C}(\Delta S) = \frac{\partial}{\partial C}\left[\tau(T) \cdot \sigma_b\right] = \tau(T)\ \frac{\partial \sigma_b}{\partial C} \qquad \text{(B16)}$$

$$= \tau(T)\ \beta \frac{\partial R}{\partial C}$$

Thus

$$\frac{\partial S}{\partial C} = (\alpha + \beta\tau(T))\ \frac{\partial R}{\partial C} \qquad \text{(B17)}$$

It now remains to evaluate the partial derivatives of R with respect to C and T.

$$\frac{\partial R}{\partial C} = \frac{\partial}{\partial C}\left[\frac{R}{R_p r_t}\right] \qquad \text{(B18)}$$

$$= \frac{1}{R_p r_t} \cdot \frac{\partial R}{\partial C} - \frac{R}{R_p^2 r_t^2}\left[r_t \frac{\partial R_p}{\partial C} + R_p \frac{\partial r_t}{\partial C}\right]$$

$$= \frac{1}{R_p r_t}\left\{\frac{\partial R}{\partial C} - R\left[\frac{1}{R_p}\frac{\partial R_p}{\partial C} + \frac{1}{r_t}\frac{\partial r_t}{\partial C}\right]\right\}$$

$$= \frac{R}{R_p r_t}\left\{\frac{1}{R}\frac{\partial R}{\partial C} - \frac{1}{R_p}\frac{\partial R_p}{\partial C} - \frac{1}{r_t}\frac{\partial r_t}{\partial C}\right\}$$

and so

$$\frac{\partial R}{\partial C} = R\left\{\frac{1}{R}\frac{\partial R}{\partial C} - \frac{1}{R_p}\frac{\partial R_p}{\partial C} - \frac{1}{r_t}\frac{\partial r_t}{\partial C}\right\} \qquad \text{(B19)}$$

But since r_t is not a function of conductivity, C.

$$\frac{\partial r_t}{\partial C} = 0 \qquad \text{(B20)}$$

and

$$\frac{\partial R}{\partial C} = R\left\{\frac{1}{R}\frac{\partial R}{\partial C} - \frac{1}{R_p}\frac{\partial R_p}{\partial C}\right\}$$

Similarly, we have

$$\frac{\partial R}{\partial C} = R\{ \frac{1}{R} \frac{\partial R}{\partial T} - \frac{1}{R_p} \frac{\partial R_p}{\partial T} - \frac{1}{r_t} \frac{\partial r_t}{\partial T} \} \tag{B21}$$

$$= -R \{ \frac{1}{R_p} \frac{\partial R_p}{\partial T} + \frac{1}{r_t} \frac{\partial r_t}{\partial T} \}$$

since $R = R(C)$.

Further evaluating, we have

$$\frac{\partial R}{\partial C} = \frac{\partial}{\partial C} \left[\frac{C}{C_o} \right] = \frac{1}{C_o}$$

$$\frac{\partial R_p}{\partial C} = - \frac{C(P)}{[B(T) + A(T) \cdot R(C)]^2} \cdot A(T) \cdot \frac{1}{C_o} \tag{B22}$$

$$= \frac{-C(P)A(T)}{C_o [B(T) + A(T) R(C)]^2}$$

$$= \frac{-A(T)}{C_o [B(T) + A(T)R(C)]} \cdot (R_p - 1)$$

$$= \frac{-A(T)}{C_o C(P)} \cdot (R_p - 1)^2$$

Thus

$$\frac{\partial R}{\partial C} = R \{ \frac{C_o}{C} \cdot \frac{1}{C_o} - \frac{1}{R_p} \cdot \frac{-A(T)}{C_o C(P)} (R_p - 1)^2 \}$$

$$= R \{ \frac{1}{C} + \frac{A(T)}{C_o C(P)} \cdot \frac{(R_p - 1)^2}{R_p} \} \tag{B23}$$

$$= \frac{R}{C_o} \{ \frac{1}{R} - \frac{\Phi \cdot A(T)}{R_p} \}$$

with

$$\Phi = - \frac{C(P)}{[B(T) + A(T)R(C)]^2}$$

Finally, evaluating $\frac{\partial R}{\partial T}$, we have

$$\frac{\partial R_p}{\partial T} = \frac{-C(P)}{[B(T) + A(T)R(C)]^2} \cdot \left[\frac{\partial B(T)}{\partial T} + R(C) \frac{\partial A(T)}{\partial T} \right] \qquad \text{(B24)}$$

and, since

$$A(T) = d_3 + d_4 T$$

$$B(T) = 1 + d_1 T + d_2 T^2,$$

we have

$$\frac{\partial A}{\partial T} = d_4$$

and

$$\frac{\partial B}{\partial T} = d_1 + 2d_2 T$$

Therefore

$$\frac{\partial R_p}{\partial T} = \frac{-C(P)}{[B(T) + A(T)R(C)]^2} \cdot [d_1 + 2d_2 T + R(C)d_4] \qquad \text{(B26)}$$

$$= \Phi(P,T,C) [d_1 + 2d_2 T + R(C)d_4]$$

and

$$\frac{\partial r_\tau}{\partial T} = \frac{\partial}{\partial T} \{ \sum_{i=0}^{4} C_i T^i \}$$

$$= \sum_{i=1}^{4} i \cdot C_i \cdot T^{i-1} = \rho(T) \qquad \text{(B27)}$$

Thus

$$\frac{\partial R}{\partial T} = -R\{ \frac{1}{R_p} \cdot \Phi \cdot [d_1 + 2d_2T + R(C)d_4] + \frac{1}{r_t} \rho(T)\} \qquad (B29)$$

$$= -R\{ \frac{\Phi}{R_p} [d_1 + 2d_2T + R(C)d_4] + \frac{\rho}{r_t}\}$$

Algorithm

In summary, we must compute the following, with constants as given by Gieskes[11]:

$$C(P) = P(e_1 + e_2P + e_3P^2),$$

$$B(T) = 1 + d_1T + d_2T^2,$$

$$A(T) = d_3 + d_4T,$$

$$R(C) = C / C_o,$$

$$\Phi(P,T,C) = \frac{-C(P)}{[B(T) + A(T)R(C)]^2},$$

$$R_p = 1 + \frac{C(P)}{[B(T) + A(T)R(C)]},$$

$$r_t = \sum_{i=o}^{4} C_i T^i,$$

$$\rho = \sum_{i=1}^{4} i\, C_i\, T^{i-1},$$

$$\Psi = \frac{R(C)}{R_p\, r_t},$$

$$\frac{\partial R}{\partial T} = -R\{ \frac{\Phi}{R_p} [d_1 + 2d_2T + R(C)d_4] + \frac{\rho}{r_t}\},$$

$$\frac{\partial R}{\partial C} = \frac{R}{C_o} \left\{ \frac{1}{R(C)} - \frac{\phi A(T)}{R_p} \right\},$$

$$\alpha = \sum_{i=1}^{5} a_i \left(\frac{i}{2}\right) R^{\left(\frac{i}{2} - 1\right)},$$

$$\beta = \sum_{i=1}^{5} b_i \left(\frac{i}{2}\right) R^{\left(\frac{i}{2} - 1\right)},$$

$$\tau = \frac{T - 15}{1 + k(T - 15)},$$

$$\sigma_b = \sum_{i=o}^{5} bi \, R^{i/2},$$

with P in decibars, T in degrees Celsius, and C in Siemens/cm. We then may compute

$$\frac{\partial S}{\partial C} = (\alpha + \beta \tau) \cdot \frac{\partial R}{\partial C}$$

and

$$\frac{\partial S}{\partial T} = (\alpha + \beta \tau) \cdot \frac{\partial R}{\partial T} + \frac{\sigma_b}{[1 + k(T-15)]^2} \cdot$$

Data arrays required to store the constants from Geiskes are

a_i, i = 0, 1, ... , 5

b_i, i = 0, 1, ... , 5

c_i, i = 0, 1, ... , 4

d_i, i = 1, ..., 4

e_i, i = 1, ..., 3

k = 0.0162

c_0 = 42.914

APPENDIX C

ESTIMATION OF VARIANCE IN SALINITY

APPENDIX C

ESTIMATION OF VARIANCE IN SALINITY*

Consider simultaneously sampled sequences of temperature and conductivity, $\{T_j\}$ and $\{C_j\}$, $j = 1, \ldots, N$, taken at constant pressure, from which a salinity sequence $\{S_j\}$ is constructed. The variance of each sequence is

$$\sigma_T^2 = \frac{1}{N} \sum_{j=1}^{N} (\bar{T} - T_j)^2 = \frac{1}{N} \sum_{j=1}^{N} \Delta T_j^2, \tag{C1}$$

$$\sigma_C^2 = \frac{1}{N} \sum_{j=1}^{N} \Delta C_j^2, \tag{C2}$$

and

$$\sigma_S^2 = \frac{1}{N} \sum_{j=1}^{N} \Delta S_j^2 \tag{C3}$$

where

$$\Delta T_j = (\bar{T} - T_j) \tag{C4}$$

$\bar{T}$ is the mean of the temperature sequence

$$\bar{T} = \frac{1}{N} \sum_{j=1}^{N} T_j \tag{C5}$$

and ΔC_j and ΔS_j are similarly defined. To a first approximation

$$\Delta S_j \cong \frac{\partial S}{\partial T}\Bigg|_{\substack{T=\bar{T} \\ C=\bar{C}}} \cdot \Delta T_j + \frac{\partial S}{\partial C}\Bigg|_{\substack{T=\bar{T} \\ C=\bar{C}}} \cdot \Delta C_j \tag{C6}$$

*Note that S is used to represent salinity in this appendix while θ is used in the main body of the report.

Squaring, we have

$$\Delta S_j^2 \cong (S_T(\bar{C},\bar{T})\,\Delta T_j)^2 + 2S_T(\bar{C},\bar{T})\,S_c(\bar{C},\bar{T})\,\Delta T_j\,\Delta C_j + (S_c(\bar{C},\bar{T})\Delta C_j)^2, \tag{C7}$$

with

$$S_T(\bar{T},\bar{C}) = \left.\frac{\partial S}{\partial T}\right|_{\substack{T=\bar{T}\\C=\bar{C}}} \tag{C8}$$

and

$$S_C(\bar{T},\bar{C}) = \left.\frac{\partial S}{\partial C}\right|_{\substack{T=\bar{T}\\C=\bar{C}}} . \tag{C9}$$

Then

$$\begin{aligned}\sigma_s^2 &= \frac{1}{N}\sum_j \Delta S_j^2 \\ &\cong S_T^2(\bar{T},\bar{C})\left[\frac{1}{N}\sum_j \Delta T_j^2\right] \\ &\quad + 2S_C(\bar{T},\bar{C})S_T(\bar{T},\bar{C})\left[\frac{1}{N}\sum_j \Delta T_j\,\Delta C_j\right] \\ &\quad + S_c^2(\bar{T},\bar{C})\left[\frac{1}{N}\sum_j \Delta C_j^2\right]\end{aligned} \tag{C10}$$

$$\sigma_s^2 \cong S_T^2(\bar{T},\bar{C})\,\sigma_T^2 + 2S_c(\bar{T},\bar{C})S_T(\bar{T},\bar{C})\left[\frac{1}{N}\sum_j \Delta T_j\,\Delta C_j\right] + S_c^2(\bar{T},\bar{C})\,\sigma_c^2 .$$

Now

$$\frac{1}{N}\sum_j \Delta T_j \Delta C_j = \left\langle \Delta T \Delta C \right\rangle \tag{C11}$$

$$\longrightarrow \iint_{\text{all } \Delta T, \Delta C} \Delta T \Delta C \; p(\Delta T \mid \Delta C)\; d(\Delta T)\; d(\Delta C)$$

for large N, where $p(\Delta T \mid \Delta C)$ is the joint probability density for ΔT and ΔC.

If we assume that the ΔT_j and ΔC_j are

1) Uncorrelated and

2) Symmetrically distributed

Then

$$\iint_{\text{all } \Delta T, \Delta C} \Delta T \Delta C \; p(\Delta T \mid \Delta C)\; d(\Delta T)\; d(\Delta C) = 0. \tag{C12}$$

Thus

$$\frac{1}{N}\sum_j \Delta T_j \Delta C_j \longrightarrow 0$$

So that

$$\sigma_s^2 = S_T^2(\bar{T},\bar{C})\,\sigma_T^2 + S_C^2(\bar{T},\bar{C})\,\sigma_C^2$$

APPENDIX D

POWER SPECTRUM OF SALINITY

APPENDIX D

POWER SPECTRUM OF SALINITY

Consider a time series of salinity, $\theta(t)$, which consists of perturbations, $\Delta\,\theta(t)$ from some average value, θ_0 . The perturbations are due entirely to perturbations in temperature, $\Delta T(t)$, and conductivity, $\Delta C(t)$. Thus

$$\theta(t) = \theta_0 + \Delta\theta(t) \tag{D1}$$

$$= \theta_0 + \{\theta_T\,\Delta T(t) + \theta_c\,\Delta C(t)\}\ , \tag{D2}$$

where θ_T and θ_c are the first partial derivatives of salinity with respect to temperature and conductivity, respectively, given by eqs. (79) and (80). The perturbation times series, $\Delta\,\theta(t)$, is a continuous, zero-mean function whose Fourier transform and power spectrum are well-behaved.

The Fourier transform of the salinity time series is

$$F\{\theta\} = F\{\theta_0\} + F\{\Delta\theta\}\ , \tag{D3}$$

where $F\{x\}$ represents the Fourier transform operating on the time series X. The Fourier transform of the constant first term in the RHS of eq. (D3) is a Dirac uelta function at zero frequency

$$F\{\theta_0\} = \frac{\delta(f/\theta_0)}{|\theta_d|}\ . \tag{D4}$$

Recalling from eq. (39) that the single-sided power spectrum of a function is given by twice the product of its Fourier transform with the conjugate, the power spectrum of the salinity time series, may be written as

$$PSD\{\theta\} = PSD\{\theta_0\} + \frac{2\delta(f/\theta_0)}{|\theta_d|}\left[F^*\{\Delta\theta\} + F\{\Delta\theta\}\right] + PSD\{\Delta\theta\}, \tag{D5}$$

For frequencies greater than zero, the first two terms in the RHS of eq. (D5) vanish, so that

$$PSD\{\theta\} \longrightarrow PSD\{\Delta\theta\} = F^*\{\Delta\theta\}\, F\{\Delta\theta\}. \tag{D6}$$

By virtue of the addition theorem for the Fourier transform, the Fourier transform of the salinity function is

$$F\{\Delta\theta\} = \theta_T\, F\{\Delta T\} + \theta_C\, F\{\Delta C\}. \tag{D7}$$

Then

$$PSD\{\theta\} = 2\,\theta_T^2\, F^*\{\Delta T\}\, F\{\Delta T\} + 2\,\theta_C^2\, F^*\{\Delta C\}\, F\{\Delta C\} + 2\,\theta_T\,\theta_C\,[F^*\{\Delta T\}\, F\{\Delta C\} + F^*\{\Delta C\}\, F\{\Delta T\}]. \tag{D8}$$

The Fourier transform may be written in polar form, as may any complex function,

$$F\{x\} = a_x\, e^{-i\phi_x}, \tag{D9}$$

Where a_x is the (real) modulus of F and ϕ_x is the (real) phase angle. Using this notation, the third term in the RHS of eq. (D8), may be expanded to yield

$$F^*\{\Delta T\}\, F\{\Delta C\} = a_{\Delta C}\, e^{i\phi_{\Delta C}}\, a_{\Delta T}\, e^{-i\phi_{\Delta T}} = a_{\Delta C} a_{\Delta T}\, e^{+i(\phi_{\Delta C} - \phi_{\Delta T})} \tag{D10}$$

and

$$F^*\{\Delta C\}\, F\{\Delta T\} = a_{\Delta C}\, a_{\Delta T}\, e^{-i(\phi_{\Delta C} - \phi_{\Delta T})}, \tag{D11}$$

so that

$$F^*\{\Delta T\}\, F\{\Delta C\} + F^*\{\Delta C\}\, F\{\Delta T\} = 2a_{\Delta C} a_{\Delta T} \cos[\phi_{\Delta C} - \phi_{\Delta T}]. \tag{D12}$$

Then, substituting into eq. (D8) the salinity spectrum becomes

$$PSD\{\theta\} = \theta_T^2\, PSD\{\Delta T\} + \theta_C^2\, PSD\{\Delta C\} + 2\theta_C\,\theta_T \sqrt{PSD\{\Delta T\}\, PSD\{\Delta C\}}\, \cos[\phi_{\Delta C} - \phi_{\Delta T}]. \tag{D13}$$

Finally, by an argument similar to that employed to obtain eq. (D6), it may be shown that for non-zero frequencies

$$PSD\{T\} \longrightarrow PSD\{\Delta T\} \tag{D14}$$

and

$$PSD\{C\} \longrightarrow PSD\{\Delta C\} \tag{D15}$$

Then for frequencies greater than zero, the salinity spectrum is

$$PSD\{\theta\} = \theta_T^2\, PSD\{T\} + \theta_C^2\, PSD\{C\} + 2\,\theta_C\,\theta_T \sqrt{PSD\{T\}\, PSD\{C\}}\, \cos[\phi_C - \phi_T]. \tag{D16}$$

The third term in the RHS of eq. (D16) may be thought of as a cross term which adds to the salinity spectrum or subtracts from it at any given frequency, depending upon the relative phases of the temperature and conductivity at that frequency. Equation (D16) is useful for determining order of magnitude estimates for the salinity spectrum. Generally, one might expect the spectra of temperature and conductivity to be comparable in magnitude. Likewise, in Section 3.3 it is shown for temperature and conductivity ranges of interest that θ_T and θ_C are comparable in magnitude. Thus, the term $2\,\theta_C\,\theta_T \sqrt{PSD\{T\}\, PSD\{C\}}$ is comparable in magnitude to the sum of the first two terms in the RHS of eq. (D16). Since the cosine term will vary from +1 to -1 as the phase difference varies from $-\pi$ to $+\pi$, it may be seen that $PSD\{\theta\}$ varies from a maximum value

$$PSD_{max}\{\theta\} \cong 2[\theta_T^2\, PSD\{T\} + \theta_C^2\, PSD\{C\}] \tag{D17}$$

to approximately zero. A median value for use as an order of magnitude estimate is

$$PSD\{\theta\} \cong \theta_T^2 \, PSD\{T\} + \theta_C^2 \, PSD\{C\}. \qquad (D18)$$

converting to the notation used in the body of the report for discrete power spectrum, eq. (D18) becomes the order of magnitude estimate of eq. (82),

$$\hat{S}_s(k\Delta f) \cong \theta_T^2(\bar{C},\bar{T})\,\hat{S}_T(k\Delta f) + \theta_C^2(\bar{C},\bar{T})\,\hat{S}_C(k\Delta f). \qquad (D19)$$

DISTRIBUTION LIST

COMNAVOCEANCOM	1
NORDA	1
JHU	1
WHOI	1
TRITON SYSTEMS, INC.	2
NAVOCEANO Code 4603	5
Code 6300	4